IFM-GEOMAR
Leibniz-Institut für Meereswissenschaften
an der Universität Kiel

Cold-water coral *Lophelia pertusa* as a high-resolution archive of paleoenvironmental conditions in the central Mediterranean

Diplomarbeit

Christian-Albrechts-Universität zu Kiel
Mathematisch-Naturwissenschaftliche Fakultät
Institut für Geowissenschaften

vorgelegt von:	**cand. geol. Jan-Rainer Riethdorf**
Studienfach:	**Geologie-Paläontologie**
Matrikelnummer:	**686440**
Erstgutachter:	**Prof. Dr. Wolf-Christian Dullo**
Zweitgutachter:	**Dr. Andres Rüggeberg**

Erklärung

Hiermit erkläre ich, dass die Diplomarbeit selbstständig und ausschließlich unter Verwendung der angegebenen Quellen und Hilfsmittel verfasst wurde.

Kiel, 17. Dezember 2008 Jan-R. Riethdorf

The Earth goeth on the Earth
Glist'ring like gold.
The Earth goes to the Earth
Sooner than it wold.
The Earth builds on the Earth
Castles and Towers.
The Earth says to the Earth
All shall be ours.

(auf einem Grabstein im Kirchhof von Melrose-Abbey, Schottland)

Zusammenfassung

Kaltwasserkorallen stellen in der Paläoklimaforschung eines der vielversprechendsten Klimaarchive dar, die sich verändernde Umweltbedingungen hochauflösend in ihrem Aragonitskelett aufzeichnen können. Diese Arbeit beschäftigt sich mit fossilen und rezenten Exemplaren der Kaltwasserkorallenart *Lophelia pertusa* aus dem zentralen Mittelmeer. Weiterhin werden Wasserproben aus diesem Gebiet, aus dem Europäischen Nordmeer und aus dem NE-Skagerrak analysiert. Ziel dieser Arbeit ist es, Paläowassertemperaturen mittels geochemischer Proxies zu rekonstruieren und die heutigen Umweltbedingungen mit denen zu Zeiten des Spätglazials und der Jüngeren Dryas zu vergleichen.

Mit der Elektronenstrahlmikrosonde werden Elementverteilungen von Mg, Ca, Sr und S bestimmt und hochauflösende Profile von Mg/Ca-, Sr/Ca- und S/Ca-Verhältnissen erstellt. Die Wasserproben, die teilweise zusammen mit den Korallen gesammelt wurden, werden mittels ICP-MS und ICP-OES auf Gehalte an Haupt- und Spurenelementen analysiert. Datierungen der fossilen Korallen erfolgten mit der U/Th-Methode. Zusätzlich werden δ^{13}C- und δ^{18}O-Messungen ausgewertet, die von Matthias López Correa (GZN-IPAL, Erlangen) an denselben Korallen durchgeführt worden sind.

Die hochauflösenden Mg/Ca-, Sr/Ca- und S/Ca-Profile werden mittels Spektralanalyse ausgewertet, während Paläotemperaturen einerseits über Sr/Ca-Verhältnisse und andererseits mit der "lines technique"-Methode (Smith et al., 2000) rekonstruiert werden. Um die Elementverhältnisse im Meerwasser zu Zeiten des Spätglazials und der Jüngeren Dryas zu rekonstruieren, erfolgt eine Kalibrierung zwischen rezenter Korallenchemie und rezenter Wasserchemie.

Bezüglich des Einbaus der untersuchten Elemente lassen sich die Ergebnisse sowohl durch Biomineralisationsprozesse als auch durch eine Beeinflussung von Umweltparametern erklären. S/Ca-Verhältnisse scheinen dabei von Temperatur, Primärproduktion und/oder Wassermassenventilation abzuhängen. Die rekonstruierten Temperaturen sind für beide Methoden unterschiedlich, aber scheinen im Vergleich zu heute vor 17,6 ka und 12,4 ka niedriger gewesen zu sein. Es hat sich ausserdem gezeigt, dass für *L. pertusa* regionale Sr/Ca-Kalibrierungen erstellt werden müssen. Konzentrationen von Haupt- und Spurenelementen im Meerwasser sind vor allem durch den Salzgehalt bestimmt, allerdings könnten die Elemente Antimon und Barium auch durch Primärproduktion beeinflusst sein. Schliesslich deuten die Ergebnisse darauf hin, dass das Mittelmeer zu Kaltzeiten von Kaltwasserkorallen besiedelt wird und dass ihre Ökosysteme in niederen Breiten deshalb glaziale Rückzugsgebiete darstellen könnten.

Abstract

Cold-water corals are one of the most promising paleoenvironmental archives in paleoclimate research that contain high-resolution records of long-term climate change. This study focuses on fossil and recent specimens of the cold-water coral *Lophelia pertusa* from the Mediterranean Sea as well as on water samples from different locations in the central Mediterranean, the Norwegian Sea and the NE-Skagerrak. The intention is to apply established geochemical proxies of seawater temperatures and to compare present-day with paleoenvironmental conditions during the late glacial period and the Younger Dryas cold interval.

Electron-probe imaging is used to map elemental distributions of Mg, Ca, Sr and S across the thecal wall of the coralline aragonite and to generate high-resolution profiles of molar element ratios. Water samples were collected together with the coral specimens and are analyzed using ICP-MS- and ICP-OES-techniques to determine concentrations of major and trace elements. Fossil coral samples were U/Th-dated after having been checked for alteration. Additionally, measurements of stable carbon (δ^{13}C) and stable oxygen (δ^{18}O) isotopes conducted on the same specimens by Matthias López Correa at GZN-IPAL, Erlangen, are evaluated.

High-resolution records of Mg/Ca-, Sr/Ca- and S/Ca-ratios are investigated using spectral analysis. Paleotemperatures are reconstructed using Sr/Ca-ratios and the "lines technique"-method (Smith et al., 2000). Furthermore, the geochemistry of the recent coral skeletons are compared and calibrated to the analysed water samples in order to reconstruct paleo-water-values with the focus lying on Mg/Ca-, Sr/Ca-, S/Ca- and B/Ca-ratios.

Results regarding element incorporation in coral skeletons can be interpreted by means of biologically controlled calcification processes and by influence of environmental parameters. S/Ca-ratios are suggested to be influenced by temperature, primary productivity and/or ventilation of intermediate water masses. Reconstructed temperatures are different for both methods applied, indicating lower temperatures than at present at 17.6 ka and at 12.4 ka, and that regional Sr/Ca-calibrations are needed for *L. pertusa*. Salinity accounts for most of the observed seawater concentrations of major and trace elements, except for antimony and barium, which might be influenced by primary productivity. Finally, results indicate that cold-water corals colonize the Mediterranean Sea during cold climates and that low latitude ecosystems act as glacial refugia in the deep sea.

Table of Contents

List of Abbreviations

$\delta^{13}C$	Ratio of stable carbon isotopes ^{13}C and ^{12}C
$\delta^{18}O$	Ratio of stable oxygen isotopes ^{18}O and ^{16}O
$\delta^{44/40}Ca$	Ratio of stable calcium isotopes ^{44}Ca and ^{40}Ca
$\delta^{88/86}Sr$	Ratio of stable strontium isotopes ^{88}Sr and ^{86}Sr
AdDW	Adriatic Deep Water
AeDW	Aegean Deep Water
ANU-RSES	Research School of Earth Sciences, The Australian National University, Canberra, Australia
AW	Atlantic Water
CNR-ISMAR	Istituto di Scienze Marine, Consiglio Nazionale delle Ricerche, Bologna, Italy
CTD	Conductivity Temperature Depth probe
DFG	Deutsche Forschungsgemeinschaft
DIC	Dissolved Inorganic Carbon
DIP	Dissolved Inorganic Phosphorus
EPMA	Electron Probe Microanalysis
eWOCE	Electronic Atlas of WOCE Data
GISP2	Greenland Ice Sheet Project 2
GKG	Box corer (Großkastengreifer)
GZN-IPAL	Geo-Center Northern Bavaria, University of Erlangen-Nuremberg, Erlangen, Germany
IAPSO	International Association for the Physical Sciences of the Oceans
ICP-MS	Inductively Coupled Plasma Mass Spectrometry
ICP-OES	ICP Optical Emission Spectrometry
ICRAM	Central Institute for Marine Research, Rome, Italy
IFM-GEOMAR	Leibniz-Institute of Marine Sciences, Kiel, Germany
ITIS	Integrated Taxonomic Information System
LIW	Levantine Intermediate Water
MARUM	Center for Marine Environmental Sciences at the University of Bremen, Bremen, Germany
MAW	Modified Atlantic Water

NASA-GISS	Goddard Institute for Space Studies, National Aeronautics and Space Administration, New York, USA
NBS	National Bureau of Standards, today National Institute of Standards and Technology (NIST), USA
NCW	Norwegian Coastal Water
NSDW	Norwegian Sea Deep Water
PDB	Pee Dee Belemnite, a carbonate standard material
ROV	Remotely Operated Vehicle
RSD	Relative Standard Deviation
SMOW	Standard Mean Ocean Water, a seawater standard
TDW	Tyrrhenian Dense Water
TRISTAN	Temperatur-Rekonstruktion aus der Isotopen-Signatur von Tiefwasserkorallen des Atlantik and der Nordsee
USNM	National Museum of Natural History, Washington, D.C., USA
WDS	Wavelength Dispersive X-ray Spectrometer
WGS84	World Geodetic System 1984 (last revised in 2004)
WOCE	World Ocean Circulation Experiment
YD	Younger Dryas cold interval

1 Introduction

1.1 Aim of this Study

This study aims to evaluate the potential of the cold-water coral *Lophelia pertusa* of being a high-resolution archive of paleoenvironmental conditions in the central Mediterranean. Its main objective is to apply established geochemical proxies of seawater temperatures to fossil and recent examples of this species. Finally it intends to reconstruct paleoenvironmental conditions of the late glacial period and the Younger Dryas cold interval in the central Mediterranean Sea.

1.1.1 Objectives

In times of noticeable and hazardous changes in Earth's climate it is more important than ever to understand the mechanisms that drive those changes. Besides instrumental records, natural archives are a source for paleoclimate data which can be used to understand climate evolution. Paleoceanographic research has access to many types of climate archives covering time intervals that range from days to millions of years. Corals are one of the most promising climate archives because they record long-term climate changes over years and decades within their skeletons. With modern instrumental techniques it is possible to analyze the coralline carbonate with up to a daily resolution, depending on the species' growth rate.

Most research nowadays regarding corals is focused on zooxanthellate (symbiont-bearing) coral species living in shallow, tropical waters, because they are easily accessible and characterized by a long lifetime. On the contrary only little is known about cold-water corals. These animals live in cold or deep waters and do not live in symbiosis with photosynthetic algae. However, there is evidence that they do record environmental changes within their aragonite skeletons as well. To this date research dealing with cold-water corals is mainly focused on cold-water coral provinces in the Atlantic and Pacific oceans and interest in their occurences in marginal seas like the Mediterranean only slowly arises. This study focuses on cold-water corals from the Mediterranean Sea and on established paleoceanographic proxies to reconstruct seawater temperatures.

In detail, the major objectives of this study are:

Coral-related objectives

- to evaluate whether cold-water corals can be used as high-resolution paleoenvironmental archives in the central Mediterranean
- to reconstruct the temperatures of intermediate water masses during the late glacial period and Younger Dryas cold interval in the central Mediterranean

Water-related objectives

- to determine element concentrations in seawater samples, in particular boron and barium
- to correlate coral geochemistry with water chemistry

Method-related objectives

- to find out whether high-resolution electron-probe analyses are useful in obtaining high-resolution paleoenvironmental records from coral chemistry
- to recommend improvements or modifications of the applied measurement strategies

1.1.2 Strategy

In this study cold-water coral specimens and seawater samples from the central Mediterranean Sea as well as water samples from the Norwegian Sea and the NE-Skagerrak were investigated.

Fossil and recent coral specimens were analyzed for concentrations of certain elements and isotopes in order to apply different methods of temperature reconstruction. The analyses include:

- Electron-probe (EPMA): mapping element distributions and determining concentrations of major elements (Ca, Mg, Sr and S)
- U/Th-dating of fossil coral specimens (carried out by Malcolm McCulloch at ANU-RSES, Canberra, Australia)
- ICP-MS: determination of stable carbon ($\delta^{13}C$) and stable oxygen ($\delta^{18}O$) isotopes (performed by Matthias López Correa at GZN-IPAL, Erlangen)

In order to calibrate recent water chemistry to recent coral geochemistry, **seawater samples** were analyzed for contents of major and trace elements:

- ICP-MS: trace elements (Li, Rb, Sr, Mo, Sb, Cs, Ba and U)
- ICP-OES: major and trace elements (Ca, Mg, Sr, B and Ba)

In addition epibenthic foraminifera from **box corer samples (GKG)** were analyzed for stable carbon and oxygen isotopic compositions using ICP mass spectrometry.

1.2 Cold-Water Corals and Reefs

1.2.1 Overview

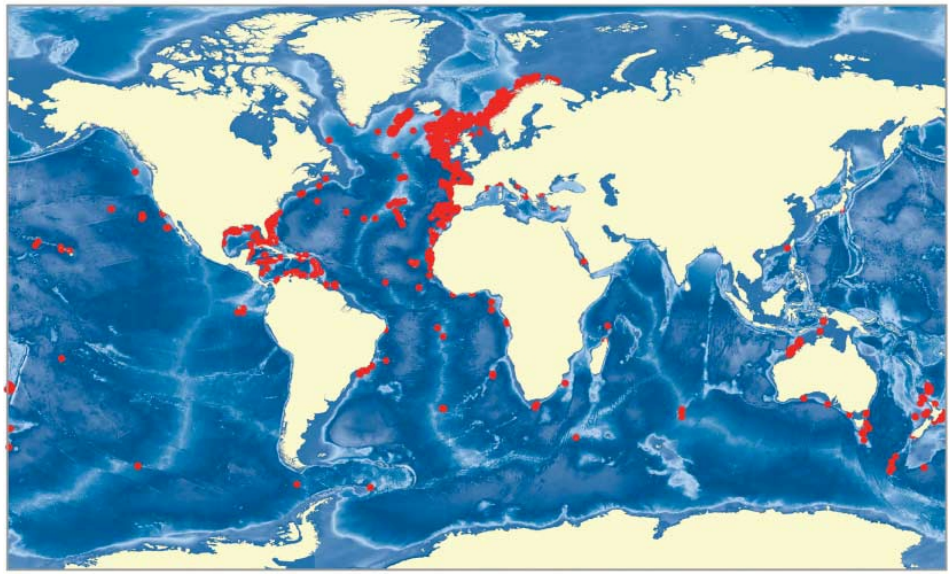

Figure 1.1: Global distribution of reef-building cold-water corals (from Roberts et al. (2006)).

Cold-water corals are azooxanthellate cnidarians encompassing stony corals (Scleractinia), soft corals (Octocorallia), black corals (Antipatharia), and hydrocorals (Stylasteridae). They either occur individually, as isolated colonies, in small patch reefs or they form large reefs or giant carbonate mounds. The knowledge about their global distribution is incomplete, but they are largely restricted to oceanic waters with temperatures ranging from 4°C to 14°C (Fig. 1.1). Deep-water reef frameworks are made up of fewer than ten species of scleractinians, occurring in depths of up to 4000 m, depending on seawater carbonate chemistry. Dominating reef-building species are *Lophelia pertusa* and *Madrepora oculata* (Freiwald et al., 2004; Roberts et al., 2006).

Reef-development seems to be controlled by the interplay of local hydrography and sedimentary dynamics. It begins with the initial settlement of a coral larva to a hard substratum and is followed by bioerosion and sediment-trapping. Finally coral growth keeps pace with sediment infill and mounds begin to form (Dorschel et al., 2005; Roberts et al., 2006).

Like shallow water scleractinians, corals in deep waters seem to be cosmopolitan consumers which are on the one hand being fueled by primary productivity in surface waters and on the other hand feed on detrital and resuspended materials (Duineveld et al., 2004). Additionally, they are reported from areas of the continental

slope where internal waves enhance food supply from the seabed (White et al., 2005). *Lophelia pertusa* seems to rely on a zooplankton diet but has also been seen capturing live zooplankton in the field (Kiriakoulakis et al., 2004; Kiriakoulakis et al., 2005). Regarding reproduction, most cold-water coral species are gonochoristic (Fadlallah, 1983), and gamete production in *Lophelia pertusa* seems to follow phytodetrital food fall in the NE-Atlantic (Waller, 2005).

While reefs in high latitudes are likely to have repeatedly diminished during glacial periods and flourished during interglacials, low latitude ecosystems seem to be important speciation centers and glacial refugia in the deep sea (de Forges et al., 2000; Roberts et al., 2006). Major threats for these ecosystems nowadays are mainly bottom trawling, hydrocarbon drilling and seabed mining, and ocean acidification (Rogers, 1999; Fosså et al., 2002; Roberts et al., 2003; Orr et al., 2005).

Most recent studies regarding cold-water coral provinces focus on the eastern North Atlantic (e.g. Foubert, 2007; Rüggeberg et al., 2007; Wheeler et al., 2007), the Norwegian Slope (e.g. Freiwald et al., 1997; Fosså et al., 2002; Wheeler et al.; 2007) and the Mediterranean Sea (e.g. Taviani et al., 2005a; Taviani et al., 2005b; Freiwald & Shipboard Scientific Party, 2006).

1.2.2 *Lophelia pertusa*

This study focuses on the colonial cold-water coral species *Lophelia pertusa* whose scientific classification is given in Tab. 1.1. Although its complete present geographic distribution is still unknown (Freiwald, 1998), this species has been reported from almost all oceans but also from marginal seas like the Mediterranean (Zibrowius, 1980). It has its highest occurrence from the eastern Atlantic margin down to West Africa (Freiwald et al., 2004).

Table 1.1: Scientific classification of *Lophelia pertusa* as found in the Integrated Taxonomic Information System (http://www.itis.gov/).

Kingdom	Animalia (animals)
Phylum	Cnidaria (cnidarians)
Class	Anthozoa (corals and sea anemons)
Order	Scleractinia (stony corals)
Family	Carophylliidae
Genus	*Lophelia*
Species	*L. pertusa* (Linnaeus, 1758)

Lophelia pertusa precipitates an aragonite exoskeleton consisting of a thick wall made up of rhythmic bands (Freiwald et al., 1997). Uniserial-erect colonies consisting of thousands of polyps are produced with either a ”zig-zag-” or dendroid-branching

pattern (Fig. 1.2) several meters in size (Freiwald, 1998). Upward extension and outward thickening happen simultaneously. Average linear extension rates are reported spanning 5.5 mm/yr (Mortensen & Rapp, 1998) to more than 1 cm/yr (Mikkelsen et al., 1982), whereas outward thickening shows a smaller rate of ca. 0.1 mm/yr (Cohen et al., 2006). Growth sequences longer than around 30 cm are difficult to find (Mortensen & Rapp, 1998) and the life span of *Lophelia pertusa* colonies is still not known (Foubert, 2007).

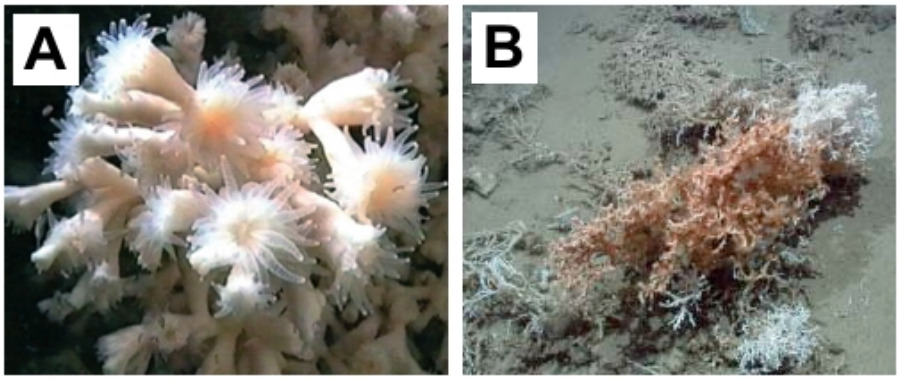

Figure 1.2: A: Living *Lophelia pertusa* with expanded tentacles, photographed by the JAGO-Team at the Sula Ridge (Norwegian Sea) (from Freiwald et al., 2004); B: White and orange coloured *L. pertusa* from the Santa Maria di Leuca Reef Province in the central Mediterranean, photographed during ROV Dive-106, station M70/1-721, in 579.4 m water depth (from Freiwald & Shipboard Scientific Party, 2006).

The distribution of *Lophelia pertusa* is mainly limited by temperature, salinity and nutrient supply (Freiwald et al., 2004). Also a connection to the bathymetric range of the oxygen minimum zone (Freiwald, 1998) as well as to a certain level of seawater density (Dullo et al., 2008) has been proposed. While the main depth distribution is within bathyal depths (Zibrowius, 1980; Freiwald, 1998), they also occur in waters as shallow as 39 m in Norwegian fjords and as deep as 3383 m at seamounts in the North Atlantic (Zibrowius, 1980). The recorded temperature range for *Lophelia pertusa* is 4–14°C and the salinity range is 35–37, although in the Mediterranean as well as in Norwegian and Swedish fjords higher and lower values are observed (Freiwald, 1998). Oldest fossil samples are reported to be of Paleogene (Eocene) age (Squires, 1957) whereas the invasion of the Mediterranean began in the Neogene after the Messinian Event (Freiwald, 1998) and their first appearance in Norwegian waters is estimated to have begun only recently, about 10,000 years ago (Henrich et al., 1996).

1.2.3 Proxies Based on Cold-Water Coral Chemistry

Paleoceanographic research using cold-water corals as a paleoenvironmental archive mainly focus on estimating past seawater temperatures or nutrient content from

skeletal chemistry or on reconstructing the ventilation history of the ocean by dating skeletal material. Their potential is mainly due to three reasons: (i) there are no photosynthetic algae present additionally influencing cold-water coral chemistry, (ii) they have a banded skeletal structure with the ability to record environmental variations through time and (iii) they exhibit cosmopolitan distributions (Roberts et al., 2006; Rüggeberg et al., 2008).

A method for inferring deep-water ventilation ages using complementary cold-water coral U/Th- and ^{14}C-studies was first proposed by Mangini et al. (1998). Since then, this method was successfully applied to recent and fossil species from the North Atlantic (Adkins et al., 1998; Schröder-Ritzrau et al., 2003) and the Southern Ocean (Goldstein et al., 2001).

Only recently, Montagna et al. (2006) observed that phosphorus incorporated into cold-water coral species *Desmophyllum dianthus* is directly proportional to the ambient seawater phosphorus concentration (DIP), making P/Ca-ratios a possible proxy of paleoproductivity.

Past seawater temperatures are reconstructed from cold-water corals using either Sr/Ca-ratios or stable isotopes. Most Sr/Ca-temperature relationships exist for tropical, zooxanthellate coral species. The relationship is linear and invers. However, Cohen et al. (2001) discovered that Sr/Ca-ratios within the daytime skeleton of symbiont-bearing tropical coral *Porites* is rather related to the calcification rate than directly to sea surface temperature. A neither constant nor predictable, but up to 65% Sr/Ca-variability in the symbiotic skeleton is related to symbiont activity (Cohen et al., 2002). Regarding cold-water corals, Montagna et al. (2005) found that the temperature-dependent elements uranium and strontium did not correlate in skeletons of *Desmophyllum dianthus* indicating that other factors than temperature are dominant. Finally, Cohen et al. (2006) published a paleotemperature-equation for *Lophelia pertusa* with a sensitivity twice as large as for tropical species and four times higher for inorganic aragonite, but stated that only about 25% of the Sr/Ca-variability are driven by temperature changes.

Mortensen & Rapp (1998) found a correlation between δ^{13}C, δ^{18}O and seawater temperature within *Lophelia pertusa*, although cold-water corals do not precipitate in equilibrium with seawater. They concluded that isotopic fractionation is controlled by kinetic isotope effects and declared that a relationship between growth rate and temperature exists. While McConnaughey (2003) also prefers the kinetic model to explain the linear relationship between carbon and oxygen isotopes, Adkins et al. (2003) proposed a mechanism for vital effects based on a thermodynamic response to a biologically induced pH-gradient in the calcifying region. Smith et al. (2000) found a linear function of temperature with a precision of about 1.0°C investigating

18 species of azooxanthellate corals from different latitudes and depths. LUTRINGER ET AL. (2005) improved the precision to 0.7°C using a micro-sampling technique published in ADKINS ET AL. (2003). However, the method is problematic since an estimate of the isotopic composition of seawater is needed to apply the equation. Because annual banding is difficult to identify and skeletal $\delta^{18}O$ varies by almost 3‰ in a non-systematic manner, sampling for 'time series' is not realizable at present (SMITH ET AL., 2002).

Relationships between temperature and stable calcium isotopes ($\delta^{44/40}Ca$) have been developed for foraminifera (NÄGLER ET AL., 2000; GUSSONE ET AL., 2003; GUSSONE ET AL., 2005), sclerosponges (HAASE-SCHRAMM ET AL., 2003), and tropical scleractinian corals (BÖHM ET AL., 2006). A recent investigation of *Lophelia pertusa* showed no clear temperature-dependent fractionation of calcium isotopes (A. Rüggeberg, personal communication).

The most recent and promising method to reconstruct past seawater temperatures from cold-water corals is the use of stable strontium isotopes ($\delta^{88/86}Sr$). FIETZKE & EISENHAUER (2006) developed a bracketing standard method for the determination of stable strontium isotopes in carbonates and showed, that the isotopic fractionation during precipitation of inorganic calcite and aragonite is temperature-dependent. The dependency was verified for the tropical coral species *Pavona clavus*. Using this approach, RÜGGEBERG ET AL. (2008) showed a temperature-dependency for stable strontium isotope fractionation in *Lophelia pertusa*, indicating a similar fractionation process to take place in both symbiotic and non-symbiotic corals.

1.3 Research Area / Setting

Sample material was collected during three different research cruises: R/V Poseidon cruise **P325** (12.07.–03.08.2005) to the so far known northernmost coral reef complexes in the Norwegian Sea, R/V Alkor cruise **AL275** (24.03.–30.03.2006) to the aphotic coral reef ecosystems in the NE-Skagerrak and R/V Meteor cruise **M70/1** (24.09.–18.10.2006) to the central Mediterranean Sea. Additionally, sample material include two fossil cold-water coral samples (*Lophelia pertusa*) from the central Mediterranean collected during R/V Urania cruises **CORSARO** (20.04.–06.05.2006) and **SETE-06** (06.05.–23.05.2007).

1.3.1 Norwegian Sea and NE-Skagerrak

Water samples collected during P325-cruise originate from two areas of the Norwegian Sea: the **Røst Reef** area (station 373) and the **Sveinsgrunnen Slope** (stations 383 & 386) (Fig. 1.3). The first area is a large reef complex along the back wall of a giant submarine slide (Trænadjupet Slide) that is about 35 km to 40 km long and 300 m to 400 m deep and shows a complex and rugged seabed topography. The Sveinsgrunnen Slope is described as a flat outer shelfbank with a steep slope resembling a slide escarpment (Freiwald & Shipboard Scientific Party, 2005).

According to Skarđhamar & Svendsen (2005), relatively cold and low-salinity Norwegian Coastal Water (NCW; $S < 35$) stretches like a wedge out over the shelf edge, merging with Atlantic Water (AW; $S > 35$) on the shelf and shelf-slope area off the North Norwegian coast. Increasing in thickness from 50 m during summer to 200 m during winter, the NCW is present above the more saline AW. The AW itself is underlain by Norwegian Sea Deep Water (NSDW; $S < 34.95$; $T < 0°C$), filling the Lofoten basin below about 800 m. During P325, Freiwald & Shipboard Scientific Party (2005) observed an increase in thickness of the NCW from 50 m to 250 m from 66°N to 71°N.

The cruise AL275 concentrated on two areas characterized by about 7 nm-long inlets of the Oslofjord, located to the east and west of the **Søster Islands** (Fig. 1.3). These inlets, which connect the main Oslofjord Trough and the Norwegian Channel, show complex seabed topography with steep inclined rock outcrops, mud-rich troughs and drumlins. Water samples investigated in this study were collected in the **Eastern Oslofjord Inlet (EOI)** (stations 420 & 425) consisting of 140 m to 200 m deep troughs separated by narrow thresholds generally less than 120 m deep (Rüggeberg & Form, 2007).

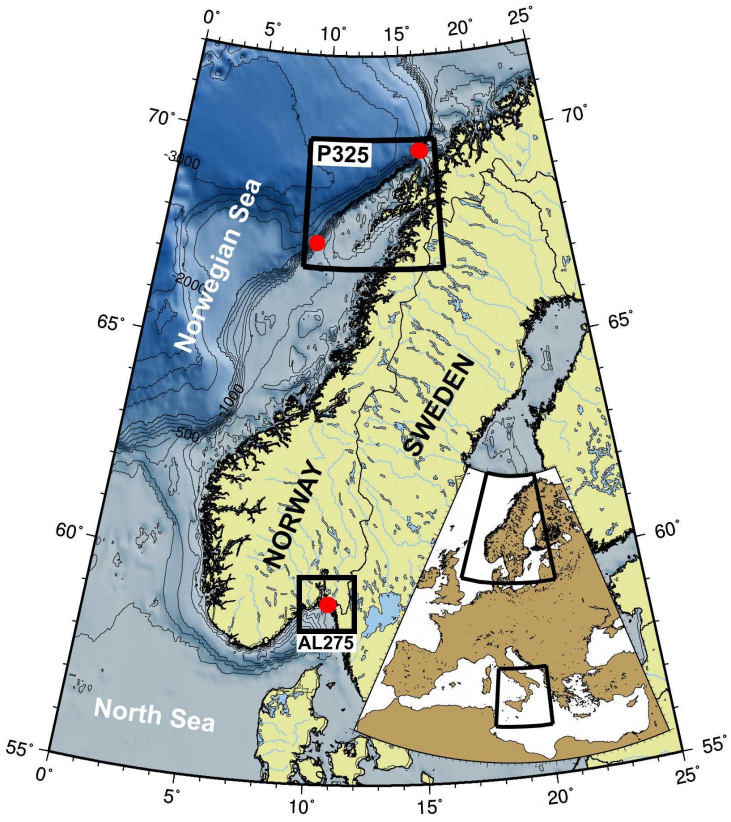

Figure 1.3: Location of water samples collected during cruises P325 and AL275.

Hydrographic investigations conducted during AL275-cruise show a well-stratified water column at the EOI-site with surface waters low in temperature and salinity (1–2°C; 24–27) and uniform T and S below 25 m water depth (about 7°C; about 36) (Rüggeberg & Form, 2007). Seasonal changes in winter and summer temperatures and salinities of these Atlantic waters lie between about 7°C and 8.5°C, and 35 and 36, respectively (Pfannkuche & Shipboard Scientific Party, 2004).

1.3.2 Central Mediterranean Sea

Coral and seawater samples from the central Mediterranean Sea were collected in three different areas during M70/1-cruise: the **southern Adriatic Sea**, the **northern Ionian Sea**, and the **Strait of Sicily** (Fig. 1.4).

In the southern Adriatic Sea samples originate from three locations (Fig. 1.5).

The first, the **Gondola Slide (GS)** (station 752), represents an 18-km-wide slump scar which is about 600 m to 700 m deep and characterized by large blocky slide deposits, up to 500 m across and up to 40 m thick. ROV Dive-111 discovered giant olistholiths derived from the upper shelf that still contain Late Pleistocene sedimentary sequences. Some of these blocks serve as substrate for coral colonies and thus are covered by fossil coral fragments and various shell debris. Live solitary

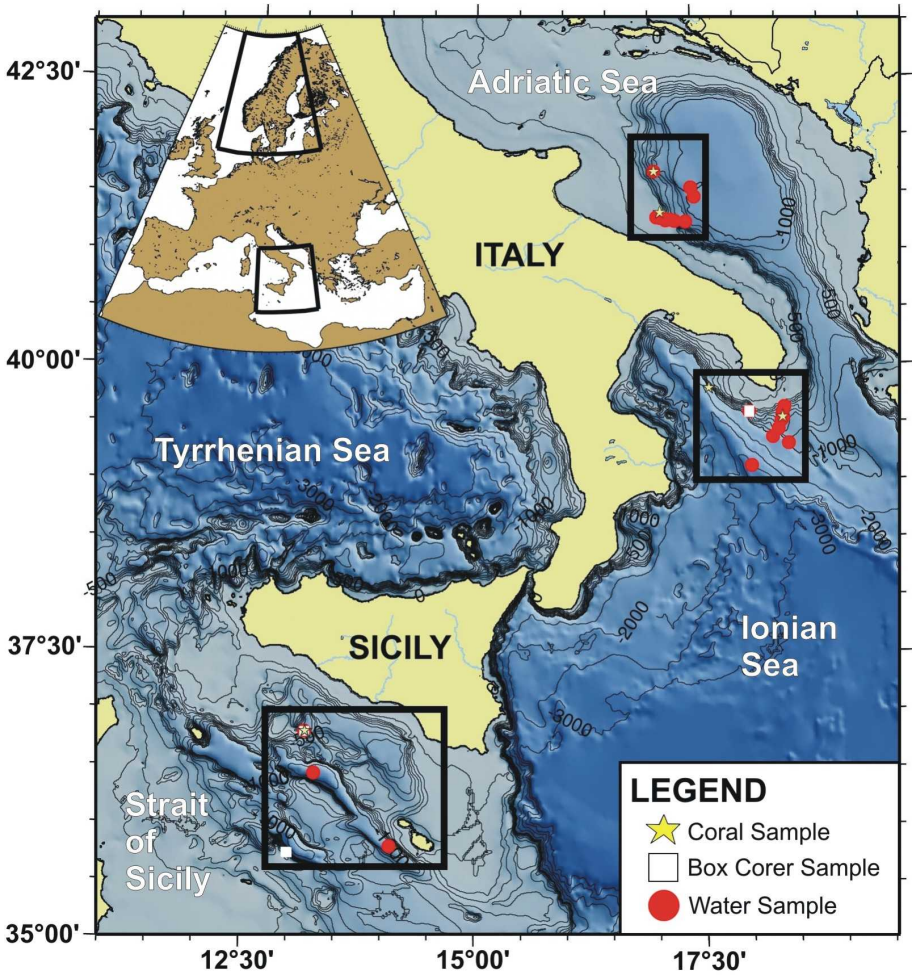

Figure 1.4: Location of samples collected during M70/1.

and colonial corals (*Desmophyllum dianthus*, *Madrepora oculata*, *Lophelia pertusa*) preferentially colonize overhangs or flanks in clusters or individually. The seafloor at station 752 is characterized by soft sediment with sandwaves (1 m wavelength, 20 cm height), boulders and pebbles. The second location, the **Bari Canyon (BC)** (stations 735, 745–750), is a large canyon system representing an asymmetric east-west striking feature that consists of two major parallel oriented canyon heads. While the shelf above the canyon lies in 200 m water depth, the slope steeply declines into depths of 1000 m with an inclination of more than 30°. Thus the steep slope acts as a barrier against dense water masses coming from the North. Sediments found here are bioturbated sandy muds, covered with boulders up to 50 cm in size that are colonized by serpulids, sponges or corals. The last study site in the southern Adriatic is the **Bari Seamount** (stations 736, 740), a seamount rising about 200 m above the seafloor (Freiwald & Shipboard Scientific Party, 2006).

The **Santa Maria di Leuca Reef Province (SML)** (stations 705, 709, 710, 712, 721–728) in the northern Ionian Sea is a well studied cold-water coral province (Taviani et al., 2005b). It is located on a gently inclined shelf ramp to the south of

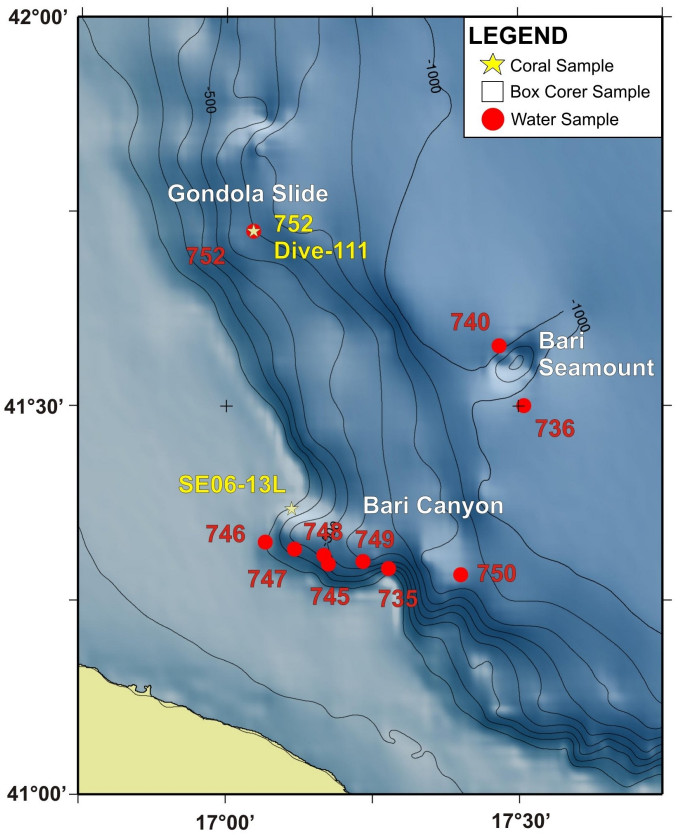

Figure 1.5: Sampling locations in the southern Adriatic Sea (M70/1).

the Apulian coast (Fig. 1.6). During ROV Dive-106 at station 721 an E-W oriented transect was investigated, that included two bigger mound structures about 50 m in height and some smaller elevations. Corals are mainly concentrated on the eastern flanks and on the top of the mounds, forming upright growing coral thickets in a dense framework. The biocoenosis is characterized by a high species variety and an orange coloured, flourishing *Lophelia pertusa* colony was first recorded here (Fig. 1.2, 6). Patch reefs, centimeters to meters across, occur as mainly dead, Fe-Mn-coated, in situ frameworks of mainly *Madrepora oculata* and *Lophelia pertusa*. On top of the dead framework and coral rubble live *Madrepora oculata* and *Lophelia pertusa*, generally 10 cm in height, can be found. On the sediment, upright growing colonies are predominantly fan-shaped while dead framework serves as substrate for various organisms. The seafloor consists of highly bioturbated sandy mud, in places with colonized boulders, 15 cm in size (Freiwald & Shipboard Scientific Party, 2006).

Within the sea area between the Strait of Sicily and the islands of Sicily and Malta, samples were collected at seven stations in three different areas (Fig. 1.7).

In the northwesternmost area, a steep NW-SE striking slope of the eastern spur of the **Urania Bank (UB)** was investigated (stations 677–679). The slope, being of volcanic origin and covered by Neogene carbonate sequences, covers a bathymetric

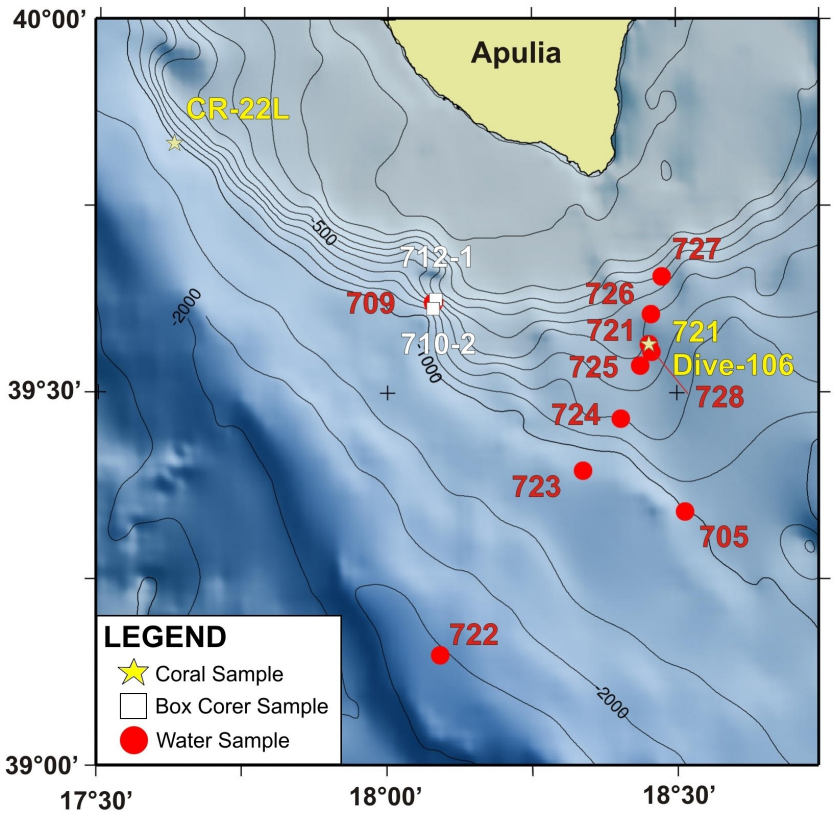

Figure 1.6: Sampling locations in the northern Ionian Sea (M70/1).

range from 800 m to 200 m water depth. ROV Dive-100 at station 677 was conducted along a cliff with steep flanks, about 50 m in height. Live colonial corals densely colonize the edges of the overhangs of the cliff while at the cliff base high amounts of coral debris accumulate on highly bioturbated sediment. The overhangs themselves are covered with dead oysters and corals, their framework serving as substrate for live solitary and colonial corals (*Madrepora oculata*, *Lophelia pertusa*, *Corallium rubrum*). Because the cliff is partially formed steplike with huge colony fragments in its horizontal areas, the live coral assemblages show a "hanging garden" growth pattern, frequently observed in the Strait of Sicily (Freiwald & Shipboard Scientific Party, 2006). The **Malta Trough** (stations 655, 675) is the easternmost deep-sea trough in the Strait of Sicily, striking NW-SE. As the central deep-sea trough in the strait, the **Linosa Trough** (stations 668, 669) is characterized by steep margins representing block-faulted horst and graben structures rich in volcanic and sedimentary sequences. A small sector at the southern slope of the trough, about 6 nm east of Linosa Island was investigated. Here the seabed shows three morphological steps in the west (1200–500 m, 500–425 m, 425–350 m) that merge into one nearly vertical escarpment further east. Box corer samples collected in the Linosa Trough consisted of hemipelagic sediment (Freiwald & Shipboard Scientific Party, 2006).

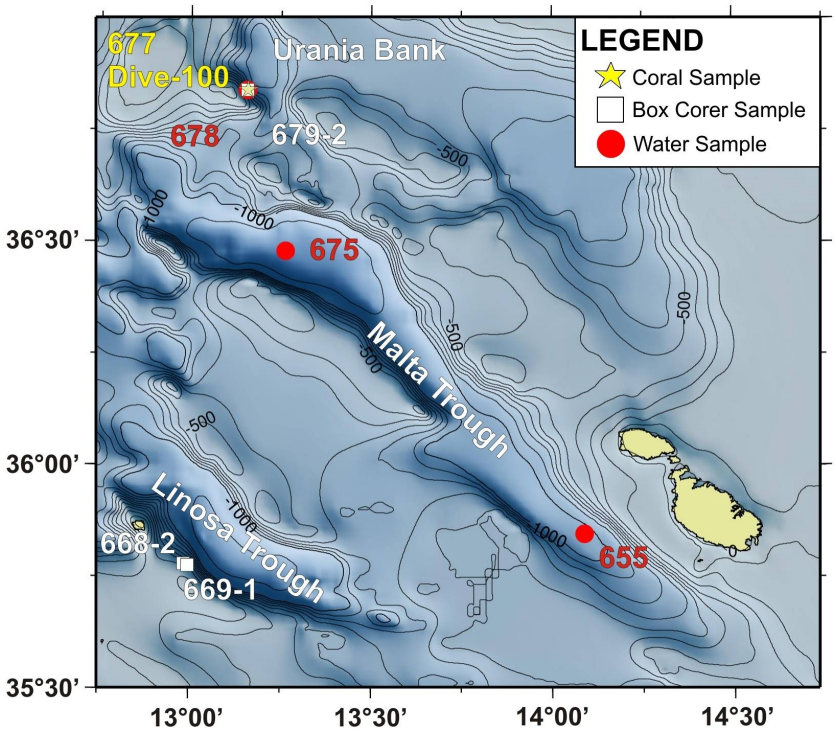

Figure 1.7: Sampling locations in the Strait of Sicily (M70/1).

1.3.3 Hydrography of the Central Mediterranean Sea

The semi-enclosed Mediterranean Sea is characterized by a thermohaline-driven, anti-estuarine circulation pattern. In the surface layer **Atlantic Water** (**AW**; T = 15–16°C, S = 36–37, σ_t = 26–27)[1,2] flows through the Strait of Gibraltar into the eastern basin, continuously being modified while flowing within the Mediterranean. The modification is due to evaporation, precipitation and mixing with other water masses. Sinking and formation of intermediate or deep Mediterranean Waters generally takes place in the northern parts of the two major basins due to two reasons: (i) in some subbasins, densified AW mixes offshore with denser waters underneath, forming subbasin-specific water masses and (ii) having only a small reservoir of heat, waters on the shelves are markedly cooled during winter. Continuously being mixed, these Mediterranean Waters then circulate and finally outflow at Gibraltar as a homogeneous water mass that is recognized at 1000–1200 m in most of

1 Here, σ refers to the density ρ of a sample of seawater at atmospheric pressure. It can either be determined from its temperature measured *in situ*, known as the density anomaly (σ_t), or from its potential temperature (Θ), known as the potential density anomaly (σ_Θ) (Bearman, 2002):

$$\sigma_t = (\rho - 1000) kg/m^3$$

2 The potential temperature (Θ) is defined as the temperature that a fluid would attain if brought adiabatically to a pressure of 100 kPa, whereas *in situ* temperature is the temperature at its actual height or depth (Bearman, 2002).

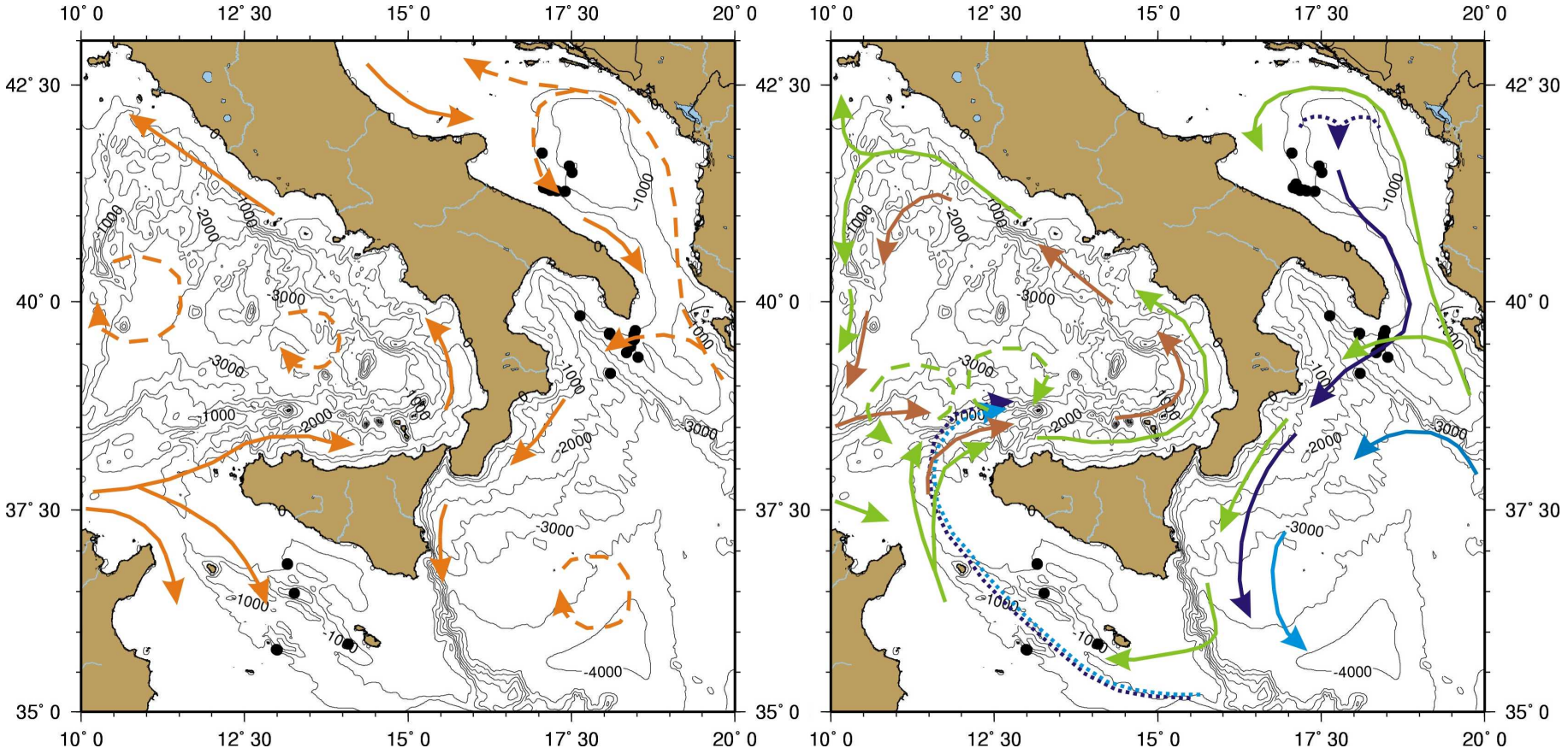

Figure 1.8: Water masses and circulation in the central Mediterranean Sea. On the left hand, orange arrows show the surface water circulation of (modified) Atlantic Water. Continuous lines indicate main paths, whereas dashed lines indicate mesoscale (seasonal) currents. On the right hand, green arrows = Levantine Intermediate Water, violet arrows = Adriatic Deep Water, blue arrows = Aegean Deep Water, brown arrows = Tyrrhenian Dense Water. Black circles represent sampling locations. Dense Water formation mainly takes place in the Adriatic, forming AdDW (compiled after Millot (1999), Astraldi et al. (2002b), and Millot & Taupier-Letage (2005)).

the northern Atlantic Ocean. About 90% of the AW inflow at Gibraltar is transformed into intermediate and deep waters, among which ca. 3/4 are formed in the eastern basin and which exhibit average residence times of 50–100 years (MILLOT & TAUPIER-LETAGE, 2005).

Detailed reviews of the circulation in both the western and eastern basin have been published (e.g. MILLOT, 1999; HAMAD ET AL., 2005).

Water masses of importance within the central Mediterranean are: **Levantine Intermediate Water (LIW)**, **Aegean Deep Water (AeDW)**, **Adriatic Deep Water (AdDW)**, and **Tyrrhenian Dense Water (TDW)** (Fig. 1.8).

LIW is the warmest and saltiest water mass of the Mediterranean sea with the largest volume. Tracked below AW in mainly 100–500 m water depth, LIW forms mainly in the northern Levantine, then flows westwards along the northern continental slopes of both basins and is involved in the offshore formation of all Mediterranean Deep Waters (Fig. 1.8). In the southern Aegean Sea, LIW mixes with AW to form AeDW during winter. Continuing to circulate in the Ionian Sea, part of LIW penetrates into the southern Adriatic Sea, where it mixes in winter with AW to form AdDW. The remainder flows alongslope into the Strait of Sicily, where most of it flows out into the Tyrrhenian Sea, circulating at 200–600 m depth. Finally the water masses either flow out through the Strait of Gibraltar or bypass it and progress eastward alongslope off Africa. Because LIW is involved in winter processes, it is expected to display everywhere an increasingly complex seasonal variability (MILLOT & TAUPIER-LETAGE, 2005). After MILLOT (1999) LIW has typical values of T = 13.2–14.0°C and S = 38.5–38.7, what is more or less confirmed by ASTRALDI ET AL. (2002a) for the central Mediterranean (Θ = 13.5–14.4°C, S = 38.55–38.76).

AeDW and AdDW have similar densities, whereas AeDW is saltier and warmer than the latter. Before outflowing through various openings and filling the eastern basin, both deep waters accumulate in the deep troughs in depths of 1000–1500 m (MILLOT & TAUPIER-LETAGE, 2005). Due to the Coriolis effect they circulate alongslope below the LIW mean level, describing a counterclockwise basin-wide gyre (MILLOT & TAUPIER-LETAGE, 2005). It was found that the hydrological characteristics of the densest bottom waters in the eastern basin vary interannually (LACOMBE ET AL., 1985), while the less dense part must flow out through the Strait of Sicily into the western basin. This outflow, which occurs mainly on the Tunisian side in the deeper part of the Strait, is denser than the water residing in the Tyrrhenian. Hence the bottom waters mix with Tyrrhenian waters and form TDW which then circulates within the western basin (MILLOT & TAUPIER-LETAGE, 2005). TDW is reported to have values of Θ = 13.1–13.2°C and S = 38.50–38.56 within the central Mediterranean (ASTRALDI ET AL., 2002a).

The cold-water coral habitats encountered during M70/1-cruise occur in different depth windows, but the environmental parameters were found to be relatively constant (Tab. 1.2). Within the Strait of Sicily reef-building *L. pertusa* and *M. oculata* thrive in waters influenced by LIW and eastern Mediterranean deep waters, while AdDW prevails at the SML-reefs, and at BC the reefs occur at the mixing depth of LIW and AdDW (Freiwald & Shipboard Scientific Party, 2006).

Table 1.2: Environmental parameters of investigated living reef-building coral habitats in the central Mediterranean Sea (from Freiwald & Shipboard Scientific Party (2006)).

Area	**Strait of Sicily**	**SML**	**BC**	**Overall**
Z [m]	450–800	560–750	315–650	315–800
T [°C]	13.7–13.9	13.5–13.8	13.4–13.7	13.4–13.9
S	38.68–38.72	38.65–38.67	38.62–38.66	38.62–38.72
O_2 [ml/l]	3.75–3.84	3.98–4.54	4.24–4.54	3.75–4.54
σ_t [kg/m^3]	29.08–29.11	29.07–29.12	29.07–29.13	29.07–29.13
pH	8.19–8.22	8.20–8.23	8.17–8.21	8.17–8.23

2 Methodology

2.1 Sampling and Sample Preparation

Apart from the two fossil coral samples (CORSARO, SETE-06), sample material includes four recent cold-water coral specimens of species *Lophelia pertusa* (M70/1). In addition box corer samples (M70/1), water samples (M70/1, P325, AL275), and CTD (**C**onductivity, **T**emperature, **D**epth) datasets (M70/1) were included. An overview of the sampling locations is given in the appendix (Tab. A.1). Sampling and sample preparation procedures are described below.

2.1.1 Coral Samples

Recent corals were collected during M70/1-cruise using the remotely operated vehicle (ROV) "QUEST 4000m", which is operated by MARUM, Center for Marine Environmental Sciences at the University of Bremen, Germany.

All coral samples were investigated for the distribution of the major elements Ca, Mg, Sr, and S within the coralline aragonite. In addition, stable carbon (δ^{13}C)[1] and stable oxygen (δ^{18}O)[2] isotope analyses performed in 2007 by Matthias López Correa (GZN-IPAL, Erlangen) were evaluated.

A list of the coral samples is given in the appendix (Tab. A.2).

Longitudinal sections of the coral samples used were embedded in epoxy prior to this study from which they were cut out using a dremel (Proxxon Micromot 40/E). After that they were reembedded in 2 cm long rigid PVC tubes, 1" in diameter, using epoxy resin and hardener (Buehler EpoThin). Subsequently samples were

1 The δ-notation reports the fractionation between the stable isotopes ^{13}C and ^{12}C within a sample compared to that within a standard material, reported in parts per thousand (‰):

$$\delta^{13}C = \frac{(^{13}C/^{12}C)_{sample} - (^{13}C/^{12}C)_{standard}}{(^{13}C/^{12}C)_{standard}} \times 1000$$

2 Analogous to the calculation of carbon isotope ratios δ^{18}O reports the fractionation between stable isotopes ^{18}O and ^{16}O.

polished to provide an even surface for electron-probe microanalyses (EPMA). This was accomplished using three different alumina suspensions (6 μm Ø, 1 μm Ø, 0.05 μm Ø, in that order) for approximately 10 minutes each on a grinding disc (Buehler Ecomet 4). Finally the surface was coated with carbon vapor.

2.1.2 Box Corer Samples (GKG)

During M70/1-cruise a box corer (GKG) with a box size of 50×50 cm and 50 cm height was used for the sampling of undisturbed surface sediments. 8 of 10 box-cores were successful and recovered an average of 40 cm sediment (Freiwald & Shipboard Scientific Party, 2006). Subsamples of the uppermost 1 cm of the sediment column, 8×8 cm in size were taken for benthic foraminifera studies, stained with rose bengal and stored at 4°C.

Five of these samples, their sampling locations being in the vicinity of the coral sampling locations, were chosen for stable isotope analysis of living foraminifera. The samples are listed in Tab. A.3. Stable isotope analysis was performed on five specimens of the two epibenthic species *Cibicidoides wuellerstorfi* and *Cibicides kullenbergi* taken from the >250–500 μm fraction.

2.1.3 Water Samples

Water was sampled during all three research cruises. During M70/1-cruise samples were taken within the water column and 10 m above seafloor with water sampler bottles (Niskin-type, 10 l) mounted on a rosette housing. Sampling during cruises P325 and AL275 was identical except for sampling seawater 13 to 15 m above seafloor.

At coral sampling locations, water samples were taken using a Niskin bottle attached to the ROV, or, in case of AL275-cruise, with a 5 l Niskin bottle attached to submersible JAGO (IFM-GEOMAR, Kiel, Germany). Tab. A.4 gives an overview of all water samples analyzed in this study.

Samples were filled on board into 125 ml glass bottles, poisened with 200 μl of saturated mercury chloride ($HgCl_2$) to prevent further degradation or oxidation, and sealed for stable isotope analysis ($\delta^{18}O_{sw}$). For major and trace element analyses, samples were filtered (0.2 μm), filled into 20 ml plastic vials and acidified with 200 μl of concentrated nitric acid (65% HNO_3) to prevent oxidation.

2.1.4 CTD Data Acquisition

On research cruise M70/1 a SeaBird Electronics (model 911 plus type) CTD system was used to measure oceanographic parameters (conductivity, temperature, pressure, dissolved oxygen, sound velocity) at 36 stations. The CTD stopped approximately 10 m above seafloor (bottom alarm) and then returned to the surface. Data were recorded continuously but were averaged per meter depth. Only the "downcast"-datasets of conductivity (salinity), temperature, and pressure (depth) measurements were used for evaluation.

Another CTD sensor was installed on the ROV for **direct measurements at sampling locations**. Salinity calculated from conductivity recorded with this device showed a constant offset of 0.31 (1σ=0.01) to the rosette-CTD values. Therefore salinity values from the ROV-CTD were corrected by adding this offset to the original value.

2.2 Methods

2.2.1 Electron-Probe Microanalysis (EPMA)

Coral aragonite was investigated for the distribution of major elements using the Jeol JXA-8200 EPMA (Electron Probe Microanalyzer) at IFM-GEOMAR, Kiel. X-ray detection took place using the device's wavelength dispersive X-ray spectrometer (WDS).

Element mappings were performed on an area of approximately 2 mm^2 within the longitudinal sections from the inside to the outside of the thecal wall. A resolution of 3×3 μm was used to determine the distribution of the elements Ca, Mg, Sr, S and P. Measurement was carried out with an acceleration voltage of 15 kV, 200 ms dwell time, a beam current of 50 nA, and a beam diameter of 1 μm. The spectrometer configuration is listed in Tab. 2.1.

Table 2.1: EPMA-configuration of the wavelength dispersive X-ray spectrometer system for element mappings.

Element	Crystal	Spectral Position [nm]
Ca	TAPH	107.687
Mg	PETH	172.131
Sr	PETJ	107.563
S	TAP	75.140
P	PETH	197.088

Quantitative measurements were carried out as discrete profile measurements within the previously mapped area to later calibrate the element mappings. An acceleration voltage of 15 kV, a beam current of 10 nA and a beam diameter of 10 μm were set. A sampling interval of 20 μm across the thecal wall was chosen, starting at the outer rim. The element mappings showed that concentrations of phosphorus were within the limits of detection (LOD), so manganese was tested instead, but the results showed that Mn-concentrations were also within LOD. Smithsonian microbeam standards (Jarosewich, 2002) were used as reference. Peak and background counting times as well as used standards are listed in Tab. 2.2.

A comparison between the measurements conducted on the microbeam standards and published data yields good deviations of ca. 1% for calcium- and magnesium-concentrations and moderate deviations of ca. 5% for the concentrations of sulfur (Tab. A.5).

Problems occurred with the chosen EPMA-configuration for the determination of strontium-concentrations. The reason for this is the general problem, that no mi-

Table 2.2: EPMA-configuration for quantitative measurements.

Element	Standard	Crystal	Peak Cnt. Time [s]	BG Cnt. Time [s]
C	Calcite	LDE1H	10	20
Ca	Calcite	PETJ	10	20
Mg	VG-2	TAP	10	20
Mn	VG-2	PETJ	15	30
S	VG-2	PETH	20	40
Sr	KAN-1	TAP	30	60

crobeam standards are available for carbonate materials, which can be used to determine Sr-concentrations. The common procedure for Sr-determination using EPMA is the calibration against the KAN-1-standard, a feldspar mineral (anorthoclase) containing also a great amount of silicon. Spectral positions for silicon and strontium are too close to precisely measure Sr within minerals like carbonates containing no silicon. In this case carbonate samples had too low Sr-concentrations by a factor of 2.

Results were calculated as wt.% of the corresponding oxides. Outlying data have been corrected for further processing, although mean total oxid masses were always > 95 wt.%. Variations in the total oxid masses are mainly due to carbon being vaporized from the sample surface by the electron beam, which normally does not influence measurement of the other elements. However, this was further controlled by means of the precision of the CaO-results. Thus, data were classified as outlying and removed from the dataset when the CaO-results were not within the interval of 51–55 wt.%, as was the case for 10 out of 676 quantitative measurements.

To obtain molar element ratios, first oxid masses of the elements were normalized to the total oxid masses and then converted into mol% (Eq. 2.1). They could then simply be calculated as fractions of element-mol% relative to calcium and are given in units of mmol/mol.

$$Oxid_i[mol\%] = \left(\frac{\left(\frac{Oxid_i[wt.\%]}{M(Oxid_i[g/mol]) \cdot \sum^i Oxid_i[wt.\%]} \right)}{\sum^i \left(\frac{Oxid_i[wt.\%]}{M(Oxid_i[g/mol]) \cdot \sum^i Oxid_i[wt.\%]} \right)} \right) \times 100 \tag{2.1}$$

Correcting Inaccurate Determinations of Strontium

Sr-concentrations were determined on the basis of an internal carbonate standard using the same measurement configuration as for the coral samples. The standard material, a carbonate powder (A-2 modern coral standard, provided by H. Elderfield, Univ. Cambridge) containing crystals > 500 μm in diameter, was pressed,

embedded with epoxy and polished. EPMA-measurements were conducted on the visible crystals only. Concentrations of strontium within this material have been determined by OHDE ET AL. (1978) using neutron activation analysis.

Because EPMA-analysis provided high-precision values for SrO (2.7%RSD, N = 19) with a deviation of -54% of the Sr-concentration to the published value, a correction factor of

$$F = 2.19 \pm 0.06$$

could have been calculated. This factor was then used to correct the quantitative measurements for Sr conducted on the cold-water coral samples. Results are in accordance with LA-ICP-MS measurements carried out by Paolo Montagna (ICRAM, Rome, Italy) at ANU-RSES, Canberra, Australia, in 2007 on the same coral samples.

Processing of EPMA-Data

To generate high-resolution profiles of molar Mg/Ca-, Sr/Ca-, and S/Ca-ratios, the element mappings were further processed. For each sample three parallel profiles, 50 μm apart from each other, were laid on the mappings at the location of the quantitative measurements, roughly perpendicular to the coral's growth banding, applying the EPMA-software. Measured intensities of the elements Ca, Mg, Sr, and S along the profiles were then converted into concentrations. This was accomplished using a linear fit between the minimum, maximum, and mean values of the measured intensities (mappings) and the measured concentrations (quantitative measurements). Molar element ratios were then calculated as fractions of the element concentrations and finally an average of the three profiles was generated. To eliminate the noise in the data, which reflect a sampling interval of 3 μm, a 10 point-smoothing (10pt) was applied to the calculated ratios, thus averaging the data over a distance of 27 μm.

To find periodicities eventually hidden within the high-resolution profiles of the molar element ratios, spectral analysis was performed. Therefore the Blackman-Tukey method (BLACKMAN & TUKEY, 1958) was applied to the unsmoothed average profiles using the program "Analyseries" (V.2.0.4.2). Results are given as power spectra over units of length.

2.2.2 ICP-MS

Water samples were analyzed for trace element concentrations using an Agilent 7500cs Quadrupol ICP-MS at the Institut für Geowissenschaften (IfG), Universität

Kiel. Measured elements were ^{7}Li, ^{85}Rb, ^{86}Sr, ^{98}Mo, ^{121}Sb, ^{133}Cs, ^{138}Ba, and ^{238}U. The experimental set-up consisted of a pneumatic nebulizer, an Ar-plasma, an interface made of Ni-Ce-cones, and a collision cell working in He-mode. Analysis included 3 replicate measurements per sample.

12 water samples representing different water depths in low saline North Atlantic and high saline Mediterranean waters were analyzed. Sample preparation included an adding of 9200 μl of diluted HNO_3 (2%) to 800 μl of the original sample, resulting in a dilution of 1:12.5, as well as an addition of an internal standard (BIR[3]).

In order to assess analytical accuracy and precision, blanks, a IAPSO seawater standard, and one duplicate sample were measured. Blanks are made of ultrapure water (ELGA, 18.2 MΩ/cm), acidified with 200 μl of HNO_3 (2%). Results for analytical assessment show a contamination of the used IAPSO with barium, moderate to poor (4–10%) accuracy and good to moderate (0.5–5%) precision of the measurements (Tab. A.6, A.7).

2.2.3 ICP-OES

Determination of major and trace element concentrations within the water samples was performed using an Spectro Ciros CCD SOP ICP-OES at the Institut für Geowissenschaften, Universität Kiel. The determination of Ca, Mg, Sr, B, and Ba, included 5 replicate measurements per sample.

Sample preparation of 45 analyzed water samples included a 1:50 dilution of 200 μl of the original sample with 9800 μl of diluted HNO_3 (2%).

Calibration of the measured intensities (counting rates) into element concentrations had to be done manually. This was accomplished by calculating calibration factors from the measurements of 3 calibration standards.

Blanks, a IAPSO seawater standard, and five duplicate samples were measured to evaluate analytical assessment. As for the ICP-MS, results show a contamination of the used IAPSO seawater standard with barium. Accuracy for calcium is excellent (0.02%), whereas accuracy for magnesium and strontium is moderate (3–4%), and poor for boron (17%). The precision of the measurements lies between 1 and 6%, except for barium with an insufficient precision of up to 116% (Tab. A.8, A.9).

The calculation of molar element ratios is based on element concentrations. Here, accuracy for Mg/Ca and Sr/Ca is moderate (3%), and poor for B/Ca (18%). Precision for Mg/Ca and Sr/Ca is excellent (<0.53%), good to moderate for B/Ca

3 **B**eryllium **I**ndium **R**henium

(<4%) and insufficient for Ba/Ca with up to 70% RSD. Therefore results for molar Ba/Ca-ratios were not evaluated (Tab. A.10, A.11).

2.2.4 U/Th-Dating

Dating of fossil corals was carried out by Malcolm McCulloch (ANU-RSES, Research School of Earth Sciences, The Australian National University, Canberra, Australia) in 2006/07 using the U/Th-method.

The method is well described in the literature (e.g. Edwards et al., 1987; Cobb et al., 2003; Turekian & Bacon, 2003) and provides reliable ^{230}Th-ages for deep-sea corals (Adkins et al., 1998; Cheng et al., 2000). As carbonates accumulate (i) from seawater that is essentially free of ^{230}Th, and (ii) without a large degree of fractionation of thorium from uranium, it is based on radioactive incorporation of ^{230}Th into the coral skeleton over time toward secular equilibrium with ^{238}U and ^{234}U. Ages can be calculated from radiogenic ^{230}Th, ^{234}U, and ^{238}U activities, if the coral remains a closed system with respect to U and Th. With current measurement techniques this method yields accurately determinable ages as great as 550 ka (Turekian & Bacon, 2003).

2.3 Paleotemperature Reconstructions

2.3.1 Sr/Ca-Ratios

Seawater temperature and strontium content of both inorganically precipitated and coral aragonite show an inverse relationship (Lea, 2003). Consequently there have been several attempts to develop paleotemperature equations based on coral Sr/Ca and seawater temperature. However, Sr/Ca-ratios in coral aragonite are known to be influenced by (i) growth rate and symbiont activity (e.g. de Villiers et al., 1994; Cohen et al., 2001; Cohen et al., 2002), and (ii) secular shifts in seawater Sr/Ca on glacial–interglacial timescales (e.g. Stoll & Schrag, 1998). Following Cohen et al. (2002) the main influence on the slope and therefore the temperature sensitivity of these linear equations might be due to algal symbionts.

Most calibrations are available for zooxanthellate coral species *Porites* (e.g. de Villiers et al., 1994; Gagan et al., 1998; Sinclair et al., 1998; Cohen et al., 2001; Cohen et al., 2002), while there are only few calibrations for inorganically precipitated aragonite (Kinsman & Holland, 1969; Cohen et al., 2006) or cold-water coral species (Cohen et al., 2002; Cohen et al., 2006).

In this study the Sr/Ca-temperature relationship from Cohen et al. (2006) for cold-water coral species *Lophelia pertusa* was used:

$$Sr/Ca[mmol/mol] = -0.18 \times T[^{\circ}C] + 11.44 \tag{2.2}$$

The slope in Eq. 2.2 represents the temperature-sensitivity estimated for Sr/Ca-variations in *Lophelia pertusa*. Dividing the residual Sr/Ca of the mean Sr/Ca by this slope thus results in a temperature anomaly.

2.3.2 "Lines Technique"

If a δ^{13}C vs. δ^{18}O regression line from an individual coral could be generated, the oxygen isotope ratio ($\delta^{18}O_i$) corresponding to the carbon isotope ratio of dissolved inorganic carbon ($\delta^{13}C_{DIC}$) and corrected for the oxygen isotope ratio of seawater ($\delta^{18}O_{sw}$) is a linear function of temperature (Smith et al., 2000):

$$T[^{\circ}C] = \frac{\delta^{18}O_i - \delta^{18}O_{sw} - 4.97}{-0.25} \tag{2.3}$$

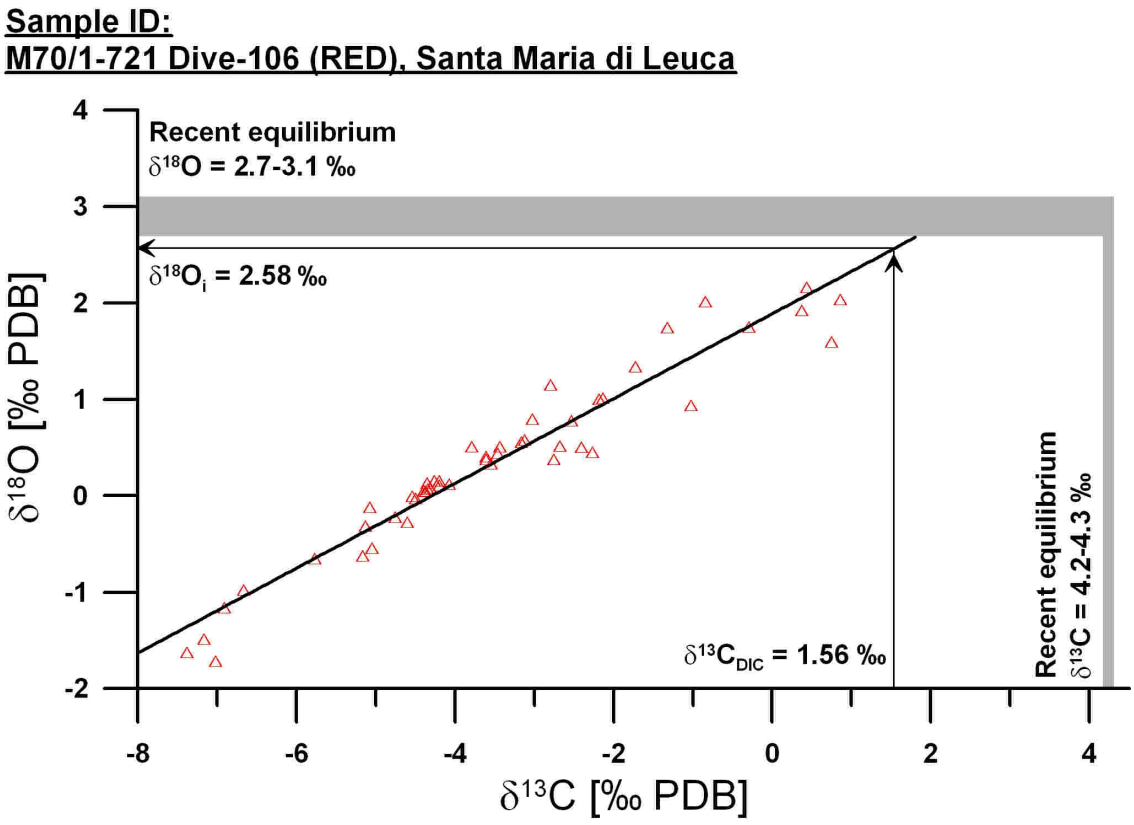

Figure 2.1: Principle of the "lines technique"-method: First a δ^{13}C vs. δ^{18}O regression line for sample M70/1-721 Dive-106 (RED) is generated. Then the $\delta^{18}O_i$ value, corresponding to $\delta^{13}C_{DIC}$ is retrieved. This value is assumed to be equal or close to the δ^{18}O value of isotopic equilibrium with seawater, and, corrected for $\delta^{18}O_{sw}$, is a linear function of temperature (Smith et al., 2000; Lutringer et al., 2005).

The principle of this method, also known as the "lines technique", of how to retrieve the $\delta^{18}O_i$ value from the regression line is illustrated in Fig. 2.1.

Coral δ^{13}C, coral δ^{18}O and $\delta^{13}C_{DIC}$ are reported against the PDB[4] standard, while the δ^{18}O value of the ambient water is reported against the SMOW[5] seawater standard. Annual average $\delta^{18}O_{sw}$ can be retrieved from the NASA-GISS global seawater oxygen-18 database (Schmidt et al., 1999).

If the isotopic composition of the seawater is not known as is the case for the fossil coral specimens, Smith et al. (2000) give the following equation, assuming that $\delta^{13}C_{DIC}$=$\delta^{18}O_{sw}$=0:

$$T[^{\circ}C] = \frac{\delta^{18}O_i - 4.51}{-0.22} \tag{2.4}$$

4 A carbonate standard material, referring to a belemnite from the Peedee Formation of South Carolina, USA (e.g. Coplen et al., 1983).

5 **S**tandard **M**ean **O**cean **W**ater

$\delta^{18}O_i$ is assumed to be equal to the $\delta^{18}O$-value of isotopic equilibrium (IE) with seawater. Recent isotopic equilibria for oxygen ($\delta^{18}O_{IE}$) in skeletal aragonite can be calculated using the temperature-fractionation relationship of BÖHM ET AL. (2000), who worked on the Caribbean coralline sponge *Ceratoporella nicholsoni*, that precipitates close to oxygen isotopic equilibrium:

$$\delta^{18}O_{IE} = \delta^{18}O_{ar} = \frac{20.0 - T_{ann.mean}[^{\circ}C]}{4.42} + \delta^{18}O_{sw} \tag{2.5}$$

Here, $\delta^{18}O_{ar}$ is the $\delta^{18}O$ value of the aragonite sample versus PDB, and T is the annual mean temperature, which can be retrieved from the eWOCE oceanographic atlas (http://www.ewoce.org/).

The calculation of carbon isotopic equilibrium with seawater ($\delta^{13}C_{IE}$) followed the result of ROMANEK ET AL. (1992), where aragonite-HCO_3^- fractionation is independent of temperature and the enrichment factor for aragonite averages 2.7‰ PDB:

$$\delta^{13}C_{IE} = \delta^{13}C_{DIC} + 2.7‰ \tag{2.6}$$

Oceanographic data to calculate paleotemperatures at coral sampling locations using the equations from SMITH ET AL. (2000) are listed in Tab. 2.3. In this table all $\delta^{18}O_{sw}$ are taken from STENNI ET AL. (1995), except for the Urania Bank location, which is taken from PIERRE ET AL. (1986). The values are close to that of the analyzed water samples collected directly at the coral sampling locations, which were used in the calculations. However, no water samples were directly collected at the Urania Bank coral sampling location. Consequently the $\delta^{18}O_{sw}$ value in Tab. 2.3 is that of water sample M70/1-678 (620 m) sampled within the immediate vicinity and within the same depth interval as the coral specimen.

In Tab. 2.3 $\delta^{13}C_{DIC}$ is the $\delta^{13}C$ value of the epibenthic foraminifera *C. wuellerstorfi* from the box corer samples. GKG sample M70/1-712-1 was assumed to best represent the $\delta^{13}C_{DIC}$ at the coral sampling locations in the Bari Canyon, Gondola Slide, and Santa Maria di Leuca Reef Province (recent coral specimens), while the $\delta^{13}C_{DIC}$ at the location of sample CR-22L (12.4 ka) is reflected by GKG sample M70/1-710-2. The stable carbon isotope value for DIC at the Urania Bank sampling location is mirrored by GKG sample M70/1-668-2 (Tab. 2.3, Tab. A.14).

Annual mean temperatures used in the calculations are from the eWOCE oceanographic atlas, that are also close to the observed temperatures during M70/1 cruise (Tab. 2.3).

Table 2.3: Recent oceanographic data and isotopic equilibria for aragonite at coral sampling locations.

Location	$\delta^{18}\mathbf{O}_{sw}$ **[‰ SMOW]**		$\delta^{13}\mathbf{C}_{DIC}$	$\mathbf{T}_{ann.mean}$ **[°C]**	
	NASA	**M70/1**	**[‰ PDB]**	**eWOCE**	**M70/1**
SE06-13L	1.62	x	1.56	13.3	13.6
CR-22L	1.47	x	1.63	12.9	13.8
M70/1-721 Dive-106	1.42	1.39	1.56	13.5	13.6
M70/1-752 Dive-111	1.51	1.40	1.56	13.3	13.5
M70/1-677 Dive-100	1.65	1.26	1.54	13.7	14.0

Location	$\delta^{18}\mathbf{O}_{IE}$ **[‰ PDB]**[a]	$\delta^{13}\mathbf{C}_{IE}$ **[‰ PDB]**[b]
SE06-13L	3.14	4.26
CR-22L	3.07	4.33
M70/1-721 Dive-106	2.86	4.26
M70/1-752 Dive-111	2.92	4.26
M70/1-677 Dive-100	2.69	4.24

a calculated after Böhm et al. (2000)
b calculated after Romanek et al. (1992)

3 Results

3.1 Dating Results

U/Th-dating resulted in ages of 17550±56 calendar years before 1950 (denoted by cal. yr BP, or 17.6 ka) for coral sample SE06-13L collected in the Bari Canyon, and of 12435±76 cal. yr BP (12.4 ka) for coral sample CR-22L originating from the Santa Maria di Leuca Reef Province. Fossil coral samples therefore lived in times of the late glacial period and the Younger Dryas cold interval.

3.2 Distributions of Elements and Isotopes in Coral Aragonite

3.2.1 Element Mappings

Element mappings were carried out to investigate the distribution of major elements within the coralline aragonite in order to (i) find suitable locations for quantitative measurements and (ii) to generate high-resolution profiles of molar element ratios.

For each coral sample the figures showing the mappings of the elements Mg, Ca, S, and Sr are given in the appendix.

In sample SE06-13L (17.6 ka) magnesium-concentrations vary between 0.059 mol% and 0.371 mol%, with a mean of 0.123 mol% (Tab. 3.1). Magnesium content increases with increasing distance from the outer rim and shows a maximum in the upper right corner of the mapping (Fig. A.1). Here a lineation of bright white carbonate crosses the mapping area. Optical dense (opaque) banding structures, difficult to identify in photographs or by optical microscope is indicated in the mapping by slightly higher Mg-concentrations. Calcium shows concentrations of 45.8–51.6 mol% ($\bar{\mu}$=49.6 mol%), with increasing values towards the outer rim. Structures like the opaque bandings cannot be clearly identified, but areas characterized by lower Ca-concentrations to a small degree reflect areas of higher Mg-concentrations. Concentrations of sulfur (0.220–0.319 mol%; $\bar{\mu}$=0.269 mol%) and strontium (0.464–0.580 mol%; $\bar{\mu}$=0.515 mol%) are more homogeneously distributed, but the content

of sulfur is slightly decreasing towards the outer rim. While strontium shows a maximum in the lower right corner of the mapping, sulfur-concentrations are minimal at the same location. Variations within the concentration of both elements indicating other structures are not clearly visible, but areas of higher S and Sr content reflect areas of higher Mg content.

Table 3.1: Average concentrations of Mg, Ca, S, and Sr as determined by the quantitative measurements of the coral specimens.

Sample ID	**N**	**Mg** [mol%]	**Ca** [mol%]	**S** [mol%]	**Sr** [mol%]
SE06-13L (17.6 ka)	145	0.123	49.6	0.269	0.515
CR-22L (12.4 ka)	101	0.132	49.0	0.265	0.484
M70/1-721 Dive-106 (RED)	143	0.161	49.3	0.314	0.490
M70/1-721 Dive-106 (WHITE)	92	0.145	49.8	0.300	0.488
M70/1-752 Dive-111	95	0.163	50.5	0.309	0.494
M70/1-677 Dive-100	90	0.149	49.7	0.306	0.497

Concentrations of Mg in sample CR-22L (12.4 ka) vary between 0.060 mol% and 0.212 mol% ($\bar{\mu}$=0.132 mol%) and are therefore on average higher than in sample SE06-13L (17.6 ka) (Tab. 3.1). Maximal Mg-concentrations are observed within the inner part of the theca, again along a line of bright white carbonate (Fig. A.2). Higher magnesium contents reflecting the opaque bands are more clearly visible here than in the previous sample. The pattern is also visible in the mapping of Ca, but in terms of lower instead of higher concentrations within the opaque bands. Variations lie between 45.3 mol% and 51.2 mol% ($\bar{\mu}$=49.0 mol%) and minima are observed at the outer rim as well as at the location of the bright white carbonate lineation to the outer right of the mapping. Sulfur contents (0.232–0.309 mol%; $\bar{\mu}$=0.265 mol%) also show a local maximum here and the banding pattern is indicated to a small degree with higher S-concentrations in the bandings. Anyway the distribution of S and Sr is again more homogeneously than that of Mg and Ca. Strontium-concentrations (0.431–0.523 mol%; $\bar{\mu}$=0.484 mol%) are lower than in sample SE06-13L (17.6 ka) and also show a maximum to the right of the mapping.

The aragonite skeleton of *Lophelia pertusa* in sample M70/1-721 Dive-106 (RED) shows homogeneously distributed concentrations of calcium (47.4–51.3 mol%; $\bar{\mu}$=49.3 mol%) and sulfur (0.243–0.346 mol%; $\bar{\mu}$=0.314 mol%) with extrema on the inner rim of the theca (Fig. A.3, Tab. 3.1). Thus, sulfur is more concentrated within this sample than in both fossil samples. High Ca-values are concentrated on the inner rim, while S is depleted. Mg-contents (0.047–0.230 mol%; $\bar{\mu}$=0.161 mol%) again reflect the opaque bands with increased concentrations within the bands. Overall Mg is higher concentrated than in the fossil specimens and minimum concentrations are observed on the inner rim. As calcium, strontium-concentrations (0.433–0.567 mol%; $\bar{\mu}$=0.490 mol%) show highest values on the inner rim and also an area roughly

500 μm apart from the outer rim has slightly higher concentrations. In this part of the skeleton also Mg has lower-than-average concentrations.

Sample M70/1-721 Dive-106 (WHITE) is characterized by Mg-concentrations of 0.052–0.244 mol% ($\bar{\mu}$=0.145 mol%), Ca-concentrations of 45.8–51.7 mol% ($\bar{\mu}$=49.8 mol%), S-concentrations of 0.205–0.342 mol% ($\bar{\mu}$=0.300 mol%), and Sr-concentrations of 0.420–0.534 mol% ($\bar{\mu}$=0.488 mol%) (Tab. 3.1). Contents of Mg and S are lowest at the inner rim, where Ca- and Sr-concentrations show a maximum (Fig. A.4). While sulfur is distributed homogeneously, magnesium, calcium and to a small extent also strontium reflect the opaque banding pattern. Mg-concentrations are higher within the bandings, whereas Ca and Sr show lower concentrations there. The shape of the banding pattern is unregularly curved.

Mg-concentrations in sample M70/1-752 Dive-111 are 0.163 mol% on average with a variation between 0.073–0.274 mol% (Tab. 3.1). Opaque banding is clearly reflected by increased Mg content (Fig. A.5). Apart from two areas in the vicinity of the inner rim with strong magnesium-concentrations, content of Mg is decreasing towards the outer rim, while a minimum is observed at the inner rim. This pattern is reflected in concentrations of sulfur (0.265–0.355 mol%; $\bar{\mu}$=0.309 mol%) and mirrored in concentrations of strontium (0.448–0.544 mol%; $\bar{\mu}$=0.494 mol%). Ca has concentrations of 48.6–52.0 mol% ($\bar{\mu}$=50.5 mol%) and runs parallel to the distribution pattern of Mg, with lowest values within the areas of the opaque banding and highest values at the inner rim.

In contrast to the other samples, mappings of sample M70/1-677 Dive-100 from the Urania Bank show more inhomogeneous distributions of S and Sr (Fig. A.6). While concentrations of sulfur vary between 0.252–0.347 mol% ($\bar{\mu}$=0.306 mol%) and that of strontium between 0.435–0.567 mol% ($\bar{\mu}$=0.497 mol%), their distribution pattern is directly opposite of each other. Sulfur contents increase toward the outer rim and are minimal in the vicinity of the inner rim where a narrow lineation with increased S content additionally crosses the mapping. As it is shown in the mapping of magnesium, which reflects the distribution pattern of sulfur, increased concentrations of Mg and S reflect the opaque banding of the coral. Mg-concentrations vary between 0.048–0.293 mol% with an average of 0.149 mol% (Tab. 3.1). Calcium on the other hand reflects the distribution pattern of strontium with concentrations varying between 47.6–51.1 mol% ($\bar{\mu}$=49.7 mol%).

Interestingly, in all samples the distribution patterns of calcium and strontium and of magnesium and sulfur are similar, while distribution patterns of magnesium and strontium seem to be opposite. This was quantitatively verified by performing correlation analyses of linear dependency between the element concentrations obtained

from the quantitative measurements. Tab. 3.2 summarizes the results of these analyses, giving the Pearson product-moment correlation coefficient (PMCC, denoted by r) with a confidence level of 95%.

Table 3.2: Results of correlation analyses (linear regression) of element concentrations obtained by the quantitative measurements of the coral specimens. Confidence level of r is 95%.

Sample ID	N	Ca vs. Sr	Mg vs. S	Mg vs. Sr
SE06-13L (17.6 ka)	145	0.221	0.508	0.482
CR-22L (12.4 ka)	101	0.448	0.418	0.088
M70/1-721 Dive-106 (RED)	143	0.410	0.341	-0.055
M70/1-721 Dive-106 (WHITE)	92	0.426	0.251	-0.212
M70/1-752 Dive-111	95	0.144	0.320	-0.235
M70/1-677 Dive-100	90	0.344	0.372	-0.635

3.2.2 High-Resolution Profiles of Molar Element Ratios

The profiles described in the following part reflect a high-resolution signal of molar Mg/Ca-, Sr/Ca-, and S/Ca-ratios from the outer rim to the internal of the coral theca, roughly perpendicular to the corals' opaque banding, which is best indicated by the mapping of magnesium-concentrations. A summary of the mean values and standard deviations (1σ) of the molar ratios observed within the coral specimens is given in Tab. 3.3.

Comparing averages and standard deviations of the ratios within the different samples give the following results: regarding Mg/Ca and S/Ca, averages are lower for the fossil than for the recent coral specimens, while the Sr/Ca-average is highest for the 17.6 kyr-old sample (Tab. 3.3). Standard deviations of Mg/Ca and Sr/Ca are also greater in the recent corals than in the fossil ones, whereas no trend can be observed for 1σ of S/Ca-ratios.

Table 3.3: Average values ($\bar{\mu}\pm1\sigma$) of Mg/Ca-, Sr/Ca-, and S/Ca-ratios as observed within the high-resolution profiles of the coral specimens.

Sample ID	N	Mg/Ca [mmol/mol]	Sr/Ca [mmol/mol]	S/Ca [mmol/mol]
SE06-13L (17.6 ka)	973	2.47±0.48	10.33±0.15	5.32±0.20
CR-22L (12.4 ka)	680	2.63±0.31	9.77±0.17	5.41±0.13
M70/1-721 Dive-106 (RED)	981	3.12±0.52	9.75±0.23	6.11±0.20
M70/1-721 Dive-106 (WHITE)	570	2.83±0.52	9.59±0.21	5.77±0.24
M70/1-752 Dive-111	635	3.30±0.67	9.77±0.18	6.19±0.20
M70/1-677 Dive-100	602	3.09±0.60	10.08±0.26	6.00±0.17

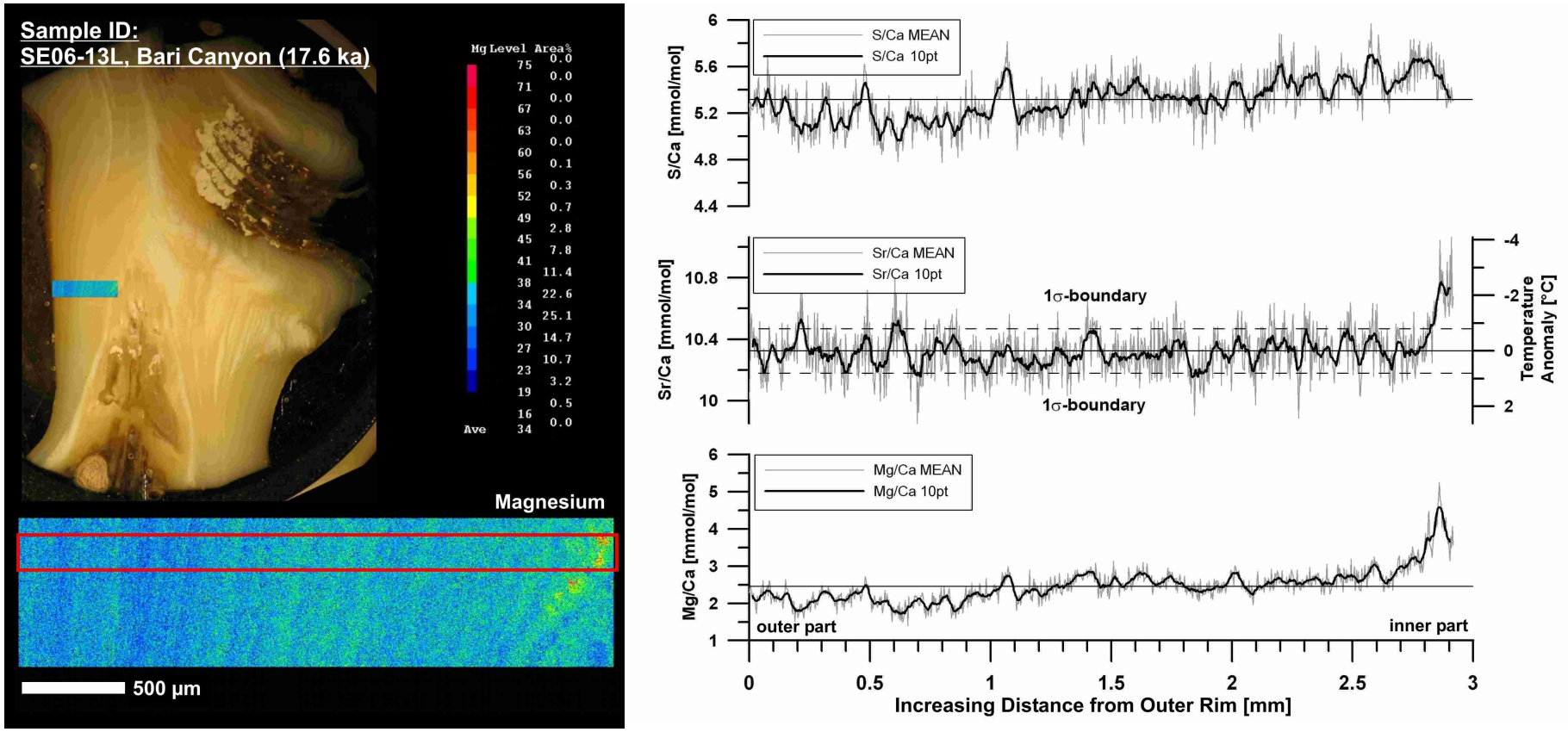

Figure 3.1: High-resolution element-ratio-profiles of sample SE06-13L (17.6 ka).

Fig. 3.1 shows the variation of molar ratios within sample SE06-13L (17.6 ka). Mg/Ca varies between 1.40–5.25 mmol/mol with an average of 2.47 mmol/mol (Tab. 3.3) and increases progressively towards the inner rim of the theca. The maximum of 5.25 mmol/mol is reached where the formerly described lineation of bright white carbonate crosses the mapping (Fig. 3.1). Sr/Ca varies less extensive than Mg/Ca between 9.85–11.06 mmol/mol ($\bar{\mu}$=10.33 mmol/mol). Although the maximum value is reached at the same location as for Mg/Ca, a general trend of increasing or decreasing values towards the inner rim cannot be observed. Rather the smoothed 10pt-curve (p. 23) reflects a cyclic variation of Sr/Ca-ratios about the average within the 1σ-boundaries of 0.15 mmol/mol. Like Mg/Ca-ratios, S/Ca-ratios show a trend of increasing values towards the inner rim. Variation lies between 4.78–5.97 mmol/mol with an average of 5.32 mmol/mol, but a single maximum clearly reflecting the carbonate lineation in the inner part of the skeleton, as observed for Mg/Ca and Sr/Ca, is not visible. A cyclic pattern of the S/Ca-curve is indicated, but not as clear as for the Sr/Ca-curve.

In sample CR-22L (12.4 ka) the average values are higher for Mg/Ca ($\bar{\mu}$=2.63 mmol/mol) and S/Ca ($\bar{\mu}$=5.41 mmol/mol) and lower for Sr/Ca ($\bar{\mu}$=9.77 mmol/mol) than in sample SE06-13L (Tab. 3.3). While variations of Mg/Ca lie between 1.72–3.60 mmol/mol, a general trend of variation within the carbonate is not as clear as in the previous sample. Local extrema reflect the opaque banding pattern visible in the Mg-mapping, most obviously on the inner rim, where the maximum is reached (Fig. 3.2). This is again not the case for Sr/Ca and S/Ca, which vary between 9.28–10.33 mmol/mol and 5.03–5.85 mmol/mol, respectively. Periodicity of the signals seems to be present in all ratio-profiles, but is most imminent for Sr/Ca with an almost stable variability of the 10pt-curve within 1σ-boundaries of $\pm$0.17 mmol/mol. For S/Ca the maximum is reached at the outer rim of the theca and a trend of increasing values towards this rim is indicated.

Both, Mg/Ca- and S/Ca-ratios in sample M70/1-721 Dive-106 (RED) are on average higher ($\bar{\mu}$=3.12 mmol/mol; $\bar{\mu}$=6.11 mmol/mol) than in the two fossil specimens (Tab. 3.3). The mean Sr/Ca-value ($\bar{\mu}$=9.75 mmol/mol) is smaller than that of sample SE06-13L (17.6 ka) but almost equal to that of sample CR-22L (12.4 ka). Mg/Ca varies between 1.12–4.41 mmol/mol, Sr/Ca between 9.18–10.57 mmol/mol, and S/Ca between 5.13–6.62 mmol/mol. Extrema are observed on the inner rim, with a maximum for Sr/Ca and minima for Mg/Ca and S/Ca (Fig. 3.3). The variability of the 10pt-Sr/Ca-curve lies within 1σ-boundaries of $\pm$0.23 mmol/mol. Again, Sr/Ca and S/Ca inhibit a cyclic pattern that is more clear for Sr/Ca and only weakly present for Mg/Ca.

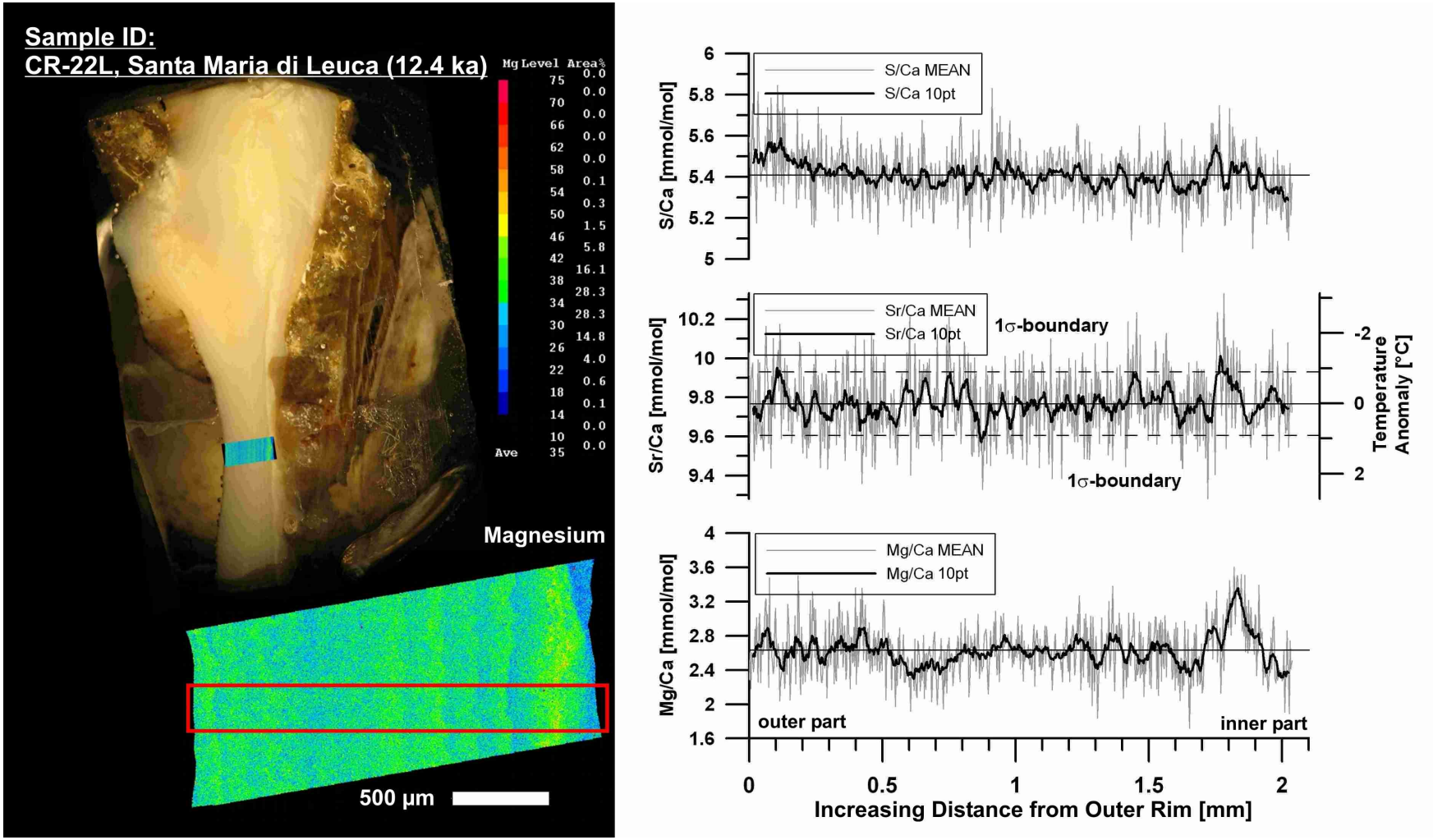

Figure 3.2: High-resolution element-ratio-profiles of sample CR-22L (12.4 ka).

In sample M70/1-721 Dive-106 (WHITE) Mg/Ca-ratios vary between 1.56–4.32 mmol/mol and are on average smaller ($\bar{\mu}$=2.83 mmol/mol) than in sample M70/1-721 Dive-106 (RED), but the average is still higher than in both fossil samples (Tab. 3.3). The same is the case for S/Ca-ratios that vary between 4.71–6.50 mmol/mol having an average around 5.77 mmol/mol. Sr/Ca lies between 8.97–10.39 mmol/mol with a mean value of $\bar{\mu}$=9.59±0.21 mmol/mol (1σ). As indicated in Fig. 3.4 the cyclicity for Sr/Ca- and S/Ca-ratios is not as imminent in the 10pt-curves as in the previous samples. Furthermore, Sr/Ca mirrors to a small degree the pattern of Mg/Ca, which clearly reflects visible skeletal structures as can be seen in the mapping of Mg-concentrations. Thus, Sr/Ca shows local maxima, where local minima for Mg/Ca are present. The opposite can be observed for S/Ca, where local maxima correspond to maxima in Mg/Ca, but within a smaller variability. However, general trends of higher or lower values towards any direction cannot be identified in any of the profiles.

Sample M70/1-752 Dive-111 from the Gondola Slide has Mg/Ca-ratios that vary between 1.64–4.96 mmol/mol ($\bar{\mu}$=3.30 mmol/mol), Sr/Ca-ratios between 9.26–10.39 mmol/mol ($\bar{\mu}$=9.77±0.18 mmol/mol, 1σ), and S/Ca-ratios between 5.47–6.81 mmol/mol ($\bar{\mu}$=6.19 mmol/mol) (Tab. 3.3). Fig. 3.5 shows highest values for Mg/Ca at the location of the two opaque bands visible in the Mg mapping. Within the approximately 0.9 mm wide area characterized by these bands, Sr/Ca and S/Ca also show stronger-than-average variations. Interestingly the maximum in Mg/Ca at a distance of about 1.3 mm from the outer rim corresponds to maxima of Sr/Ca and S/Ca, while the Mg/Ca maximum at a distance of about 1.6 mm from the outer rim corresponds to local minima in both Sr/Ca and S/Ca. Periodicities within the signal of all three ratio profiles can not be clearly identified at first glance.

Urania Bank sample M70/1-677 Dive-100 shows an average Sr/Ca value of 10.08 mmol/mol (±0.26 mmol/mol, 1σ) that lies between that of the recent coral specimens and that of sample SE06-13L (17.6 ka) (Tab. 3.3). However, Sr/Ca varies between 9.36–10.98 mmol/mol and its smoothed 10Pt-curve is characterized by a clear periodicity of the signal (Fig. 3.6). Mg/Ca lacks this periodicity in terms of a stable variation. The signal varies between 1.68–5.42 mmol/mol with an average of 3.09 mmol/mol. Highest values are observed at locations of opaque bands. Towards the inner rim ratios abruptly decrease at a distance of about 1.3 mm from the outer rim. At the same location a minimum is present in S/Ca-ratios, but no global extremum can be observed for Sr/Ca. S/Ca-ratios are increasing towards the outer rim from their minimum at 1.3 mm, varying between 5.49–6.45 mmol/mol ($\bar{\mu}$=6.00 mmol/mol). It might be of importance, that from 0.6–1.2 mm distance from the outer rim Sr/Ca-ratios drop below average and show less intense variation, while Mg/Ca-ratios are highest from 0.8–1.2 mm distance from the outer rim. Here,

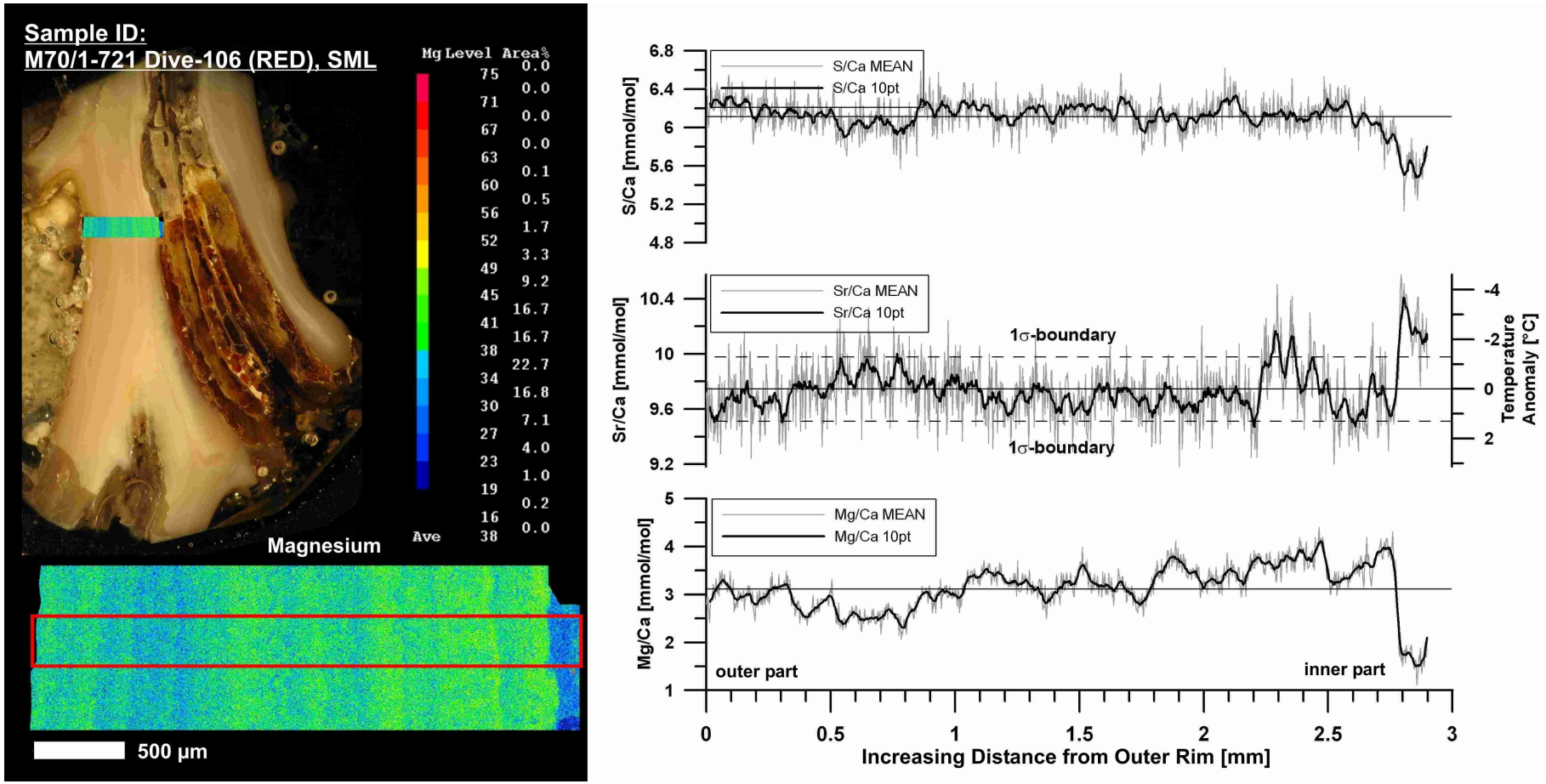

Figure 3.3: High-resolution element-ratio-profiles of sample M70/1-721 Dive-106 (RED).

S/Ca-ratios show no abnormal variations.

Results of linear correlation analyses between the obtained (unsmoothed) high-resolution profiles of molar ratios is given in Tab. 3.4. As for the correlation analyses of element concentrations (Tab. 3.2), the Pearson product-moment correlation coefficient is calculated with a confidence level of 95% and shows similar results.

Highest correlation coefficients are found for linear regressions between Mg/Ca and S/Ca, with positive values only, ranging from 0.076 to 0.594. r is also positive for correlations between Mg/Ca and Sr/Ca in fossil corals, but it is negative for recent specimens. Maximum positive values are found for fossil sample SE06-13L (17. 6 ka) (r=+0.305) and maximum negative values are present for both recent corals from the Santa Maria di Leuca Reef Province (r=-0.349, r=-0.347; Tab. 3.4). Except for sample M70/1-721 Dive-106 (RED) where r is negative (-0.244), correlation coefficients are positive for correlations between Sr/Ca and S/Ca in recent and fossil coral specimens, ranging from 0.032 to 0.207.

Table 3.4: Results of correlation analyses (linear regression) of molar element ratios from the high-resolution profiles of the coral specimens. Confidence level of r is 95%.

Sample ID	**N**	**Mg/Ca vs. Sr/Ca**	**Mg/Ca vs. S/Ca**	**Sr/Ca vs. S/Ca**
SE06-13L (17.6 ka)	973	0.305	0.594	0.135
CR-22L (12.4 ka)	680	0.028	0.076	0.107
M70/1-721 Dive-106 (RED)	981	-0.349	0.389	-0.244
M70/1-721 Dive-106 (WHITE)	570	-0.347	0.114	0.154
M70/1-752 Dive-111	635	-0.002	0.530	0.207
M70/1-677 Dive-100	602	-0.105	0.202	0.032

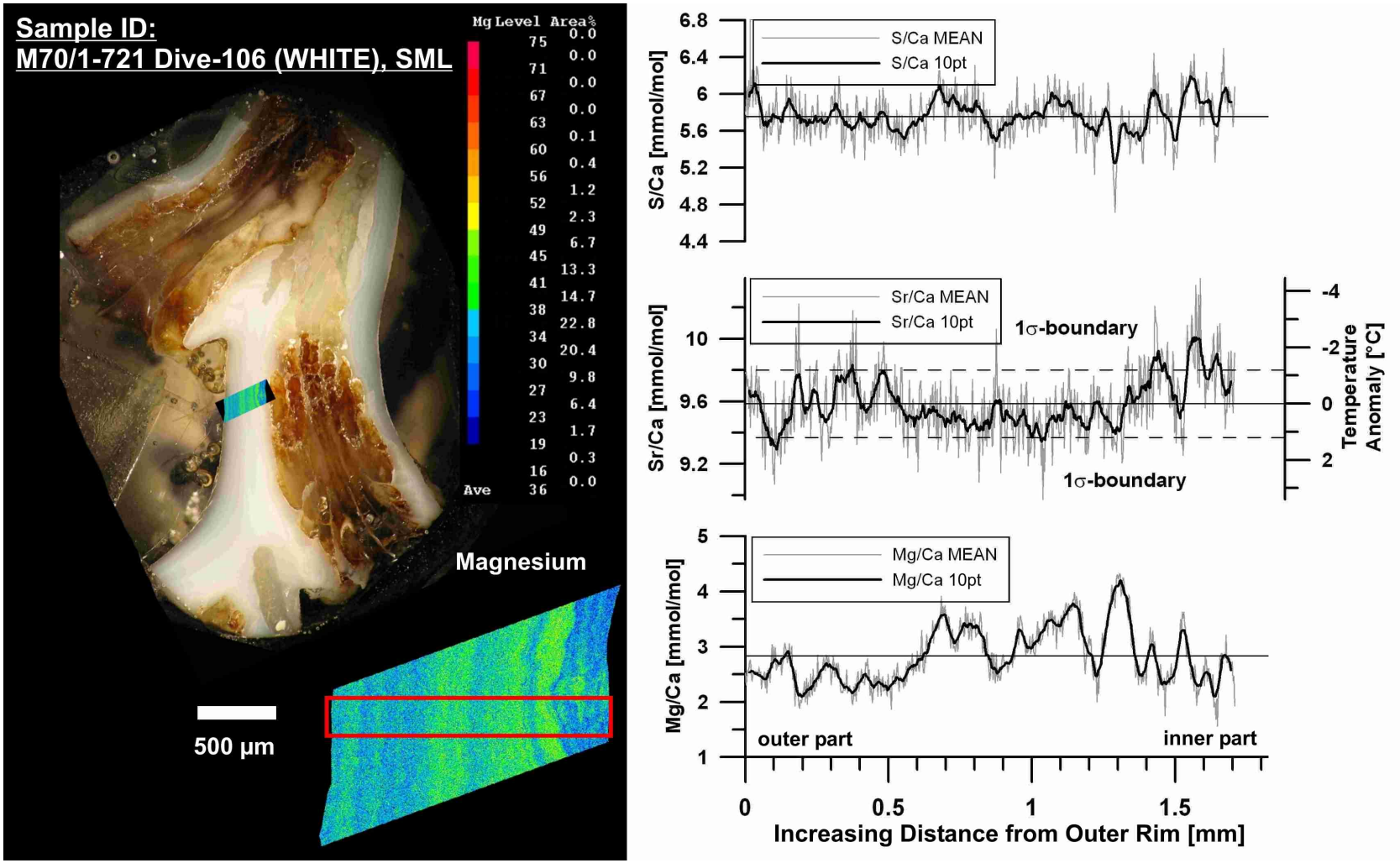

Figure 3.4: High-resolution element-ratio-profiles of sample M70/1-721 Dive-106 (WHITE).

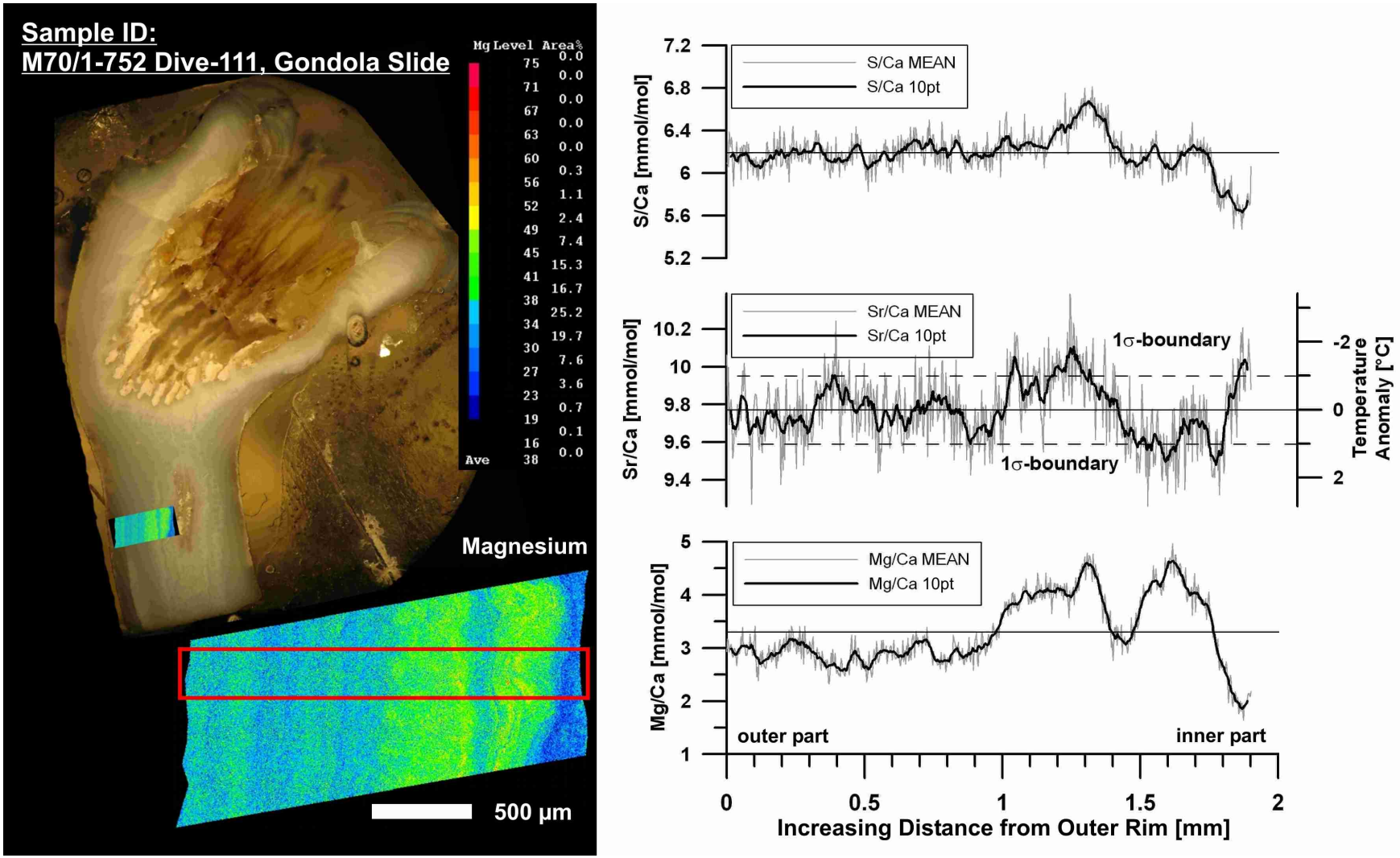

Figure 3.5: High-resolution element-ratio-profiles of sample M70/1-752 Dive-111.

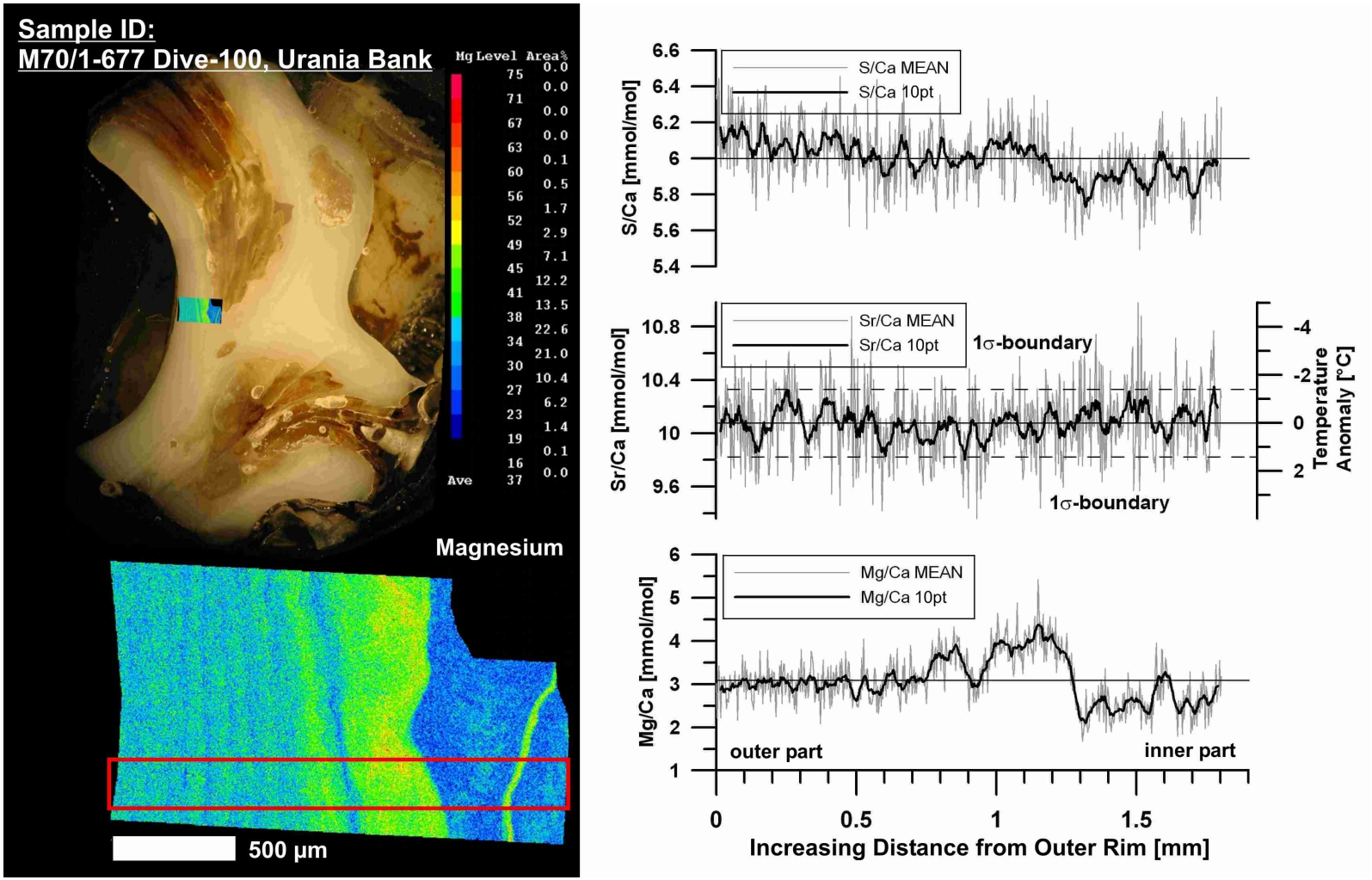

Figure 3.6: High-resolution element-ratio-profiles of sample M70/1-677 Dive-100.

3.2.3 Spectral Analysis

Within the high-resolution profiles of molar ratios a frequency interval of 0–25 mm^{-1} was investigated with a sample rate of 0.05 mm^{-1}, corresponding to a range of 0.040–20 mm. Only 7 of a total of 113 maxima in spectral power found within the profiles have a periodicity that is greater than 300 μm.

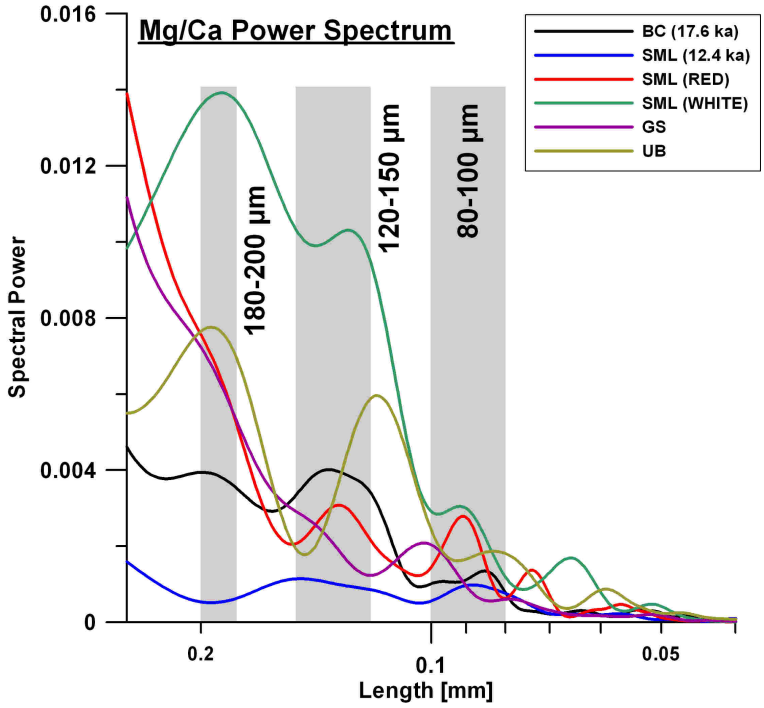

Figure 3.7: Spectral analysis of high-resolution Mg/Ca-ratio profiles.

The Blackman-Tukey power spectrum of the Mg/Ca-profiles of the analyzed coral specimens is shown in Fig. 3.7. Strongest maxima are found for sample M70/1-721 Dive-106 (WHITE) at 189 μm and 128 μm and for sample M70/1-677 Dive-100 at 194 μm and 118 μm. Weaker maxima are found at 92 μm and 66 μm for the white *L. pertusa* and at 83 μm for the specimen from the Urania Bank. At 200 μm an extremum is observed for fossil sample SE06-13L (17.6 ka), as well as at 136 μm and 85 μm. For the second fossil sample, CR-22L (12.4 ka), weak extrema are present at 148 μm and 88 μm. Close to these values are extrema for sample M70/1-721 Dive-106 (RED): 132 μm, 91μm, and 74 μm. Only one maximum could be identified for sample M70/1-752 Dive-111 from the Gondola Slide (102 μm).

Extrema reflecting periodicities within the Mg/Ca-profiles, that are present in more than one sample, group within three intervals: 189–200 μm (Bari Canyon, SML WHITE, Urania Bank), 118–148 μm (all samples except for the Gondola Slide specimen), and 83–102 μm (all samples).

Spectral power of the maxima, found within the Sr/Ca-profiles, is by a factor of 10 lower than in the Mg/Ca-profiles and lowest values are observed within samples

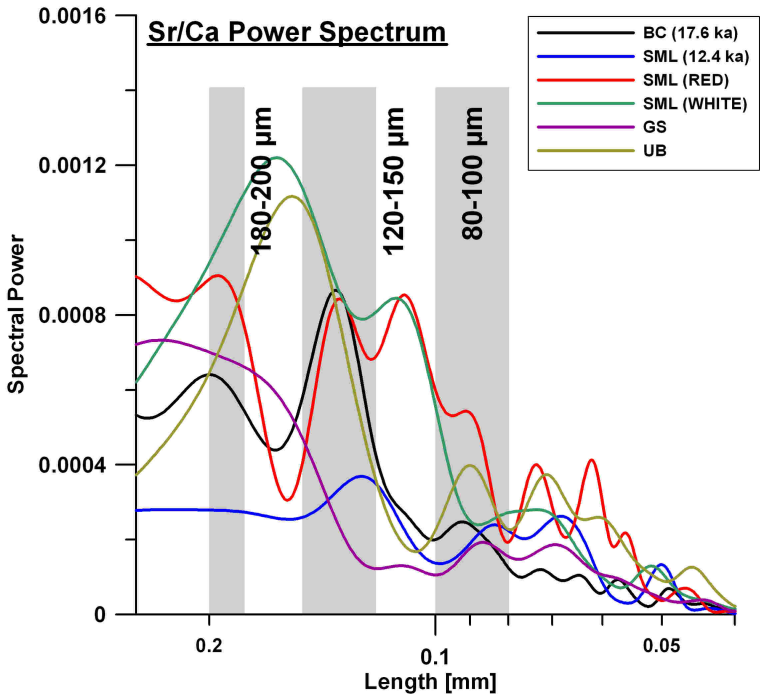

Figure 3.8: Spectral analysis of high-resolution Sr/Ca-ratio profiles.

CR-22L (12.4 ka) (at 126 μm, 83 μm, 68 μm) and M70/1-752 Dive-111 (at 233 μm, 111 μm, 87 μm, 69 μm). Most maxima are present for sample M70/1-721 Dive-106 (RED) (194 μm, 134 μm, 110 μm, 91 μm, 74 μm, 62 μm), while the remaining samples only show three distinguishable extrema (Fig. 3.8): SE06-13L (17.6 ka) at 200 μm, 136 μm, and 92 μm, M70/1-721 Dive-106 (WHITE) at 163 μm, 113 μm, and 73 μm, and the specimen from the Urania Bank at 155 μm, 90 μm, and 71 μm.

A grouping of maximum values is observable: 194–200 μm (SE06-13L (17.6 ka), M70/1-721 Dive-106 (RED)), 126–155 μm (all samples except the white *L. pertusa* from SML and the specimen from the Gondola Slide), and 83–92 μm (all samples except for sample M70/1-721 Dive-106 (WHITE)).

The power spectrum observed for the S/Ca-ratio-profiles is comparable to that for Sr/Ca regarding spectral power. The strongest peak is found for sample M70/1-721 Dive-106 (WHITE), at 145 μm, while a minor one is present at 71 μm (Fig. 3.9). Second in strength are extrema for fossil sample SE06-13L (17.6 ka), at 190 μm, 142 μm, and 85 μm, followed by the red *L. pertusa* from SML with maxima at 211 μm, 137 μm, 88 μm, and 67 μm. Only weak undulations are found within the curves representing samples CR-22L (12.4 ka) (at 192 μm, 116 μm, 87 μm) and M70/1-677 Dive-100 (at 185 μm, 117 μm, 80 μm), while the Gondola Slide specimen shows maxima at 127 μm and 90 μm.

The peaks within the power spectrum of S/Ca concentrate in three intervals, like

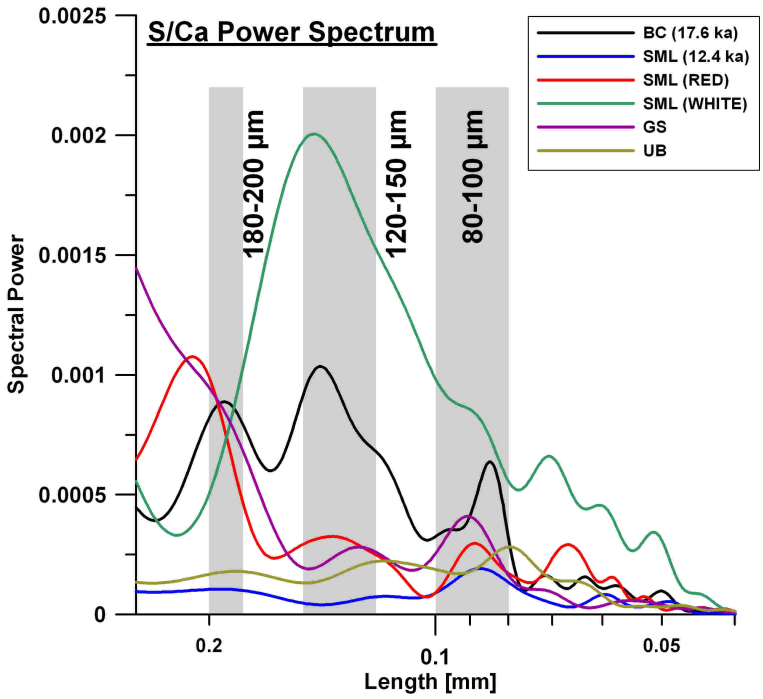

Figure 3.9: Spectral analysis of high-resolution S/Ca-ratio-profiles.

peaks for Mg/Ca and Sr/Ca: 185–211 μm (SE06-13L (17.6 ka), CR-22L (12.4 ka), M70/1-721 Dive-106 (RED), M70/1-677 Dive-100), 116–145 μm (all samples), and 80–90 μm (all samples except for the white *L. pertusa* from SML).

3.2.4 Stable C- and O-Isotopes

Of the six cold-water coral specimens investigated in this study, both fossil and two of the recent examples were investigated for distributions of stable carbon (δ^{13}C) and stable oxygen (δ^{18}O) isotopes. Analyses were carried out in 2007 by Matthias López Correa (GZN-IPAL, Erlangen) along profiles across the thecal wall, up to 7 mm in length and with a sampling resolution of 100 μm and in one case of about 73 μm. Results can be found in the appendix (Tab. A.13).

As can be seen in Fig. 3.10 linear relationships between carbon and oxygen isotopes are present in all of the coral samples with both isotopic ratios becoming more positive towards the outer rim.

While in sample SE06-13L (17.6 ka) δ^{13}C varies between -4.14‰ and +3.72‰ ($\bar{\mu}$=+1.70‰), the average in sample CR-22L (12.4 ka) is more negative ($\bar{\mu}$=-1.41‰) as is the range of variation (-5.09‰ to +1.32‰). The recent coral specimens are even more negative regarding the content of stable carbon isotopes, i.e. ^{12}C is more enriched in relation to the PDB-standard: $\bar{\mu}$=-3.50‰ (-7.39‰ to +0.86‰) in sample M70/1-721 Dive-106 (RED), and $\bar{\mu}$=-2.66‰ (-6.89‰ to +1.25‰) in sample M70/1-752 Dive-111.

Similar trends can be observed for δ^{18}O with average values being more positive in the fossil samples (Fig. 3.10), indicating that ^{18}O is more enriched in relation to the PDB-standard. These vary between -1.71‰ and +2.16‰ ($\bar{\mu}$=+0.35‰) in sample M70/1-721 Dive-106 (RED) and between -0.92‰ and+2.59‰ ($\bar{\mu}$=+0.99‰) in the Gondola Slide coral sample. In the fossil specimen from SML (12.4 ka) an average of $\bar{\mu}$=+2.82‰ varying within a range of +0.96‰ to +4.06‰ is observed and in the oldest sample, SE06-13L (17.6 ka), values are even more positive ranging from +2.33‰ to +5.50‰ ($\bar{\mu}$=+4.53‰).

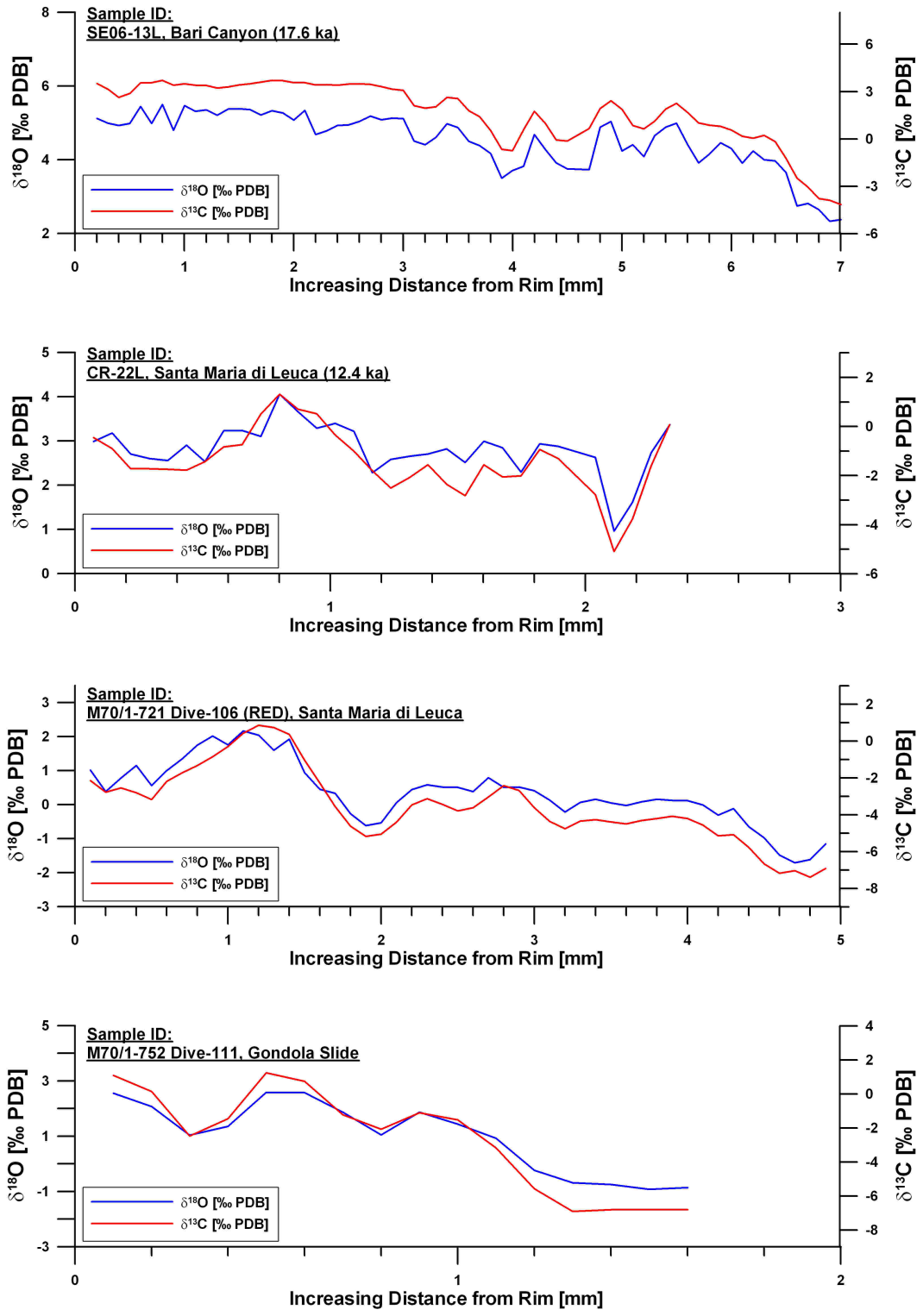

Figure 3.10: Profiles of stable C- and O-isotopes across the theca of two fossil and two recent cold-water coral specimens starting at the outer rim. The measurements were carried out by Matthias López Correa (GZN-IPAL, Erlangen) in 2007. Note the different scaling of the abscissae within the graphs.

3.3 Element Concentrations in Water Samples

3.3.1 Trace Elements (ICP-MS)

Trace elements, i.e. elements with average concentrations of less than 100 mg/l, have been determined within water samples collected in the Norwegian Sea (P325-cruise), NE-Skagerrak (AL275-cruise), and central Mediterranean Sea (M70/1-cruise).

Depth profiles representing the concentrations of the elements lithium, rubidium, strontium, and molybdenum are illustrated in Fig. 3.11, and illustrated in Fig. 3.12 for the elements antimony, caesium, barium, and uranium. Results of the analyses are listed in the appendix (Tab. A.15).

All elements except Sb and Ba show a similar distribution pattern: lowest element concentrations are observed for the AL275-samples with a high variation between 10–85 m water depth, while P325- and M70/1-samples are characterized by almost constant concentrations within the depth ranges of 170–600 m and 200–1200 m, respectively, but always with higher element concentrations in water samples from the Mediterranean (Figs. 3.11, 3.12).

Alkali Metals

Variations of Li lie between 133–166 μg/l (AL275), 164–174 μg/l (P325), and 188–201 μg/l (M70/1), similar to that of Rb varying between 96–123 μg/l (AL275), 124–126 μg/l (P325), and 134–144 μg/l (M70/1). Concentrations of Cs are by a factor of 400 smaller, ranging between 0.244–0.303 μg/l (AL275), 0.297–0.303 μg/l (P325), and 0.324–0.336 μg/l (M70/1).

Alkaline Earth Metals

Sr shows highest concentrations of the investigated trace elements: 6351–8391 μg/l (AL275), 8489–8528 μg/l (P325), 9210–9768 μg/l (M70/1), while alkaline earth metal Ba only varies between 7.51–9.96 μg/l (AL275), 5.70–6.05 μg/l (P325), and 8.47–9.92 μg/l (M70/1). Concentrations of barium are higher in AL275-samples than in P325-samples and close to that in M70/1-samples, what is not observed for the other elements.

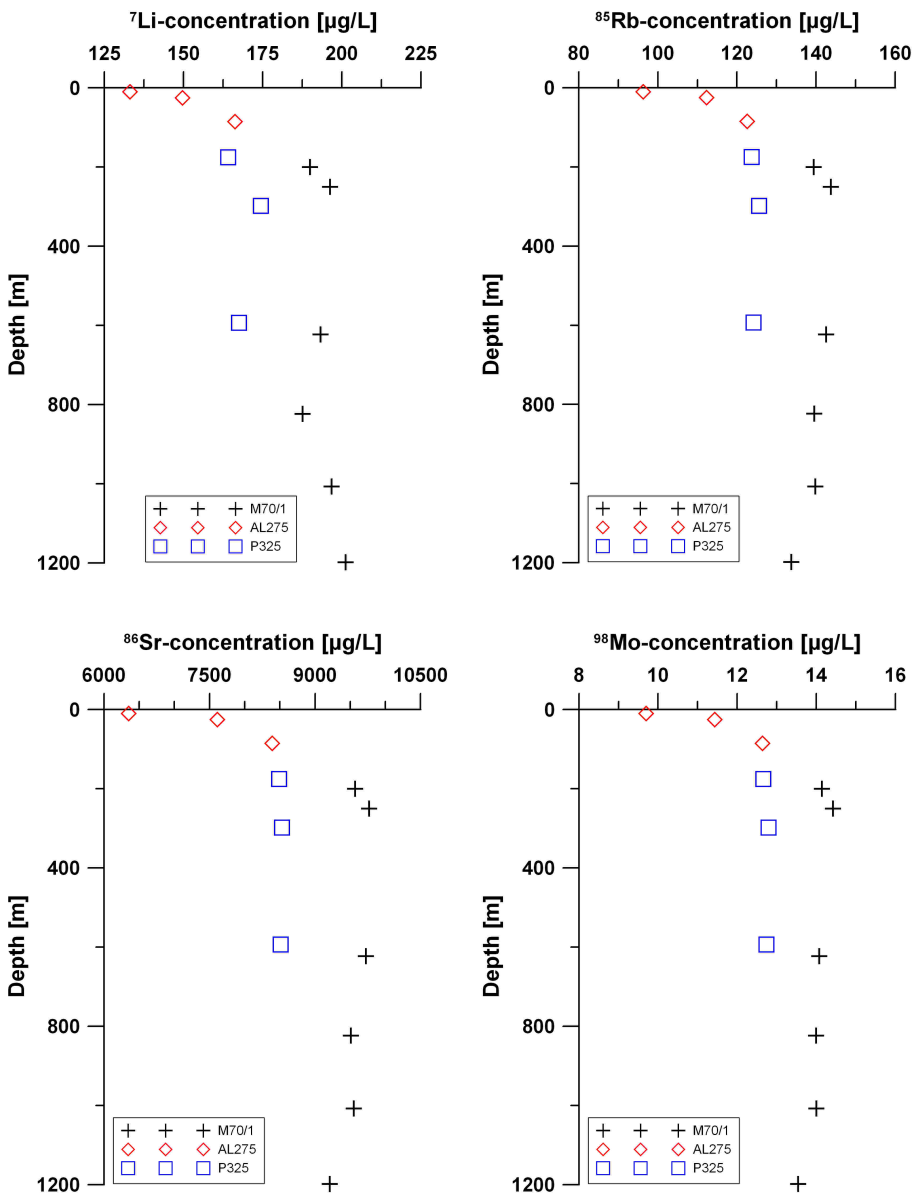

Figure 3.11: Depth profiles of trace elements Li, Rb, Sr, and Mo.

Other Elements

The transition element Mo has concentrations similar to that of Ba, ranging between 9.7–12.6 μg/l (AL275), 12.7–12.8 μg/l (P325), and 13.5–14.4 μg/l (M70/1), while concentrations of the metalloid Sb are close to that of Cs: 0.186–0.210 μg/l (AL275), 0.187–0.236 μg/l (P325), 0.213–0.239 μg/l (M70/1). Although concentrations of antimony are higher within M70/1-samples than in water samples from AL275- and P325-cruises, variations observed are stronger than for the other elements. Finally, actinid metal U was found to have concentrations between 2.57–3.23 μg/l (AL275), 3.20–3.26 μg/l (P325), and 3.47–3.59 μg/l (M70/1).

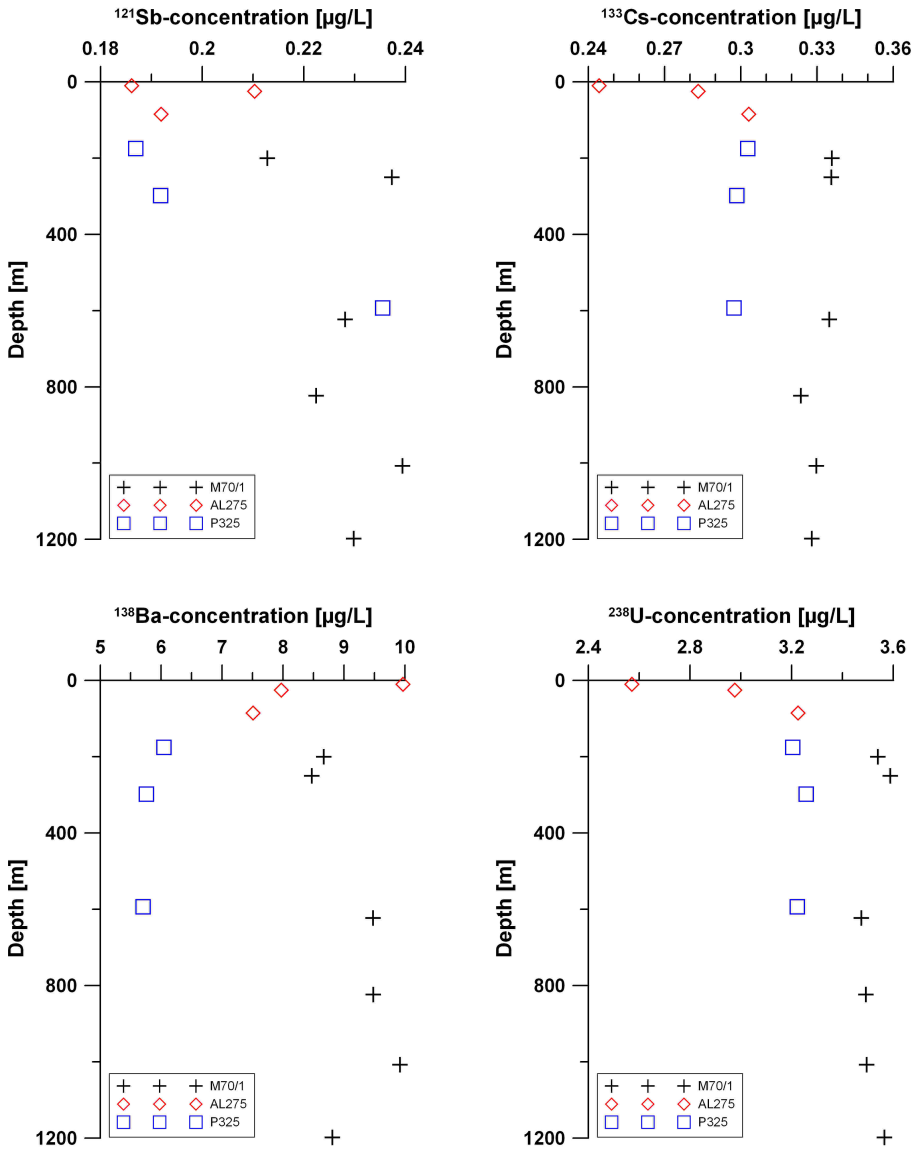

Figure 3.12: Depth profiles of trace elements Sb, Cs, Ba, and U.

3.3.2 Major and Trace Elements (ICP-OES)

Results for concentrations of the major elements calcium and magnesium, as well as for the trace elements strontium and boron, determined by ICP-OES, are listed in the appendix (Tab. A.16) and shown as depth profiles in Fig. 3.13.

The distribution pattern found for the ICP-MS-determined trace element concentrations is again observable. Highest element concentrations are found in Mediterranean water samples and lowest in water samples from AL275-cruise, although the depth range for M70/1-samples is extended (20–2510 m).

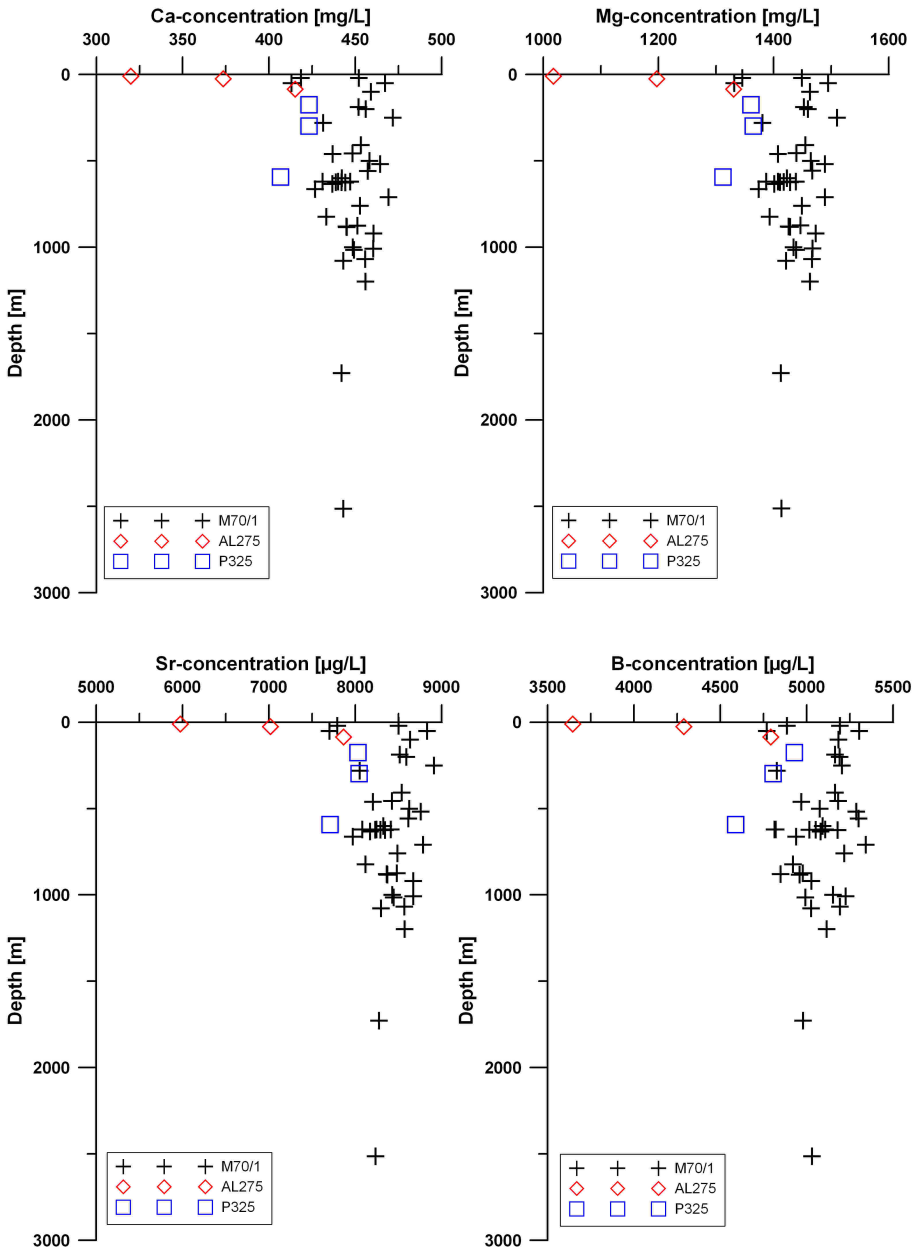

Figure 3.13: Depth profiles of major and trace elements Ca, Mg, Sr, and B.

Alkaline Earth Metals

Calcium-concentrations vary between 320–415 mg/l (AL275), 407–423 mg/l (P325), and 413–472 mg/l (M70/1), while highest concentrations are found for Mg, ranging between 1017–1331 mg/l (AL275), 1312–1364 mg/l (P325), and 1331–1510 mg/l (M70/1). Sr-concentrations are lower by a factor of 200: 5973–7866 μg/l (AL275), 7709–8044 μg/l (P325), 7702–8912 μg/l (M70/1).

Interestingly, concentrations of strontium determined by ICP-OES are 5% to 15% lower than those determined by ICP-MS. However, analytical assessment documents that concentrations obtained by ICP-OES are more accurate (-2.38% vs. +9.38% deviation from published IAPSO-value) but less precise (5.80% vs. 1.31% RSD)

than concentrations determined by ICP-MS. This can not be explained by a contamination of the IAPSO seawater standard, but possibly by a systematical error regarding the calculation of Sr-concentrations from the ICP-MS-measured intensities of this element. It is therefore possible that all ICP-MS-obtained results are defective.

Metalloid Boron

Boron is characterized by low concentrations in the investigated seawater samples, ranging between 3644–4791 μg/l (AL275), 4588–4929 μg/l (P325), and 4768–5342 μg/l (M70/1).

Molar Ratios

Molar element ratios of the ICP-OES-determined element concentrations only vary to a small degree within the analyzed water samples. A distribution pattern with respect to sampling locations as for the element concentrations is not observed. Results are also found in the appendix (Tab. A.16).

The range of Sr/Ca-variation lies between 8.47–8.59 mmol/mol (AL275), 8.60–8.62 mmol/mol (P325), and 8.44–8.58 mmol/mol (M70/1). That of B/Ca is slightly greater, with 42.2–42.7 mmol/mol (AL275), 41.7–43.1 mmol/mol (P325), and 40.2–43.3 mmol/mol (M70/1), while that of Mg/Ca is by a factor of 100 greater: 5.20–5.24 mol/mol (AL275), 5.26–5.28 mol/mol (P325), 5.19–5.27 mol/mol (M70/1).

4 Discussion

4.1 Paleotemperature Reconstructions

4.1.1 Sr/Ca-Ratios

To calculate paleotemperatures ($T_{Sr/Ca}$), equation 2.2 (p. 26) was applied to the (unsmoothed) high-resolution Sr/Ca-profiles of the coral specimens. The results are summarized in Tab. 4.1. Additionally, the residual Sr/Ca from its arithmetic mean was divided by the slope in equation 2.2, thus generating high-resolution records of a paleotemperature anomaly (T-anomaly), reflecting the Sr/Ca-variability (Figs. 3.1 to 3.6, pp. 34 to 42).

As indicated in Tab. 4.1, average and standard deviation of $T_{Sr/Ca}$ are lowest for 17.6 kyr-old sample SE06-13L (6.2±0.8°C). Temperatures vary between 2.1°C and 8.8°C or rather -4.1°C to +2.6°C by means of the T-anomaly (Fig. 3.1). Variability in fossil sample CR-22L (12.4 ka) is similar with a T-anomaly ranging from -3.1°C to +2.7°C (Fig. 3.2), i.e. a $T_{Sr/Ca}$-variation between 6.2°C and 12.0°C about an average of 9.3±0.9°C (1σ).

Table 4.1: Average values ($\bar{\mu}\pm1\sigma$) of calculated paleotemperatures after applying the temperature equation of Cohen et al. (2006) to the generated high-resolution Sr/Ca-profiles of the coral specimens, as well as observed water temperatures at coral sampling locations. Note that the standard deviation also reflects the variability of the temperature anomaly.

Sample ID	**N**	$\mathbf{T}_{Sr/Ca}$ [°C]	$\mathbf{T}_{obs.}$ [°C]	$\mathbf{\Delta T}$ [°C]
SE06-13L (17.6 ka)	973	6.2±0.8	x	x
CR-22L (12.4 ka)	680	9.3±0.9	x	x
M70/1-721 Dive-106 (RED)	981	9.4±1.3	13.6	-4.2
M70/1-721 Dive-106 (WHITE)	570	10.3±1.2	13.6	-3.3
M70/1-752 Dive-111	635	9.3±1.0	13.5	-4.2
M70/1-677 Dive-100	602	7.6±1.4	14.0	-6.4

Recent coral specimens show a higher variability of the T-anomaly than the fossil corals, but all averages of $T_{Sr/Ca}$ are offset from observed in situ temperatures at coral sampling locations. Observed temperatures (Tab. 2.3, p. 29) are all higher

than the mean of the calculated paleotemperatures, with differences (ΔT) up to -6°C, and even within 2σ-boundaries $T_{Sr/Ca}$ do not match the observed temperatures (Tab. 4.1).

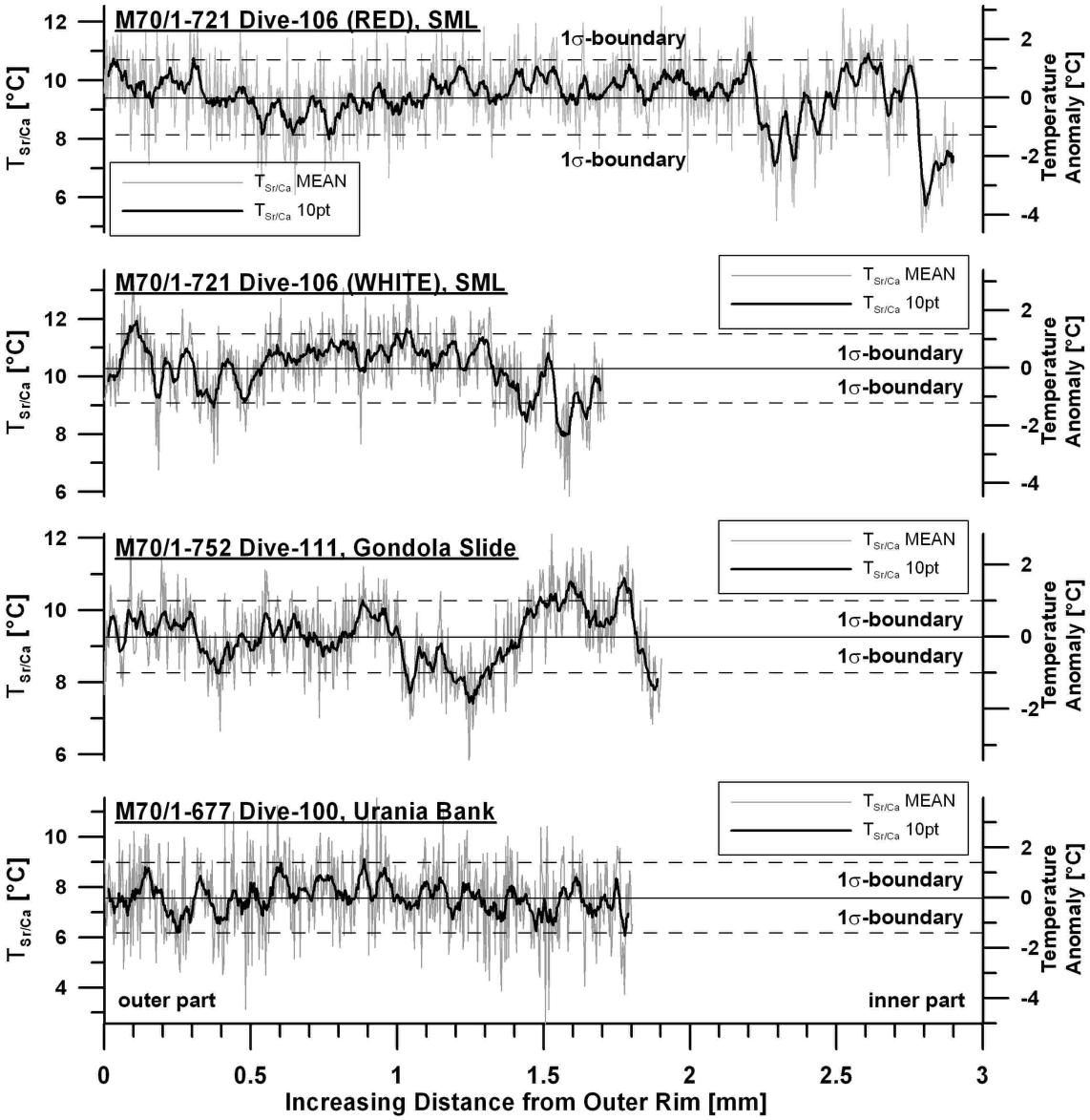

Figure 4.1: High-resolution paleotemperature-profiles of recent coral specimens.

$T_{Sr/Ca}$ is highest for sample M70/1-721 Dive-106 (WHITE) (10.3±1.2°C) and lowest for sample M70/1-677 Dive-100 (7.6±1.4°C). However, the variability of the T-anomaly is similar for all recent samples, ranging from -4.6°C to +3.1°C for sample M70/1-721 Dive-106 (RED) (1σ=1.3°C), from -4.5°C to +3.4°C for sample M70/1-721 Dive-106 (WHITE), from -3.4°C to +2.8°C for sample M70/1-752 Dive-111 (1σ=1.0°C), and from -5.0°C to +4.0°C for sample M70/1-677 Dive-100 (Fig. 4.1).

It is therefore evident, that the Sr/Ca-temperature relationship for *Lophelia pertusa* from COHEN ET AL. (2006) is not applicable to samples of the same species from the central Mediterranean. However, considering Mediterranean intermediate waters to be relatively stable with respect to their environmental parameters at

coral sampling locations (Tab. 1.2, p. 17), the smoothed curves of the T-anomaly, mainly plotting within 1σ-boundaries of the unsmoothed dataset, reflect realistic changes in seawater temperature. This is supported by analytical assessment of the EPMA-measurements. Here, the precision for Sr/Ca and thus for the T-anomaly is only about 3%RSD, indicating that the undulations of the T-anomaly reflect a true signal. Furthermore, the range of absolute coral Sr/Ca-variation in the investigated recent coral specimens is similar to that observed within the coral that was used by COHEN ET AL. (2006) to generate the published Sr/Ca-temperature relationship. Lower average Sr/Ca-content of the Mediterranean corals, indicating higher temperatures, further implies that the T-sensitivity (slope of the equation) might be correct, while the offset is not. Thus a local temperature calibration is needed for the Mediterranean *Lophelia pertusa*. Remaining questions are to what extent changes in temperature account for the observed Sr/Ca-variability and to what degree the relationship between coral Sr/Ca and temperature stays constant in time and space. COHEN ET AL. (2006) provide an answer to the first question and give an estimate of about 25%.

4.1.2 "Lines Technique"

Paleotemperatures were calculated using the "lines technique"-method published by SMITH ET AL. (2000) for fossil samples SE06-13L (17.6 ka) and CR-22L (12.4 ka), and for recent coral specimens M70/1-721 Dive-106 (RED) and M70/1-752 Dive-111.

First, δ^{13}C vs. δ^{18}O regression lines were created for coral samples, based on stable isotope analyses. Linear regression was performed with a confidence level of 95% and resulted in linear equations with similar slopes ranging between 0.370 and 0.440 and in high coefficients of determination ($0.827<R^2<0.989$) (Tab. 4.2). From these regression lines the $\delta^{18}O_i$ values, corresponding to the δ^{13}C values of DIC at the sampling locations, were obtained afterwards.

Together with the oceanographic data listed in Tab. 2.3 (p. 29) single paleotemperature estimates were then calculated using equation 2.3 (p. 26) for the recent specimens and equation 2.4 (p. 27) for the fossil coral samples. Results are listed in Tab. 4.2.

For the recent samples, the reconstructed temperatures range from 14.3°C for sample M70/1-752 Dive-111 to 15.1°C for sample M70/1-721 Dive-106 (RED). These values are within an error of ±1.0°C (SMITH ET AL., 2000) very close to the observed temperatures of 13.5°C and 13.6°C, respectively. The obtained temperatures for fossil coral samples are lower with respect to the recent samples: 5.1°C for sample

Table 4.2: Summary of important variables for applying the "lines technique"-method published by SMITH ET AL. (2000). R^2 is the coefficient of determination of the linear regression with a confidence level of 95%. $\delta^{18}O_i$ is in ‰ PDB.

Sample ID	**N**	**Slope**	**Intercept**	$\mathbf{R^2}$	$\delta^{18}\mathbf{O}_i$	**T [°C]**
SE06-13L (17.6 ka)	68	0.370	3.90	0.933	3.90	2.8
CR-22L (12.4 ka)	31	0.395	3.38	0.827	3.38	5.1
M70/1-721 Dive-106 (RED)	49	0.440	1.89	0.933	2.58	15.1
M70/1-752 Dive-111	16	0.428	2.13	0.989	2.80	14.3

CR-22L (12.4 ka) and 2.8°C for sample SE06-13L (17.6 ka), while SMITH ET AL. (2000) give here an error estimate of ±1.1°C.

Fig. 4.2 shows that neither the investigated fossil nor the recent cold-water corals precipitated their carbonate in isotopic equilibrium with seawater. However, the assumption that $\delta^{18}O_i$ is equal or close to the $\delta^{18}O_{IE}$ with seawater is verified for the two recent specimens. The main uncertainty for the calculation of $\delta^{18}O_i$ for the fossil samples arises from the fact that the isotopic composition of the seawater is not known. Equation 2.4 therefore assumes that $\delta^{13}C_{DIC}$=$\delta^{18}O_{sw}$=0, although oxygen isotope ratios of seawater are assumed to be more positive during glacial times than at present due to the build-up of ice-sheets. This is consistent with shifts towards lighter carbon and lighter oxygen isotopes within the coral skeletons since 17.6 ka (Fig. 4.2), and the result of CACHO ET AL. (2006) who suggest a dominance of a heavier water end member during glacial times in the western Mediterranean Sea.

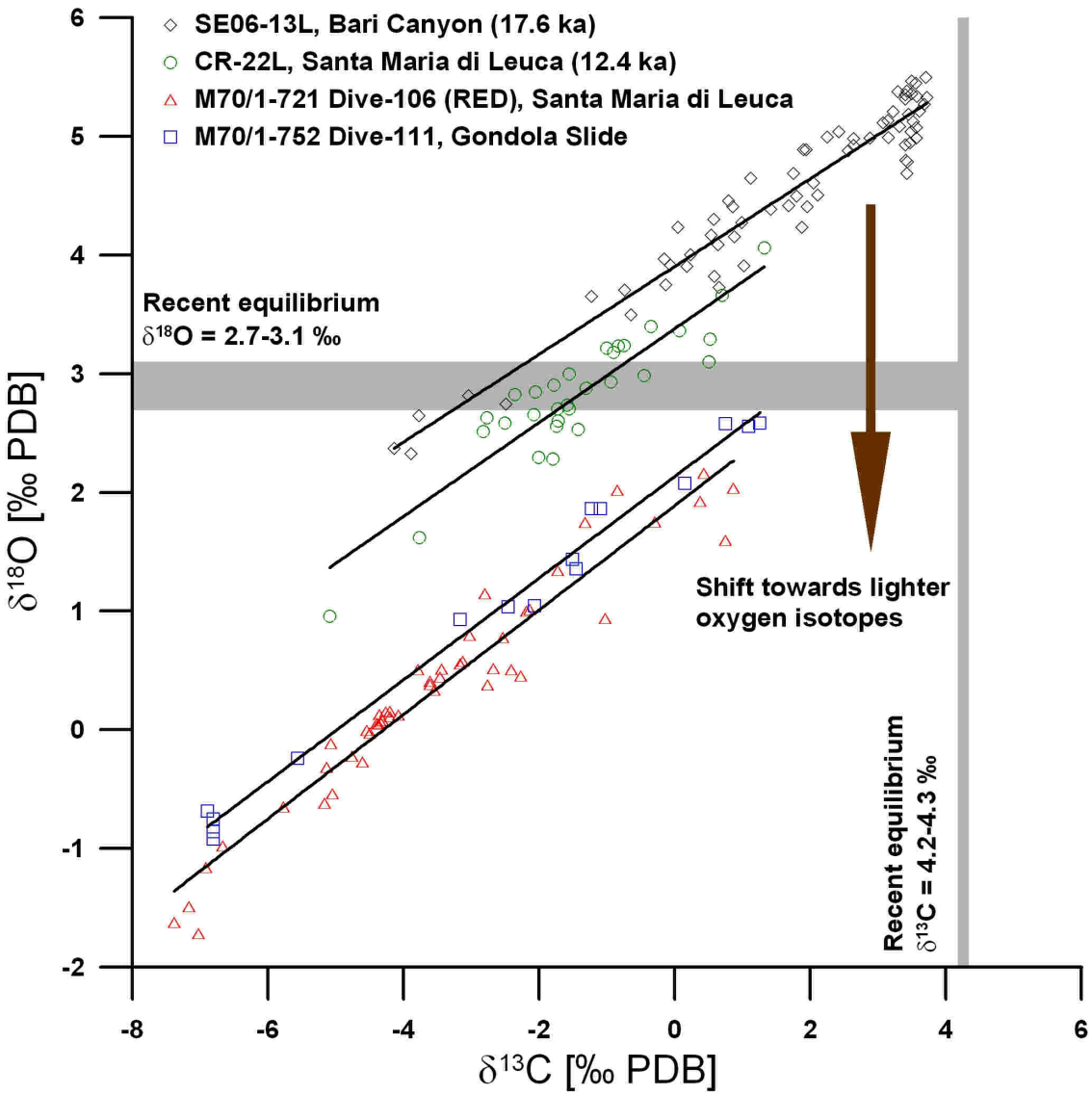

Figure 4.2: Linear correlations between stable C- and O-isotopes observed within the cold-water coral specimens.

4.2 Seawater Composition

4.2.1 T- and S-Relationships

Results of correlation analyses (linear regression) between element concentrations and recorded environmental parameters within a confidence level of 95%, are listed in Tab. 4.3 and Tab. 4.4.

Except for elements Sb and Ba coefficients of determination for the ICP-MS-analyses of trace elements vary between 0.782 and 0.856 regarding temperature and between 0.902 and 0.965 regarding salinity. All slopes of the resulting linear equations are positive. In contrast, R^2 is <0.5 for correlation analyses between trace element concentrations and water depth (Tab. 4.3).

Table 4.3: Correlation analyses (linear regression) between concentrations of trace elements from the ICP-MS analyses of the water samples and water temperature, salinity, and depth. Confidence level of the coefficient of determination is 95%.

R^2 (95%)	N	T	S	Depth
^{7}**Li**	12	0.843	0.902	0.502
^{85}**Rb**	12	0.830	0.936	0.320
^{86}**Sr**	12	0.814	0.948	0.329
^{98}**Mo**	12	0.782	0.940	0.299
^{121}**Sb**	12	0.397	0.492	0.481
^{133}**Cs**	12	0.856	0.965	0.306
^{138}**Ba**	12	0.232	0.030	0.093
^{238}**U**	12	0.798	0.958	0.371

ICP-OES-derived analyses produce the same result regarding correlations between element concentrations, temperature, and salinity, although coefficients of determination are smaller (Tab. 4.4). Here, R^2 varies between 0.342 and 0.406 with reference to temperature and between 0.689 and 0.755 for salinity. Again R^2 is higher for linear relationships between element concentration and salinity than for those involving temperature, of which all are positive. Contrary to these results, coefficients of determination are <0.1 for correlations between (i) element concentrations and water depth, (ii) molar ratios and all environmental parameters, and (iii) molar ratios among each other, indicating absent linear relationships.

Apparently, concentrations of trace and major elements in the analyzed water samples, except for Sb and Ba, are related to variations in seawater temperature and salinity, while salinity accounts for most of the observed change. At least for strontium and calcium this is supported by DE VILLIERS ET AL. (1994) who investigated the variability of both elements in seawater from the Pacific Ocean. For both elements they report conservative behaviour that is clearly related to salinity.

Table 4.4: Correlation analyses (linear regression) between concentrations and ratios of major and trace elements from the ICP-OES analyses of the water samples and water temperature, salinity, and depth. Confidence level of the coefficient of determination is 95%.

R^2 (95%)	N	T	S	Depth	Mg/Ca	Sr/Ca	B/Ca
Ca	45	0.388	0.738	0.086	x	x	x
Mg	45	0.390	0.755	0.080	x	x	x
Sr	45	0.342	0.689	0.068	x	x	x
B	45	0.406	0.689	0.048	x	x	x
Mg/Ca	45	0.000	0.019	0.030	x	0.052	0.071
Sr/Ca	45	0.127	0.025	0.099	0.052	x	0.007
B/Ca	45	0.000	0.028	0.072	0.071	0.007	x

The difference between depth-distribution patterns of Sb and Ba and those of the other elements, cannot be explained by means of analytical precision. Here, other factors than T and S must be responsible for the observed values. A possible explanation might be that both elements are related to biological productivity, which in the literature is at least considered for fluxes of particulate barium (e.g. Dymond & Collier, 1996).

While element concentrations are different in the Norwegian Sea, in the NE-Skagerrak, and in the Mediterranean region, all molar ratios are found to be within the same range of spatial and depth variability. Regarding Sr/Ca-ratios, this observation is consistent with the investigation of de Villiers et al. (1994) and de Villiers (1999) that seawater Sr/Ca shows spatially gradients of 2–3% globally. The range of variation is equivalent to a seawater Sr/Ca-amplitude of 1–2% that arise by reason of Quaternary sea level changes (Stoll & Schrag, 1998).

Furthermore de Villiers et al. (1994) and de Villiers (1999) announce a depletion of Sr/Ca in oligotrophic surface waters, while deep waters and surface waters in upwelling regions and at high latitudes are enriched. The fact that seawater Sr/Ca-values are highest in samples from P325 cruise (67–70°N) supports this. The assumption of de Villiers et al. (1994) that water samples from areas characterized by river runoff should be depleted in Sr/Ca is also confirmed. Of the analyzed water samples, sample AL275-425-2#63, collected in 10 m depth of low-salinity water from the Oslofjord, has second-lowest values regarding Sr/Ca and Mg/Ca.

On the other hand, a 'labile nutrient-like' behaviour of Sr/Ca (de Villiers, 1999) is not observed. However, this cannot be concluded with certainty, considering an analytical precision for Mg/Ca of up to 0.50%RSD, for Sr/Ca of up to 0.53%RSD, and for B/Ca of up to 3.6%RSD. de Villiers (1999) explains her observed vertical Sr gradient within the upper 200 m of the water column with the production of celestite skeletons of surface-dwelling acantharia and calcium carbonate cycling.

4.2.2 Correlations Between Coral- and Water-Chemistry

To find relationships between the chemical compositions of the coral specimens and the water samples, correlation analyses (linear regressions) were performed between molar element ratios and environmental parameters with a confidence level of 95%. Results are listed in Tab. 4.5.

The database is represented by the arithmetic means of the molar ratios of the recent cold-water coral specimens obtained by the quantitative EPMA-analyses, the ICP-OES-determined molar ratios of the seawater samples collected directly at the coral sampling locations, and records of temperature and salinity.

Table 4.5: Correlation analyses between molar element ratios obtained from the quantitative analyses of the coral samples and the ICP-OES analyses of the water samples, as well as water temperatures and salinities. Confidence level of the coefficient of determination is 95%.

R^2 (95%)	N	Water Mg/Ca	Water Sr/Ca	Water B/Ca	T	S
Coral Mg/Ca	4	0.184	0.003	0.056	0.244	0.291
Coral Sr/Ca	4	0.137	0.193	0.444	0.783	0.788
Coral S/Ca	4	0.044	0.020	0.007	0.002	0.007

Results show highest coefficients of determination for relationships between coral-Sr/Ca and seawater temperature (0.783) and between coral-Sr/Ca and seawater salinity (0.788) (Tab. 4.5). However, both resulting linear equations are characterized by positive slopes. Applying the Sr/Ca-temperature relationship to the mean Sr/Ca-ratios observed within the fossil coral samples results in paleotemperatures of +14.6°C for sample SE06-13L (17.6 ka) and of +13.7°C for sample CR-22L (12.4 ka), respectively. These are similar to the present annual mean temperatures at the sampling locations, which can be retrieved from the eWOCE oceanographic atlas. Same is the case for the Sr/Ca-salinity relationship, producing paleosalinities for samples SE06-13L (17.6 ka) and CR-22L (12.4 ka) of 38.80 and 38.67, values similar to recently observable salinities within the central Mediterranean.

Coral-Mg/Ca-temperature relationships (R^2=0.244) and coral-Mg/Ca-salinity relationships (R^2=0.291) have negative slopes. For fossil coral samples they result in paleotemperatures and paleosalinities close to that retrieved by the T- and S-relationships for Sr/Ca. Calculated paleo-values for sample SE06-13L (17.6 ka) are T=14.1°C and S=38.73, and T=13.9°C and S=38.71 for sample CR-22L (12.4 ka).

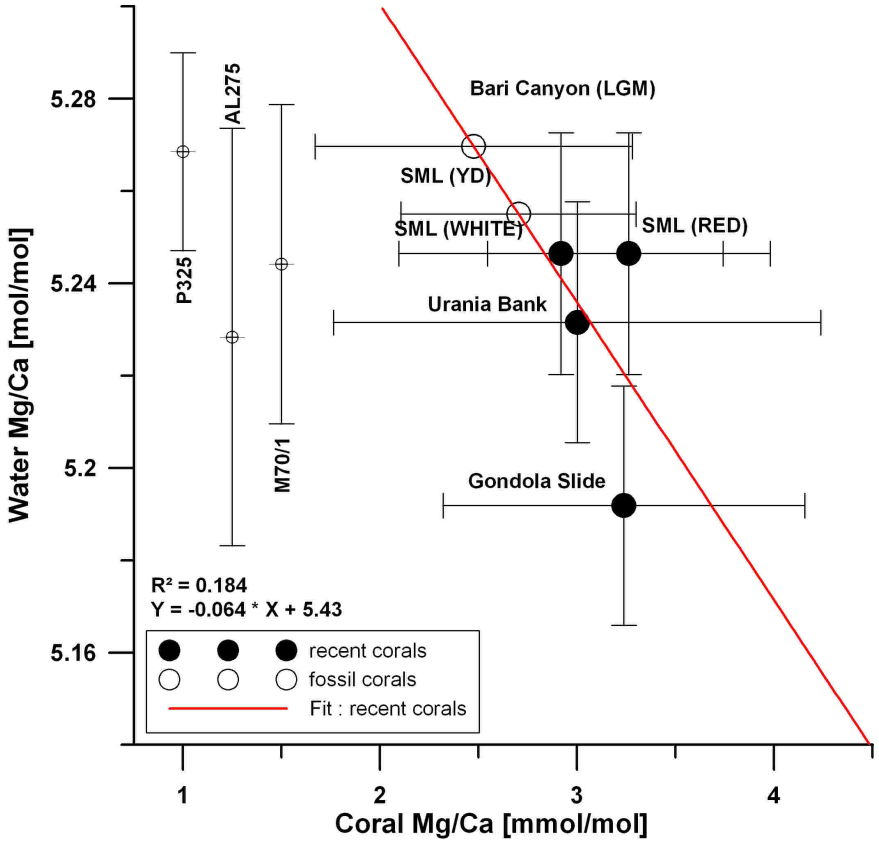

Figure 4.3: Correlations between coral and water Mg/Ca-ratios. Recent coral specimens are represented by black dots and fossil samples by open circles. Horizontal error bars stand for the standard deviation (1σ) of the Mg/Ca-signal determined by quantitative EPMA-analysis, whereas vertical error bars illustrate the precision of the ICP-OES-measurement for the particular water sample. For comparison the average and standard deviation (2σ) determined within all seawater samples from the respective cruises are shown. Note that the mean of the Mg/Ca-ratio observed within the fossil samples is projected onto the regression line, which is calculated for the recent coral specimens only.

Only few of the remaining coefficients of determination in Tab. 4.5 lie between 0.18 and 0.5. These are (i) coral Mg/Ca vs. water Mg/Ca, (ii) coral Sr/Ca vs. water Sr/Ca, and (iii) coral Sr/Ca vs. water B/Ca.

The linear relationship between coral and water Mg/Ca-ratios is negative and characterized by a R^2 of 0.184 (Fig. 4.3). Interestingly a recent seawater Mg/Ca variability of about 5.18–5.29 mol/mol is reflected by a recent coral Mg/Ca-variability of only about 1.8–4.2 mmol/mol. Projecting the mean Mg/Ca-ratios of the fossil coral samples onto the regression line results in water paleo-Mg/Ca-ratios of 5.25 mol/mol for sample CR-22L (12.4 ka) and of 5.27 mol/mol for sample SE06-13L (17.6 ka). These values are within the observed variability of Mg/Ca-ratios of all of the analyzed water samples. In Figs. 4.3, 4.4, and 4.5, this variability is represented by the standard deviation (2σ) of the ratios observed within all water samples of the respective cruises.

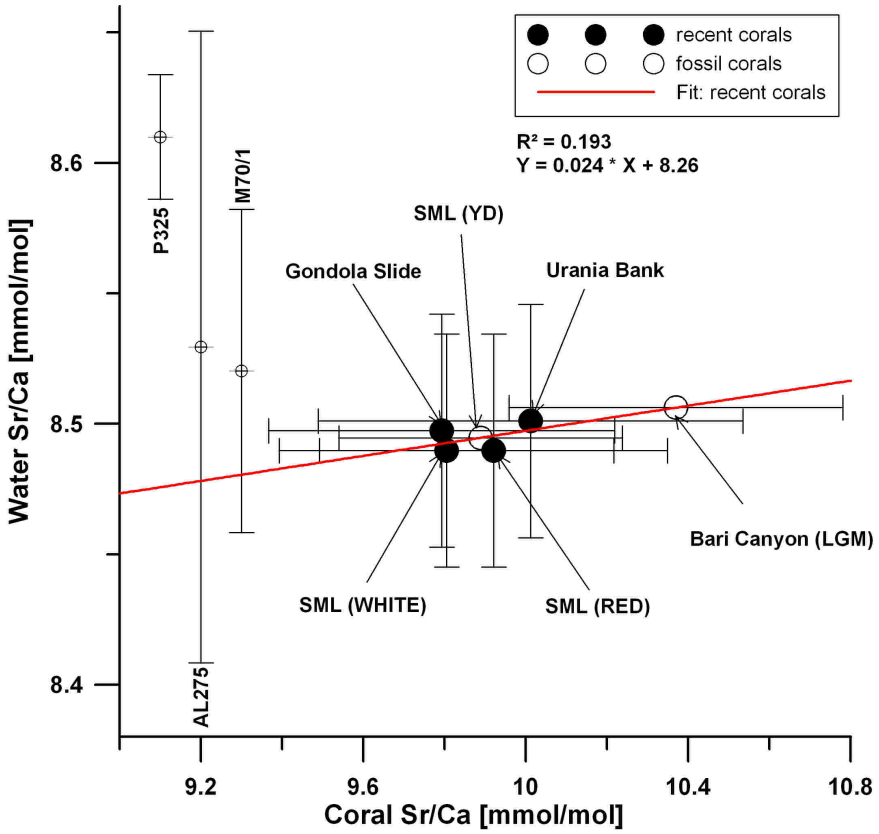

Figure 4.4: Correlations between coral and water Sr/Ca-ratios. For explanations see Fig. 4.3.

Coral- and water-Sr/Ca-ratios are positively correlated with a R^2 of the linear regression of 0.193 (Fig. 4.4). Recent coral specimens are slightly enriched in Sr/Ca (ca. 9.4–10.5 mmol/mol) with respect to seawater (ca. 8.41–8.65 mmol/mol). Applying the linear relationship, paleo-water-Sr/Ca-values calculated for the sample CR-22L (12.4 ka) and the sample SE06-13L (17.6 ka) are 8.49 mmol/mol and 8.51 mmol/mol. These values are very similar to the ratios determined within the water samples collected at the sampling locations of the recent coral specimens. They are also within the range of Sr/Ca-ratios observed within analyzed seawater samples from cruises AL275 and M70/1.

A coefficient of determination, that is twice as great as for the previous relationship is present for a linear correlation between coral-Sr/Ca-ratios and water-B/Ca-ratios (R^2=0.444) (Tab. 4.5). As can be seen in Fig. 4.5, the slope of the equation is negative and produces paleo-water-B/Ca-ratios of 42.1 mmol/mol for sample CR-22L (12.4 ka) and of 38.2 mmol/mol for sample SE06-13L (17.6 ka). While the first value is close to that of the recent water samples, the value for the paleo-water-B/Ca-ratio related to the fossil coral from the Bari Canyon is not within the range of recently observable water-B/Ca-ratios (ca. 40.3–43.8 mmol/mol).

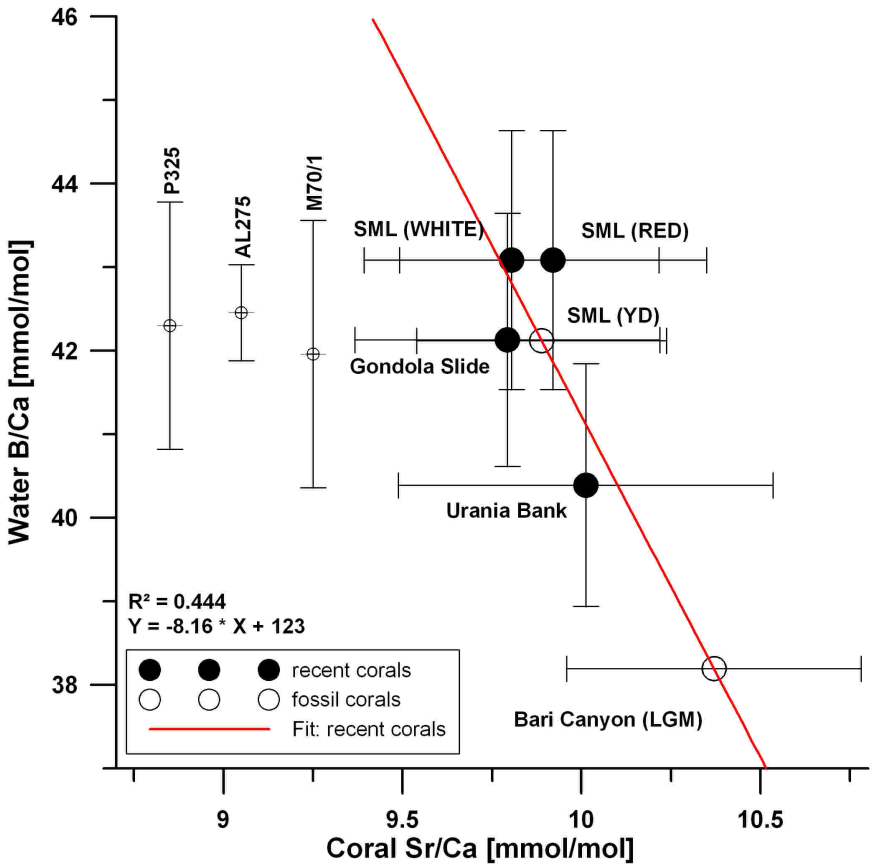

Figure 4.5: Correlations between coral Sr/Ca- and water B/Ca-ratios. For explanations see Fig. 4.3.

There are several limitations regarding the conducted correlations between recent coral- and water-chemistry. First, there is the assumption, that the average values of the obtained molar ratios of the coral skeleton best represent the environmental conditions in which carbonate precipitation took place. Considering the observed relative stability of Mediterranean intermediate waters, this might be a realistic background. Second, for a distinct calibration function between the parameters involved, these should span a wide range to eliminate uncertainties. This is definitely not the case here with molar ratios of the investigated coral specimens varying within the same small interval and molar ratios of the investigated water samples varying within analytical precision. Third, with only four recent coral samples involved, the total number of count is far from being sufficient for an accurate linear regression analysis. Finally, performed correlation analyses are methods to find linear relationships only between the involved parameters. Thus, the obtained correlation coefficients do not reveal whether there are non-linear relationships present. Therefore, the paleo-water-values inferred from the calibration functions should be considered with caution. This becomes most obvious from the fact that the discovered relationships (i) between temperature and coral-Sr/Ca-ratios are positive, and (ii) between temperature and coral-Mg/Ca-ratios are negative. For most coral species the exact opposite is reported (e.g. Lea, 2003).

If the relationships between coral- and water-chemistry are correct, both fossil coral samples would have precipitated their aragonite skeleton in waters slightly enriched in Mg/Ca. The coefficient of determination, however, is very small (0.184), indicating an absent linear relationship. Anyway, the obtained paleo-water-Mg/Ca-values are within the range of recently observable water-Mg/Ca-ratios and within measurement-precision. Hence, a clear difference between recent and paleo-Mg/Ca-ratios cannot be stated.

Ratios of Mg/Ca in corals appear to serve as paleothermometers (Lea, 2003). For example, Sinclair et al. (1998) found a linear correlation between Mg/Ca and sea surface temperature (SST) in tropical shallow-water coral species *Porites*, but with a greater variability of the annual seasonal variation in comparison with other elements. If temperature also applies as the primary control on incorporation of Mg in the skeleton of *L. pertusa*, then the on average smaller Mg/Ca-ratios in fossil samples SE06-13L (17.6 ka) and CR-22L (12.4 ka) indicate lower temperatures.

Given a low R^2 of 0.193 of the relationship between Sr/Ca-ratios of coral and water samples, fossil samples experienced water Sr/Ca-ratios that are not different from those that are recently observable. However, regarding Sr/Ca, shelf recrystallization fluxes during glacial maxima have the potential to change seawater Sr/Ca by 1–2% (Stoll & Schrag, 1998). Thus, at least for the end of the last glacial period, an increase of seawater Sr/Ca should be observable. This is indicated by the fact that the fossil sample SE06-13L (17.6 ka) has on average higher Sr/Ca-values than the other specimens, but can also be interpreted by means of lower temperatures. As a result, the calculated relationship must be considered inaccurate.

Hart & Cohen (1996) report B/Ca-ratios in zooxanthellate species *Porites* to be 100 times lower than in seawater, showing seasonal variation trends, and a positive co-variation with coral Sr/Ca-ratios. Sinclair et al. (1998) developed B/Ca-ratios in this species as a proxy of SST, characterized by a negative correlation, and only recently a similar relationship was discovered by Montagna et al. (2008) for Mediterranean cold-water coral species *Cladocora caespitosa*. Regarding the results for the relationship between coral-Sr/Ca-ratios and water-B/Ca-ratios, the fossil sample SE06-13L (17.6 ka) would have thrived in waters depleted in B/Ca, while the sample CR-22L (12.4 ka) would have not (R^2=0.444).

B/Ca-ratios being lower in coral aragonite than in seawater indicate a biological control on incorporation of boron, rather than changes in the amount of boron in seawater. Consequently, if incorporation processes of B are similar in cold-water coral *L. pertusa*, lower seawater B/Ca-ratios at 17.6 ka remain speculation.

4.3 Cold-Water Corals as Paleoenvironmental Archives

4.3.1 High-Resolution Mappings and Profiles

Mechanisms responsible for the observed element distributions and the variations of the molar element ratios within the coralline aragonite are either a thermodynamic temperature effect or a biomineralization effect. The question is to what extent element incorporation in coral skeletons is linked to calcification.

Results of the correlation analyses amongst element concentrations from the quantitative measurements, and amongst molar element ratios along the high-resolution profiles, indicate (i) co-variant incorporation of magnesium and sulfur, (ii) co-variant incorporation of calcium and strontium, (iii) a relationship between Mg/Ca and S/Ca, (iv) a relationship between Sr/Ca and S/Ca, and (v) an inverse relationship between Mg/Ca and Sr/Ca. However, most of the obtained Pearson product-moment correlation coefficients have values of $r<0.5$ (Tab. 3.2, p. 33; Tab. 3.4, p. 39), equal to coefficients of determination (R^2) smaller than 0.25, and thus they only weakly indicate linear correlations. Considering Mg/Ca and Sr/Ca as paleothermometers in *L. pertusa* would explain the inverse relationship between Mg/Ca and Sr/Ca. Then, however, it is not clear why r is negative for correlations between Mg/Ca and Sr/Ca (and Mg vs. Sr) in recent coral specimens only, while fossil samples are characterized by positive values.

At present, no records or paleoceanographic proxy studies exist for S/Ca-ratios within the cold-water coral *Lophelia pertusa*. Willenz et al. (2006) report a temperature effect and significant latitudinal influence on incorporation of Mg and S to be evident in juvenile wide-ranged temperate starfish *Asterias rubens* (Echinodermata). The correlation is positive and is assumed to be linear. If S/Ca can be confirmed being a paleothermometer in cold-water corals as well, this would explain the co-variant incorporation of Mg and S, the positive correlation between Mg/Ca and S/Ca, and the negative correlation between Sr/Ca and S/Ca in sample M70/1-721 Dive-106 (RED). However, it would not explain that in all other investigated coral samples the correlation between Sr/Ca and S/Ca is positive (Tab. 3.4, p. 39).

An additional argument for the assumption that incorporation of Mg, Sr and S is to some extent temperature-dependent is apparent, when comparing the average values of the investigated fossil and recent coral specimens. Fossil samples are characterized by on average lower Mg/Ca-ratios and S/Ca-ratios, and sample SE06-13L (17.6 ka)

by higher Sr/Ca-ratios (Tab. 3.3, p. 33). This could be explained by assuming that intermediate water temperatures were lower in the late glacial period and the Younger Dryas cold interval than at present. This assumption is supported by on average more positive $\delta^{18}O$ values in both fossil corals (chapter 3.2.4, p. 46), indicative of the presence of continental ice sheets and/or lower temperatures. That Sr/Ca-ratios in fossil sample SE06-13L (17.6 ka) are higher than in fossil sample CR-22L (12.4 ka), with values in the 12.4 kyr-old sample being similar to those observed within the recent coral specimens, could be explained by a reduced or even absent influence of shelf recrystallization fluxes on seawater Sr/Ca-ratios during the Younger Dryas cold interval.

There is evidence, however, that element ratios are more linked to calcification processes. An experimental precipitation study showed that Sr/Ca-ratios and Mg/Ca-ratios in abiogenic aragonite decrease with increasing temperature (Gaetani & Cohen, 2006). Cohen et al. (2006) found a dependence of Sr/Ca on temperature, as well as an inverse correlation between Sr/Ca and Mg/Ca in *L. pertusa* and therefore concluded that the influence of temperature on partitioning is not the primary control on skeletal chemistry. This is consistent with results of Shirai et al. (2005) who found only weak correlations between temperature and Mg/Ca-ratios and between temperature and Sr/Ca-ratios in deep-sea coral taxa *Flabellum* sp. and *Caryophillia* sp. They observed large variations among individuals collected from similar temperatures and explained these by means of calcification as controlling factor (Shirai et al., 2005).

If Sr/Ca is considered as a reliable proxy for paleotemperature in *L. pertusa*, then both recent specimens derived from the Santa Maria di Leuca Reef Province from almost the same spot, should exhibit equivalent Sr/Ca-profiles, at least, on a relative scale. As both corals must have experienced changing environmental parameters simultaneously, both Sr/Ca-profiles should show co-variant behaviour. This is not the case and can also not be observed for Mg/Ca nor S/Ca (Fig. 3.3, p. 38; Fig. 3.4, p. 40; Fig. 4.1, p. 54). A possible explanation for this might be intra-species differences between orange and white coloured *L. pertusa*, which by now have not been investigated. Another possibility to explain the absent co-variant behaviour of all three ratios, when comparing both coral samples, are the selected locations for the EPMA-measurements. Samples M70/1-721 Dive-106 (RED and WHITE) were probed on areas located between two different polyps (Fig 3.3, p. 38, and Fig. 3.4, p. 40). Freiwald et al. (2004) reported that in living *L. pertusa* each new polyp generation coincides with the formation of a new incremental calcareous layer, secreted around the skeleton of the older polyps as well. Thus, both samples may have recorded signals of at least two different polyps, making a comparison between Sr/Ca-profiles impossible by means of paleothermometry. To prevent interferences

of this kind, it is reommended to probe horizontal cross sections of single polyps only.

S/Ca-ratios and Mg/Ca-ratios can also be assumed to be influenced by calcification processes. Although not verified by microstructural data, PINGITORE ET AL. (1995) interpreted sulfur in coral carbonate as SO_4^{2-} ions being substituted for CO_3^{2-}. On the contrary, sulfur is interpreted by DAUPHIN (2001) as organic sulfated polysaccharides. This is also favoured by CUIF & DAUPHIN (2005) who report that coral fibres are built by superimposition of a few micron-thick growth layers, which are made of mineral nanograins densely packed within an organic component containing sulfur bearing glycoproteins. If this applies to *L. pertusa* as well, a link to calcification can be established, but until now no investigations concerning this matter exist.

However, it would not explain why S/Ca-ratios are on average lower in the fossil coral samples than in the recent specimens. Reminding the result of PINGITORE ET AL. (1995), a possible explanation would be lower concentrations of SO_4^{2-} in seawater, which then are incorporated into the coral aragonite. Lower seawater SO_4^{2-}-concentrations would then be a result of (i) a higher pH, as SO_4^{2-} is produced by dissociation of sulfuric acid (H_2SO_4), (ii) less oxidized sulfur compounds from decomposed organic matter indicating a relationship to primary productivity, or (iii) less anoxic conditions due to stronger ventilation of intermediate water masses. Evidence supporting the second and third argument comes from CACHO ET AL. (2000) and BÁRCENA ET AL. (2001) who worked on sediment cores from the Alboran Sea (western Mediterranean). Results of CACHO ET AL. (2000) indicate that rapid changes in the western Mediterranean thermohaline circulation occurred in parallel to SST oscillations with enhanced deep water ventilation occurring during cold intervals between 20–50 kyr BP. Analyses of windblown particles, diatom assemblages and total organic carbon (TOC) suggest intensified winds and an increase in paleoproductivity during the Younger Dryas cold interval compared to 17.6 ka (BÁRCENA ET AL., 2001), which then would explain the slightly higher average values of S/Ca in sample CR-22L (12.4 ka). However, the findings of CACHO ET AL. (2000) and BÁRCENA ET AL. (2001) must not consequently apply for the central Mediterranean.

Assuming that all sulfur in seawater is present in the form of SO_4^{2-}, the S/Ca-ratio in standard seawater is about 2.75 mol/mol (MILLERO ET AL., 2008). Thus, coral S/Ca-ratios are depleted by a factor of 1000, indicating that incorporation of sulfur does not occur in equilibrium with seawater. This further implies that incorporation of S, like Mg and Sr, is to some extent influenced by factors controlling calcification.

Regarding Mg/Ca, results of MEIBOM ET AL. (2004) indicate a biological control on the crystallization process in coral fibrous tissues, investigated in tropical species *Pavona clavus*. Concerning cold-water corals, ADKINS ET AL. (2003) found that Mg/Ca-variability in skeletons of *D. cristagalli* and *L. pertusa* exceeds what can be explained by influence of physiological processes. This indicates that these species are also linked to the biomineralization process. This is consistent with the conclusion of SINCLAIR ET AL. (2006) that similar vital effects in tropical and deep-sea corals are associated with internal structure and that bio/geochemical processes fractionate trace elements. GAGNON ET AL. (2007) explain inverse Mg/Ca and Sr/Ca in *D. dianthus* by Rayleigh fractionation implying a closed system during precipitation, which lacks to explain large increases of Mg/Ca in optical dense bands.

Extraordinary variations occurring synchronously in all three ratios within a coral specimen would give additional evidence of calcification processes influencing element incorporation. This can be observed in sample M70/1-721 Dive-106 (RED) (Fig. 3.3, p. 38). In this sample Mg/Ca clearly reflects the coral's opaque bands, but the banding within the inner 0.7 mm of the thecal wall also seems to influence Sr/Ca-ratios and S/Ca-ratios. Here the variability of the 10pt-Sr/Ca-curve is stronger than in the outer part of the profile and it is out of the 1σ-boundaries of ± 0.23 mmol/mol, while S/Ca-ratios like Mg/Ca-ratios rapidly decrease towards the inner rim. A similar observation can be made for sample M70/1-677 Dive-100. While Mg/Ca-ratios are highest from 0.8 mm to 1.2 mm distance from the outer rim, Sr/Ca-ratios drop below average from 0.6–1.2 mm (Fig. 3.6, p. 42). Although S/Ca-ratios show no abnormal variations within this interval, Mg/Ca and S/Ca both rapidly increase from 1.3 mm to 1.2 mm while Sr/Ca decreases. The maximum in Mg/Ca at about 1.3 mm distance from the outer rim in sample M70/1-752 Dive-111 corresponds to maxima of Sr/Ca and S/Ca, while the Mg/Ca-maximum at about 1.6 mm distance from the outer rim corresponds to local minima in both Sr/Ca and S/Ca (Fig. 3.5, p. 41). All these examples show extraordinary variations which could be interpreted by means of strong calcification influences on element incorporation.

Further evidence comes from the results of the spectral analyses (chapter 3.2.3). Comparing the location of the extrema found within the ratios for each sample shows interesting similarities: in sample SE06-13L (17.6 ka) maxima for Mg/Ca and Sr/Ca are present at 200 μm and at 136 μm, and for Mg/Ca and S/Ca at 85 μm. A grouping can be detected for the intervals 190–200 μm, 136–142 μm, and 85–92 μm, where all three ratios are simultaneously present. The same is observable for sample CR-22L: although periodicities are not identical within any ratio, all are present within 83–88 μm, and Sr/Ca- and S/Ca-maxima can be found between 116 μm and 126 μm. Extrema for Mg/Ca and Sr/Ca in sample M70/1-721 Dive-106

(RED) coincide at 91 μm and 74 μm, while intervals containing peaks of all ratios are observed at 132–137 μm, 88–91 μm, and 67–74 μm. Sr/Ca-maxima and S/Ca-maxima are present between 194 μm and 211 μm. Correlations are not obvious for samples M70/1-721 Dive-106 (WHITE) and M70/1-752 Dive-111. While in the former sample all ratios are present only within the range of 66–73 μm, in the Gondola Slide sample Sr/Ca-peaks and S/Ca-peaks are only found between 87 μm and 90 μm. Spectral maxima in sample M70/1-677 Dive-100 from the Urania Bank are observed between 185–194 μm and 117–118 μm for Mg/Ca and S/Ca, while extrema for all ratios are present within 80–90 μm.

Thus, it is obvious that all ratios in all samples are affected simultaneously and that the incorporation of Mg, Sr and S is related to each other and occurrs periodical. Significant periodicities in fossil and recent corals are similar and can be grouped into three intervals: ca. 80-100 μm, ca. 120-150 μm, and ca. 180-200 μm. Assuming the 120-150 μm interval to reflect an annual signal, then the 80-100 μm interval will reflect a time interval of 8 to 9 months and the 180-200 μm interval a time interval of 17 to 19 months, if coral growth occurs at a constant rate.

Comparable to that result, Cohen et al. (2006) also found highest Mg/Ca-ratios and lowest Sr/Ca-ratios in opaque bands across the thecal wall of *Lophelia pertusa* and state an average thecal "thickening" rate of about 100 μm/yr if these oscillations are annual. On the contrary, de Villiers et al. (1994) found that variations in skeletal Sr/Ca-values in the zooxanthellate species *Pavona clavus* are associated with variable extension and possibly variable calcification rates, with higher values associated with slower extension rates. Therefore, it is also possible that these intervals reflect phases of slower calcification. To verify whether the results of the spectral analyses reflect an annual periodicity or different extension rates, it is necessary to provide an "age-model" based on high-resolution dating across the corals' thecal wall and to conduct in situ observations of cold-water coral calcification.

4.3.2 Temperature Reconstructions and Climatic Implications

Climatic implications can be made by assuming that (i) paleotemperatures calculated by applying the "lines technique" reflect realistic temperatures, and (ii) that the temperature anomaly calculated by applying the Sr/Ca-temperature relationship of Cohen et al. (2006) reflects a realistic temperature variability.

The stable isotope composition of accumulated ice is assumed to reflect paleotemperature, because colder air masses are more depleted of heavy water (containing ^{18}O or ^{2}H) and produce lighter precipitation (containing ^{16}O or ^{1}H) (e.g. Dansgaard,

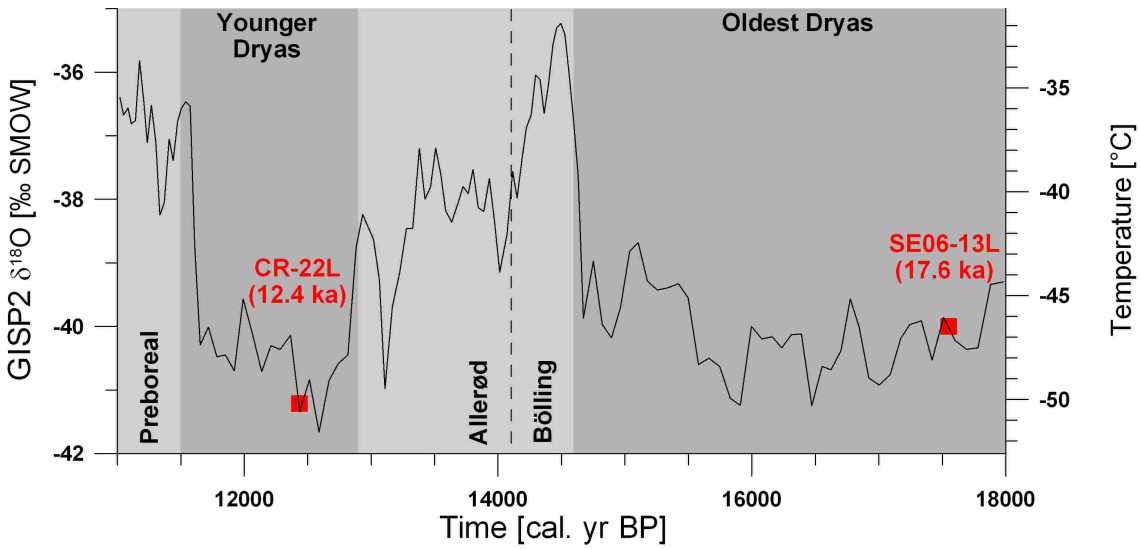

Figure 4.6: GISP2 ice core record (Greenland) of oxygen isotopes between 11 and 18 cal. kyr BP. Dated fossil corals are represented by red squares, while durations of cold and warm periods are highlighted by different grey shadings. The temperature scale was created by applying the glacial-interglacial calibration of Cuffey et al. (1995) to the δ^{18}O-record of Grootes & Stuiver (1997).

1964). Ice cores from central Greenland are exceptionally robust and independent paleothermometers (Alley, 2000) and a paleotemperature relationship for oxygen isotope ratios measured in Greenland Ice Sheet Project 2 core (GISP2) has been published by Cuffey et al. (1995).

Paleotemperatures in central Greenland from 11,000–18,000 cal. yr BP have been reconstructed by applying the relationship of Cuffey et al. (1995) to the δ^{18}O-record of Grootes & Stuiver (1997). The result is illustrated in Fig. 4.6. Ice-core data are available on "The Greenland Summit Ice Cores CD-ROM", 1997, National Snow and Ice Data Center, University of Colorado at Boulder, and the World Data Center-A for Paleoclimatology, National Geophysical Data Center, Boulder, Colorado (http://www.ngdc.noaa.gov/paleo/ icecore/greenland/summit/index.html).

Fig. 4.6 shows that temperatures in central Greenland were about -15°C to -20°C colder than at present (ca. -30°C) when fossil coral samples were alive. The GISP2-record indicates that temperatures were even lower at 12.4 ka BP (ca. -50°C) than at 17.6 ka BP (ca. -46°C).

For the Adriatic Sea it could have been shown that paleoclimatic changes during the last 370 kyr appear in phase with the North Atlantic climate system (Piva et al., 2008a), although results of Cacho et al. (2001) show a shorter cooling phase for the Younger Dryas cold interval (700 years) in the western Mediterranean Sea than that observed in the North Atlantic region (1200 years).

The fact that temperatures were colder in the past than at present is supported by

the results of the "lines technique" temperature reconstruction. Paleotemperature estimates of intermediate water masses in the central Mediterranean are +2.8°C for sample SE06-13L (17.6 ka) and +5.1°C for sample CR-22L (12.4 ka). Thus, in contrast to paleotemperature reconstructions from central Greenland, the sample from the Younger Dryas cold interval appears to have lived in warmer water masses.

The reconstructed values for both fossil samples are calculated by assuming that $\delta^{13}C_{DIC}=\delta^{18}O_{sw}=0$, because the isotopic composition of seawater is not known. However, a shift towards lighter carbon and towards lighter oxygen isotope ratios from the 17.6 ka to the 12.4 ka old sample is observable (Fig. 4.2, p. 57). This indicates that the reconstructed temperatures are to some unknown extent inaccurate and that temperatures at 12.4 ka could as well have been colder.

On the other hand, BÁRCENA ET AL. (2001) report 2–3°C higher SST in the Alboran Sea at 12.4 ka compared to 17.6 ka based on alkenone-SST-studies. However, they confirmed the trend towards lighter oxygen isotope ratios. Higher SST at 12.4 ka is also consistent with results of PIVA ET AL. (2008a) who presented alkenone-derived SST-values of about 8°C at 17 ka and of about 11°C at 12 ka in the central Adriatic Sea. On the contrary, CACHO ET AL. (2006) stated that even deep-water temperatures were about 11°C at 17.6 ka and at 12.4 ka, based on Mg/Ca-analyses of benthic foraminifera in a sediment core from the Alboran Sea. These values are significantly higher than those reconstructed by the "lines technique"-method and those reconstructed by applying the Sr/Ca-temperature relationship of COHEN ET AL. (2006) (Tab. 4.1, p. 53). Thus, paleotemperatures from the Alboran Sea might not be comparable to those of the central Mediterranean Sea.

Direct comparisons between fossil and recent coral specimens living at same locations indicate that temperature variability recorded in cold-water corals has been lower during glacial periods. While the fossil sample from the Bari Canyon (SE06-13L, 17.6 ka) is characterized by a temperature anomaly of ±0.8°C (Tab. 4.1, p. 53), the recent coral sample from the Gondola Slide (M70/1-752 Dive-111) has a value of ±1.0°C. Same is observable for corals from the Santa Maria di Leuca Reef Province. The fossil sample CR-22L (12.4 ka) has a temperature anomaly of ±0.9°C while samples from M70/1-721 Dive-106 have values of ±1.3°C and ±1.2°C, respectively (Tab. 4.1, p. 53). That corals can record changes in seasonal temperature cycles has been shown for zooxanthellate species *Porites* from the Red Sea, indicating increased seasonality during the last interglacial period (FELIS ET AL., 2004). Furthermore, PIVA ET AL. (2008b) inferred from assemblages of planktonic and benthic foraminifera in sediment cores from the Adriatic Sea that production of LIW (p. 16) was weakened during colder and wetter intervals of the last 6000 years. Thus, it is possible that also the fossil cold-water corals from the central Mediterranean

recorded a lower temperature variability of intermediate water masses at 17.6 ka and at 12.4 ka. The reason for this observation might be linked to lower inter-seasonal temperature changes and reduced production of intermediate water masses in the central Mediterranean during the late glacial period and the Younger Dryas cold interval.

It is very interesting that both fossil coral samples lived in times characterized by a cool climate. For the last 50,000 years CACHO ET AL. (1999) found that SST-oscillations in a sediment core from the Alboran Sea show strong parallelism to Dansgaard-Oeschger events (D/O-events)[1]. Furthermore, based on abundances of planktonic foraminifera species *Neogloboquadrina pachyderma* sinistral and the isotopic record, they present evidence of significant SST drops (4°C) in association with Heinrich events (HE-events)[2] recorded in the GISP2 ice core (CACHO ET AL., 1999).

Sample SE06-13L is dated to 17.6 ka. This is very close to the time interval of HE1 in the Alboran Sea of about 16–17 kyr BP (CACHO ET AL., 1999; PÉREZ-FOLGADO ET AL., 2003). Thus, it is possible that cold-water corals colonize the Mediterranean in a batch-wise manner only during intervals of cold climates. This argument is strengthened by the result of MCCULLOCH ET AL. (2006) that prolific growth of Mediterranean cold-water corals ended abruptly at about 11 ka, although they flourished during the glacial-like conditions of the Younger Dryas. Their demise was probably due to the combined effects of a rapid 6–8°C rise in ocean temperatures at the end of the Younger Dryas and unusually high sediment influx from increased river discharge (MCCULLOCH ET AL., 2006). The argument is furthermore consistent with the assumption that low latitude cold-water coral ecosystems are important speciation centers and glacial refugia in the deep sea (DE FORGES ET AL., 2000; ROBERTS ET AL., 2006).

1 Dansgaard-Oeschger (D/O) events are large-amplitude, abrupt climate changes that have occurred with a periodicity of about 1,500 years during the past 120,000 years. They are characterized by an initial rapid warming of 5–10°C in Greenland ice cores (RAHMSTORF, 2002).

2 Heinrich events (HE) are climatic events that occurred at irregular intervals of the order of 10,000 years, mostly in the latter half of the last glacial. Distinct layers of ice-rafted debris in sediments from the North Atlantic are characteristic for these events. It is suggested that Heinrich events reflect massive episodic iceberg discharges leading to a subsequent breakdown of the Atlantic thermohaline circulation (RAHMSTORF, 2002).

5 Conclusions and Recommendations

This study shows that high-resolution mappings and profiles of major and trace elements can be produced for fossil and recent specimens of cold-water coral species *Lophelia pertusa* from the central Mediterranean Sea using electron-probe microanalysis (EPMA). A procedure to correct inaccurate EPMA-determinations of strontium in marine carbonate has been successfully developed by applying an internal carbonate standard.

Interpretation of the obtained high-resolution mappings and profiles indicates that element incorporation in coral aragonite of *L. pertusa* is linked to both, biologically controlled calcification processes and environmental parameters. Co-variant behaviour of Mg/Ca and S/Ca as well as an inverse relationship between Mg/Ca and Sr/Ca is partially explained by temperature-dependency. This is consistent with the observation of significant differences of average element composition when comparing fossil and recent coral specimens. However, high-resolution element profiles of recent coral samples collected within immediate vicinity of each other show no similarities, and thus do not confirm a possible application as high-resolution paleothermometers. Since there remains the problem that locations sampled on these specimens can not be clearly attributed to one single polyp, it is recommended for future studies to sample horizontal cross sections of the coral theca that can be attributed to a single polyp.

S/Ca-ratios seem to reflect growth layers containing organic compounds, but an influence of temperature, primary productivity and ventilation of intermediate water masses on S/Ca-ratios is suggested as well.

Results of spectral analyses indicate a dominant control of kinetic vital effects on calcification processes, as variations of element ratios occur synchronously and periodically. Periodicities found are similar in fossil and recent coral specimens and occur within three distinct intervals (80-100 μm, 120-150 μm, and 180-200 μm). These intervals are assumed to reflect either constant growth rates, with coral growth occurring annual and in cycles of 8 to 9 months, and of 17 to 19 months, respectively, or, to reflect phases of slower calcification. These assumptions remain unproofed until high-resolution dating techniques are applied to the coral skeleton and until in situ observations of calcification are conducted on *L. pertusa*.

It is the main conclusion of this study that more fundamental research is needed regarding element incorporation processes in *Lophelia pertusa* and possibly in other calcifying organisms. As long as it is not clear to what extent calcification influences element incorporation and specifically what controls S/Ca, the obtained high-resolution profiles should be regarded as reflecting paleoenvironmental records rather than specific parameters like temperature.

Reconstructions of paleotemperature using the "lines technique"-method (SMITH ET AL., 2000) generates single paleotemperature estimates which indicate that the temperature of intermediate water masses in the central Mediterranean were colder at 17.6 ka and at 12.4 ka than at present. This is consistent with paleotemperature data from ice cores. As the estimates are calculated without knowledge of the seawater isotopic composition they are to an unknown extent inaccurate. However, the temperature difference between 17.6 ka and 12.4 ka is similar to a difference in sea surface temperature observed at the same time in the Alboran Sea and the Adriatic Sea, although deep-water temperatures in the western Mediterranean seem to have been significantly higher.

Applying the Sr/Ca-temperature relationship of COHEN ET AL. (2006) shows that this relationship can not be applied to samples of *L. pertusa* from the central Mediterranean and it is therefore recommended to generate a regional Sr/Ca-calibration for this species. Anyway, the generated temperature anomaly seems to mirror a realistic picture of the relative temperature variability of intermediate water masses. This variability seems to have been lower within cold intervals, possibly due to a decreased seasonality and/or reduced production of intermediate water masses.

To verify the obtained paleotemperature estimates it is necessary to apply different proxies of temperatures. Regarding cold-water coral *L. pertusa*, the most promising proxy are stable strontium isotopes ($\delta^{88/86}$Sr). Thriving in about 14°C warm waters, specimens from the Mediterranean could extend the temperature relationship published by RÜGGEBERG ET AL. (2008) which only covers a range between 6–9°C. Additionally, this proxy could be evaluated as to whether it is possible to obtain high-resolution records of paleotemperature.

The second aim of this study was to determine concentrations of major and trace elements in seawater samples. It is shown that this is possible using ICP-MS- and ICP-OES-techniques. It is inferred from analytical assessment of the ICP-OES measurements, that accuracy and precision were poor for element boron and even insufficient for element barium. It is therefore recommended for future studies to use dilutions smaller than 1:50 or to measure these elements in undiluted samples.

Except for elements antimony and barium it is shown that salinity accounts for most of the observed concentration changes. There is the possibility that the ele-

ments Sb and Ba are influenced by biological productivity, which should be further investigated.

Element ratios are found to be more stable than element concentrations by means of their variability, and to be independent of temperature, salinity, and depth. For Sr/Ca, the published global spatial and depth variability has been confirmed.

The conducted correlations between coral- and water-chemistry are found to be insignificant, mainly because of statistical limitations. Thus, the reconstructed values for paleo-water-chemistry should be considered with caution.

On behalf of these conclusions and because of the fact that only two fossil coral specimens of different age were investigated, it is not possible to reconstruct the distribution of intermediate water masses in the central Mediterranean during the late glacial period and during the Younger Dryas cold interval. But it is possible to assume that cold-water corals colonize the Mediterranean in a batch-wise manner during cold climates and that low latitude ecosystems act as glacial refugia in the deep sea.

Danksagung / Acknowledgement

Zuerst möchte ich mich ganz herzlich bei Herrn Prof. Dr. Wolf-Christian Dullo bedanken. Sowohl für die Vergabe des Diplomarbeitsthemas, als auch für die Möglichkeit die Arbeit am IFM-GEOMAR zu schreiben und nicht zuletzt für die Betreuung und die Anregungen hinsichtlich der Dateninterpretation, vor allem in der Endphase der Arbeit.

Dr. Andres Rüggeberg war als Zweitbetreuer nahezu ständig verfügbar, sogar bei Abwesenheit. Wenn es darum ging, methodische Ansätze oder Ergebnisse zu diskutieren, die verschiedenen Messungen zu betreuen oder Lösungen für die Strontium-Problematik zu suchen, war immer auf ihn Verlass, auch über die Forschungsarbeit hinaus. Ich kann nur jedem Diplomanden/-in eine so gute Betreuung wünschen, wie ich sie bei Dr. Rüggeberg bekommen habe. Dafür bin ich ihm zu sehr großem Dank verpflichtet.

Für seine Diskussionsbereitschaft, seine unvorstellbare Fähigkeit zur Aufmunterung und seine Korrekturarbeiten möchte ich Dipl.-Geogr. Jacek Raddatz danken. Seine Unterstützung bei der Arbeit, zuletzt sogar als Bürokollege, und natürlich auch im Wulfsbrook, waren für mich von unvorstellbarem Wert, und haben zu einer Freundschaft geführt, die ich nicht missen möchte.

Die Messungen an der Mikrosonde und die Lösung des Strontium-Problems wären nicht möglich gewesen ohne die technische Betreuung durch Mario Thöner, sowie Diskussionen mit PD Dr. Thor Hansteen, Dr. Jan Fietzke, Julia Mahlke und Edgars Rudzitis.

Für die Wasseranalytik und die Nutzung des ICP-MS-Labors am Institut für Geowissenschaften der Christian-Albrechts-Universität zu Kiel, sowie eine vorbildliche, praxisnahe geochemische Ausbildung während des Studiums möchte ich Dr. C.-Dieter Garbe-Schönberg danken. Dies gilt auch für Frau Dipl.-Ing. Ulrike Westernströer und Frau Karin Kißling, die mich bei den Messungen an der ICP-MS und der ICP-OES betreut haben.

Sozusagen für die logistische und mentale Unterstützung zu Hause und ein so angenehmes WG-Leben danke ich Harald Meyer, Dr. jur. Tilman Scheinert und Anne Westhues. Michael Struck half mir mit der englischen Sprache. Dafür und für eine fast lebenslange Freundschaft bin ich ihm sehr dankbar.

Mein größter Dank gebührt jedoch meiner Familie, ohne deren stete Unterstützung mir weder dieses Studium noch der Abschluß dieser Arbeit jemals in dieser Form gelungen wären. Diese Arbeit sei Ihr deshalb gewidmet, in Dankbarkeit.

Zuletzt gilt mein Dank den Besatzungen und Fahrtteilnehmern der Ausfahrten P325, AL275 und M70/1, die das Probenmaterial und die Datenbasis dieser Arbeit lieferten.

Acknowledgements

This work is part of DFG-Project Paläo-TRISTAN.

Fossil coral samples were collected by Marco Taviani (CNR-ISMAR, Bologna) on R/V Urania.

Stable isotopes were measured by Matthias López Correa at GZN-IPAL, University of Erlangen, Germany.

U/Th-dating was carried out by Malcolm McCulloch at ANU-RSES, Canberra, Australia.

References

Adkins, J.F., Cheng, H., Boyle, E.A., Druffel, E.R.M. & Edwards, R.L. (1998): Deep-Sea Coral Evidence for Rapid Change in Ventilation of the Deep North Atlantic 15,400 Years Ago. *Science* **280**, 725–728.

Adkins, J.F., Boyle, E.A., Curry, W.B. & Lutringer, A. (2003): Stable isotopes in deep-sea corals and a new mechanism for "vital effects". *Geochimica et Cosmochimica Acta* **67**(6), 1129–1143.

Alley, R.B. (2000): The Younger Dryas cold interval as viewed from central Greenland. *Quaternary Science Reviews* **19**, 213–226.

Astraldi, M., Conversano, F., Civitarese, G., Gasparini, G.P., Ribera d'Alcalà, M. & Vetrano, A. (2002a): Water mass properties and chemical signatures in the central *Mediterranean* region. *Journal of Marine Systems* **33-34**, 155–177.

Astraldi, M., Gasparini, G.P., Vetrano, A. & Vignudelli, S. (2002b): Hydrographic characteristics and interannual variability of water masses in the central Mediterranean: a sensitivity test for long-term changes in the Mediterranean Sea. *Deep-Sea Research I* **49**, 661–680.

Bárcena, M.A., Cacho, I., Abrantes, F., Sierro, F.J., Grimalt, J.O. & Flores, J.A. (2001): Paleoproductivity variations related to climatic conditions in the Alboran Sea (western Mediterranean) during the last glacial–interglacial transition: the diatom record. *Palaeogeography, Palaeoclimatology, Palaeoecology* **167**, 337–357.

Bearman, G. (Ed.) (2002): Seawater: Its composition, properties and behaviour. Butterworth-Heinemann, Oxford, Second edition 1995 reprinted with corrections 1997, 1999, 2002, 168 pp.

Blackman, R.B. & Tukey, J.W. (1958): The Measurement of Power Spectra from the Point of View of Communication Engineering. Dover Publications, New York, 190 pp.

Blamart, D., Rollion-Bard, C., Cuif, J.-P., Juillet-Leclerc, A., Lutringer, A., van Weering, T.C.E. & Henriet, J.-P. (2005): C and O isotopes in a deep-sea coral (*Lophelia pertusa*) related to skeletal microstructure.

In Freiwald, A. & Roberts, J. (Eds.): Cold-water Corals and Ecosystems, pp. 1005–1020, Springer-Verlag Berlin Heidelberg.

Blamart, D., Rollion-Bard, C., Meibom, A., Cuif, J.-P., Juillet-Leclerc, A. & Dauphin, Y. (2007): Correlation of boron isotopic composition with ultrastructure in the deep-sea coral *Lophelia pertusa*: Implications for biomineralization and paleo-pH. *Geochemistry Geophysics Geosystems* **8**, Q12001, doi:10.1029/2007GC001686.

Böhm, F., Joachimski, M.M., Dullo, W.-Chr., Eisenhauer, A., Lehnert, H., Reitner, J. & Wörheide, G. (2000): Oxygen isotope fractionation in marine aragonite of coralline sponges. *Geochimica et Cosmochimica Acta* **64**, 1695–1703.

Böhm, F., Gussone, N., Eisenhauer, A., Dullo, W.-Chr., Reynaud, S. & Paytan, A. (2006): Calcium isotope fractionation in modern scleractinian corals. *Geochimica et Cosmochimica Acta* **70**, 4452–4462.

Burton, J.D. (1996): The ocean: a global geochemical system. *In* Summerhayes, C.P. & Thorpe, S.A. (Eds.): Oceanography. An illustrated guide, Chapter 11, pp. 165–181, Manson Publishing Ltd.

Cacho, I., Grimalt, J.O., Pelejero, C., Canals, M., Sierro, F.J., Flores, J.A. & Shackleton, N. (1999): Dansgaard-Oeschger and Heinrich event imprints in Alboran Sea paleotemperatures. *Paleoceanography* **14**(6), 698–705.

Cacho, I., Grimalt, J.O., Sierro, F.J., Shackleton, N. & Canals, M. (2000): Evidence for enhanced Mediterranean thermohaline circulation during rapid climatic coolings. *Earth and Planetary Science Letters* **183**, 417–429.

Cacho, I., Grimalt, J.O., Canals, M., Sbaffi, L., Shackleton, N.J., Schönfeld, J. & Zahn, R. (2001): Variability of the western Mediterranean Sea surface temperature during the last 25,000 years and its connection with the Northern Hemisphere climatic changes. *Paleoceanography* **16**(1), 40–52.

Cacho, I., Shackleton, N., Elderfield, H., Sierro, F.J. & Grimalt, J.O. (2006): Glacial rapid variability in deep-water temperature and δ^{18}O from the Western Mediterranean Sea. *Quaternary Science Reviews* **25**, 3294–3311.

Cheng, H., Adkins, J., Edwards, R.L. & Boyle, E.A. (2000): U-Th dating of deep-sea corals. *Geochimica et Cosmochimica Acta* **64**(14), 2401–2416.

Cobb, K.M., Charles, C.D., Cheng, H., Kastner, M. & Edwards, R.L. (2003): U/Th-dating living and young fossil corals from the central tropical Pacific. *Earth and Planetary Science Letters* **210**, 91–103.

Cohen, A.L. & McConnaughey, T.A. (2003): Geochemical Perspectives on Coral Mineralization. *Reviews in Mineralogy and Geochemistry* **54**, 151–187.

Cohen, A.L. & Sohn, R.A. (2004): Tidal modulation of Sr/Ca ratios in a Pacific reef coral. *Geophysical Research Letters* **31**, L16310, doi:10.1029/2004GL020600.

Cohen, A.L., Layne, G.D. & Hart, S.R. (2001): Kinetic control of skeletal Sr/Ca in a symbiotic coral: Implications for the paleotemperature proxy. *Paleoceanography* **16**(1), 20–26.

Cohen, A.L., Owens, K.E., Layne, G.D. & Shimizu, N. (2002): The Effect of Algal Symbionts on the Accuracy of Sr/Ca Paleotemperatures from Coral. *Science* **296**, 331–333.

Cohen, A.L., Smith, S.R., McCartney, M.S. & van Etten, J. (2004): How brain corals record climate: an integration of skeletal structure, growth and chemistry of *Diploria labyrinthiformis* from Bermuda. *Marine Ecology Progress Series* **271**, 147–158.

Cohen, A.L., Gaetani, G.A., Lundälv, T., Corliss, B.H. & George, R.Y. (2006): Compositional variability in a cold-water scleractinian, *Lophelia pertusa*: New insights into "vital effects". *Geochemistry Geophysics Geosystems* **7**, Q12004, doi:10.1029/2006GC001354.

Coplen, T.B., Kendall, C. & Hopple, J. (1983): Comparison of stable isotope reference samples. *Nature* **302**, 236–238.

Cuffey, K.M., Clow, G.D., Alley, R.B., Stuiver, M., Waddington, E.D. & Saltus, R.W. (1995): Large Arctic temperature change at the Wisconsin-Holocene glacial transition. *Science* **270**, 455–458.

Cuif, J.P. & Dauphin, Y. (2005): The Environmental Recording Unit in coral skeletons – a synthesis of structural and chemical evidences for a biochemically driven, stepping-growth process in fibres. *Biogeosciences* **2**, 61–73.

Dansgaard, W. (1964): Stable isotopes in precipitation. *Tellus* **16**, 436–468.

Dauphin, Y. (2001): Comparative studies of skeletal soluble matrices from some Scleractinian corals and Molluscs. *International Journal of Biological Macromolecules* **28**, 293–304.

Dixon, J.E., Clague, D.A. & Stolper, E.M. (1991): Degassing of water, sulfur, and carbon in submarine lavas from Kilauea volcano, Hawaii. *Journal of Geology* **99**, 371–394.

Dorschel, B., Hebbeln, D., Rüggeberg, A., Dullo, W.-Chr. & Freiwald, A. (2005): Growth and erosion of a cold-water coral covered carbonate mound in the Northeast Atlantic during the Late Pleistocene and Holocene. *Earth and Planetary Science Letters* **233**, 33–44.

Duineveld, G.C.A., Lavaleye, M.S.S. & Berghuis, E.M. (2004): Particle flux

and food supply to a seamount cold-water coral community (Galicia Bank, NW Spain). *Marine Ecology Progress Series* **277**, 13–23.

Dullo, W.-Chr., Flögel, S. & Rüggeberg, A. (2008): Cold-water coral growth in relation to the hydrography of the Celtic and Nordic European continental margin. *Marine Ecology Progress Series* **371**, 165–176.

Dymond, J. & Collier, R. (1996): Particulate barium fluxes and their relationships to biological productivity. *Deep-Sea Research II* **43**(4–6), 1283–1308.

Edwards, R.L., Chen, J.H. & Wasserburg, G.J. (1987): ^{238}U-^{234}U-^{230}Th-^{232}Th systematics and the precise measurement of time over the past 500,000 years. *Earth and Planetary Science Letters* **81**, 175–192.

Fadlallah, Y.H. (1983): Sexual reproduction, development and larval biology in scleractinian corals: A review. *Coral Reefs* **2**(3), 129–150.

Farkaŝ, J., Böhm, F., Wallmann, K., Blenkinsop, J., Eisenhauer, A., van Geldern, R., Munnecke, A., Voigt, S. & Veizer, J. (2007): Calcium isotope record of Phanerozoic oceans: Implications for chemical evolution of seawater and its causative mechanisms. *Geochimica et Cosmochimica Acta* **71**, 5117–5134.

Felis, T., Lohmann, G., Kuhnert, H., Lorenz, S.J., Scholz, D., Pätzold, J., Al-Rousan, S. & Al-Moghrabi, S.M. (2004): Increased seasonality in Middle East temperatures during the last interglacial period. *Nature* **429**, 164–168.

Fietzke, J. & Eisenhauer, A. (2006): Determination of temperature-dependent stable strontium isotope (^{88}Sr/^{86}Sr) fractionation via bracketing standard MC-ICP-MS. *Geochemistry Geophysics Geosystems* **7**, Q08009, doi:10.1029/2006GC001243.

Fietzke, J., Liebetrau, V., Günther, D., Gürs, K., Hametner, K., Zumholz, K., Hansteen, T.H. & Eisenhauer, A. (2008): An alternative data acquisition and evaluation strategy for improved isotope ratio precision using LA-MC-ICP-MS applied to stable and radiogenic strontium isotopes in carbonate. *Journal of Analytical Atomic Spectrometry*, doi: 10.1039/b717706b.

Fine, M. & Tchernov, D. (2007): Scleractinian Coral Species Survive and Recover from Decalcification. *Science* **315**, 1811.

de Forges, B.R., Koslow, J.A. & Poore, G.C.B. (2000): Diversity and endemism of the benthic seamount fauna in the southwest Pacific. *Nature* **405**, 944–947.

Fosså, J.H., Mortensen, P.B. & Furevik, D.M. (2002): The deep-water coral *Lophelia pertusa* in Norwegian waters: distribution and fishery impacts. *Hydrobiologia* **471**, 1–12.

Foubert, A. (2007): Nature and significance of the carbonate mound record: The Mound Challenger code. Dissertation, Universiteit Gent, 341 pp.

Frank, N., Paterne, M., Ayliffe, L., van Weering, T., Henriet, J.-P. & Blamart, D. (2004): Eastern North Atlantic deep-sea corals: tracing upper intermediate water Δ^{14}C during the Holocene. *Earth and Planetary Science Letters* **219**, 297–309.

Freiwald, A. (1998): Geobiology of *Lophelia pertusa* (Scleractinia) reefs in the North Atlantic. Habilitation Thesis, Universität Bremen, 116 pp.

Freiwald, A. & Shipboard Scientific Party (2005): Cruise Report, RV Poseidon Cruise 325, Bremerhaven – Tromsø, 12 July – 3 August 2005. – Report.

Freiwald, A. & Shipboard Scientific Party (2006): METEOR Cruise M70, Mediterranean Sea 2006, Leg 1, Deep-water Coral Ecosystems in the Central Mediterranean Sea. – Report.

Freiwald, A., Henrick, R. & Pätzold, J. (1997): Anatomy of a deep-water coral reef mound from Stjernsund, West-Finnmark, Northern Norway. *SEPM, Special Publication* **56**, 141–161.

Freiwald, A., Fosså, J.H., Grehan, A., Koslow, T. & Roberts, J.M. (2004): Cold-water coral reefs. UNEP-WCMC, Cambridge, UK, 84 pp.

Gaetani, G.A. & Cohen, A.L. (2006): Element partitioning during precipitation of aragonite from seawater: A framework for understanding paleoproxies. *Geochimica et Cosmochimica Acta* **70**, 4617–4634.

Gagan, M.K., Ayliffe, L.K., Hopley, D., Cali, J.A., Mortimer, G.E., Chappell, J., McCulloch, M.T. & Head, M.J. (1998): Temperature and Surface-Ocean Water Balance of the Mid-Holocene Tropical Western Pacific. *Science* **279**, 1014–1017.

Gagnon, A.C., Adkins, J.F., Fernandez, D.P. & Robinson, L.F. (2007): Sr/Ca and Mg/Ca vital effects correlated with skeletal architecture in a scleractinian deep-sea coral and the role of Rayleigh fractionation. *Earth and Planetary Science Letters* **261**, 280–295.

Goldstein, S.J., Lea, D.W., Chakraborty, S., Kashgarian, M. & Murrell, M.T. (2001): Uranium-series and radiocarbon geochronology of deep-sea corals: implications for Southern Ocean ventilation rates and the oceanic carbon cycle. *Earth and Planetary Science Letters* **193**, 167–182.

Grootes, P.M. & Stuiver, M. (1997): Oxygen 18/16 variability in Greenland snow and ice with 10^{-3}- to 10^{5}-year time resolution. *Journal of Geophysical Research* **102**(C12), 26455–26470.

Gussone, N., Eisenhauer, A., Heuser, A., Dietzel, M., Bock, B., Böhm, F., Spero, H.J., Lea, D.W., Bijma, J. & Nägler, T.F. (2003): Model for kinetic effects on calcium isotope fractionation (δ^{44}Ca) in inorganic aragonite and cultured planktonic foraminifera. *Geochimica et Cosmochimica Acta* **67**(7), 1375–1382.

Gussone, N., Böhm, F., Eisenhauer, A., Dietzel, M., Heuser, A., Teichert, B.M.A., Reitner, J., Wörheide, G. & Dullo, W.-Chr. (2005): Calcium isotope fractionation in calcite and aragonite. *Geochimica et Cosmochimica Acta* **69**(18), 4485–4494.

Haase-Schramm, A., Böhm, F., Eisenhauer, A., Dullo, W.-Chr., Joachimski, M.M., Hansen, B. & Reitner, J. (2003): Sr/Ca ratios and oxygen isotopes from sclerosponges: Temperature history of the Caribbean mixed layer and thermocline during the Little Ice Age. *Paleoceanography* **18**(3), 1073, doi:10.1029/2002PA000830.

Hamad, N., Millot, C. & Taupier-Letage, I. (2005): A new hypothesis about the surface circulation in the eastern basin of the mediterranean sea. *Progress in Oceanography* **66**, 287–298.

Hart, S.R. & Cohen, A.L. (1996): An ion probe study of annual cycles of Sr/Ca and other trace elements in corals. *Geochimica et Cosmochimica Acta* **60**(16), 3075–3084.

Henrich, R., Freiwald, A., Wehrmann, A., Schäfer, P., Samtleben, C., & Zankl, H. (1996): Nordic cold-water carbonates: Occurrences and controls. *In* Reitner, J., Neuweiler, F. & Gunkel, F. (Eds.): Global and regional controls on biogenic sedimentation, I, Reef Evolution, Research Reports. – Göttinger Arb. Geol. Paläontol., pp. 35–52.

Hippler, D., Schmitt, A.-D., Gussone, N., Heuser, A., Stille, P., Eisenhauer, A. & Nägler, T.F. (2003): Calcium Isotopic Composition of Various Reference Materials and Seawater. *Geostandards Newsletter* **27**(1), 13–19.

Jarosewich, E. (2002): Smithsonian microbeam standards. *Journal of Research of the National Institute of Standards and Technology* **107**, 681–685.

Jarosewich, E. & MacIntyre, I.G. (1983): Carbonate reference samples for electron microprobe and scanning electron microscope analyses. *Journal of Sedimentary Petrology* **52**(2), 677–678.

Jarosewich, E., Nelen, J.A. & Norbers, J.A. (1980): Reference samples for electron microprobe analysis. *Geostandards Newsletter* **4**(1), 43–47.

Jones, C.E. & Jenkyns, H.C. (2001): Seawater strontium isotopes, oceanic anoxic

events, and seafloor hydrothermal activity in the Jurassic and Cretaceous. *American Journal of Science* **301**, 112–149.

Kinsman, D.J.J. & Holland, H.D. (1969): The co-precipitation of cations with $CaCO_3$–IV. The co-precipitation of Sr^{2+} with aragonite between 16° and 96°C. *Geochimica et Cosmochimica Acta* **33**, 1–17.

Kiriakoulakis, K., Bett, B.J., White, M. & Wolff, G.A. (2004): Organic biogeochemistry of the Darwin Mounds, a deep-water coral ecosystem, of the NE Atlantic. *Deep-Sea Research I* **51**, 1937–1954.

Kiriakoulakis, K., Fisher, E., Wolff, G.A., Freiwald, A., Grehan, A. & Roberts, J.M. (2005): Lipids and nitrogen isotopes of two deep-water corals from the North-East Atlantic: initial results and implications for their nutrition. *In* Freiwald, A. & Roberts, J. (Eds.): Cold-water Corals and Ecosystems, pp. 715–729, Springer-Verlag Berlin Heidelberg.

Lacombe, H., Tchernia, P. & Gamberoni, L. (1985): Variable Bottom Water in the Western Mediterranean Basin. *Progress in Oceanography* **14**, 319–338.

Lea, D.W. (2003): Elemental and Isotopic Proxies of Past Ocean Temperatures. *In* Elderfield, H. (Ed.): The Oceans and Marine Geochemistry Vol. 6 Treatise on Geochemistry (Eds. H.D. Holland and K.K. Turekian), pp. 365–390, Elsevier-Pergamon, Oxford.

Lutringer, A., Blamart, D., Frank, N. & Labeyrie, L. (2005): Paleotemperatures from deep-sea corals: scale effects. *In* Freiwald, A. & Roberts, J. (Eds.): Cold-water Corals and Ecosystems, pp. 1081–1096, Springer-Verlag Berlin Heidelberg.

Malakoff, D. (2003): Deep-Sea Science: Cool Corals Become Hot Topic. *Science* **299**, 195.

Mangini, A., Lomitschka, M., Eichstädter, R., Frank, N., Vogler, S., Bonani, G., Hajdas, I. & Pätzold, J. (1998): Coral provides way to age deep water. *Nature* **392**, 347–348.

McConnaughey, T.A. (2003): Sub-equilibrium oxygen-18 and carbon-13 levels in biological carbonates: carbonate and kinetic models. *Coral Reefs* **22**, 316–327.

McCulloch, M.T., Taviani, M., Montagna, P., Mortimer, G. & Remia, A. (2006): Proliferation and demise of Mediterranean deep-sea corals. *Geochimica et Cosmochimica Acta* **70**(18), Suppl. 1, A407.

Meibom, A., Cuif, J.-P., Hillion, F., Constantz, B.R., Juillet-Leclerc, A., Dauphin, Y., Watanabe, T. & Dunbar, R.B. (2004): Distribution of magnesium in coral skeleton. *Geophysical Research Letters* **31**, L23306, doi:10.1029/2004GL021313.

Meibom, A., Yurimoto, H., Cuif, J.-P., Domart-Coulon, I., Houlbreque, F., Constantz, B., Dauphin, Y., Tambutté, E., Tambutté, S., Allemand, D., Wooden, J. & Dunbar, R. (2006): Vital effects in coral skeletal composition display strict three-dimensional control. *Geophysical Research Letters* **33**, L11608, doi:10.1029/2006GL025968.

Meibom, A., Mostefaoui, S., Cuif, J.-P., Dauphin, Y., Houlbreque, F., Dunbar, R. & Constantz, B. (2007): Biological forcing controls the chemistry of reef-building coral skeleton. *Geophysical Research Letters* **34**, L02601, doi:10.1029/2006GL028657.

Mikkelsen, N., Erlenkeuser, H., Killingley, J.S. & Berger, W.H. (1982): Norwegian corals: radiocarbon and stable isotopes in *Lophelia pertusa*. *Boreas* **11**(2), 163–171.

Millero, F.J., Feistel, R., Wright, D.G. & McDougall, T.J. (2008): The composition of standard seawater and the definition of the reference-composition salinity scale. *Deep-Sea Research I* **55**, 50–72.

Millot, C. (1999): Circulation in the Western Mediterranean Sea. *Journal of Marine Systems* **20**, 423–442.

Millot, C. & Taupier-Letage, I. (2005): Circulation in the Mediterranean Sea. *In* Saliot, A. (Ed.): The Handbook of Environmental Chemistry, 5 (K), pp. 29–66, Springer-Verlag, Heidelberg.

Montagna, P., McCulloch, M., Taviani, M., Remia, A. & Rouse, G. (2005): High-resolution trace and minor element compositions in deep-water scleractinian corals (*Desmophyllum dianthus*) from the Mediterranean Sea and the Great Australian Bight. *In* Freiwald, A. & Roberts, J. (Eds.): Cold-water Corals and Ecosystems, pp. 1109–1126, Springer-Verlag Berlin Heidelberg.

Montagna, P., McCulloch, M., Taviani, M., Mazzoli, C. & Vendrell, B. (2006): Phosphorous in Cold-Water Corals as a Proxy for Seawater Nutrient Chemistry. *Science* **312**, 1788–1791.

Montagna, P., Silenzi, S., Devoti, C., Mazzoli, C., McCulloch, M., Scicchitano, G. & Taviani, M. (2008): Climate Reconstructions and Monitoring in the Mediterranean Sea: A Review on Some Recently Discovered High-Resolution Marine Archives. *Rendiconti Lincei* **19**, 121–140.

Mortensen, P.B. & Rapp, H.T. (1998): Oxygen and carbon isotope ratios related to growth line patterns in skeletons of *Lophelia pertusa* (L) (anthozoa, scleractinia): Implications for determination of linear extension rates. *Sarsia* **83**, 433–446.

Nägler, T.F., Eisenhauer, A., Müller, A., Hemleben, C. & Kramers, J.

(2000): The δ^{44}Ca-temperature calibration on fossil and cultured *Globigerinoides sacculifer*: New tool for reconstruction of past sea surface temperatures. *Geochemistry Geophysics Geosystems* **1**, Paper number 2000GC000091.

Ohde, S., Ohta, N. & Tomura, K. (1978): Determination of trace elements in carbonates by instrumental neutron activation analysis. *Journal of Radioanalytical Chemistry* **42**, 159–167.

Orr, J.C., Fabry, V.J., Aumont, O., Bopp, L., Doney, S.C., Feely, R.A., Gnanadesikan, A., Gruber, N., Ishida, A., Joos, F., Key, R.M., Lindsay, K., Maier-Reimer, E., Matear, R., Monfray, P., Mouchet, A., Najjar, R.G., Plattner, G.-K., Rodgers, K.B., Sabine, C.L., Sarmiento, J.L., Schlitzer, R., Slater, R.D., Totterdell, I.J., Weirig, M.-F., Yamanaka, Y. & Yool, A. (2005): Anthropogenic ocean acidification over the twenty-first century and its impact on calcifying organisms. *Nature* **437**, 681–686.

Pérez-Folgado, M., Sierro, F.J., Flores, J.A., Cacho, I., Grimalt, J.O., Zahn, R. & Shackleton, N. (2003): Western Mediterranean planktonic foraminifera events and millennial climatic variability during the last 70 kyr. *Marine Micropaleontology* **48**, 49–70.

Pfannkuche, O. & Shipboard Scientific Party (2004): Geobiological investigations of aphotic coral reef ecosystems in the NE- Skagerrak, RV ALKOR cruise AL232, Kiel – Strömstad (Sweden) – Kiel, 30.10. – 11.11.2003. IFM-GEOMAR. – Report (unpubl.).

Pierre, C., Vergnaud Grazzini, C., Thouron, D. & Saliège, J.-F. (1986): Compositions isotopiques de l'oxygène et du carbone des masses d'eau en Méditerranée. *Memorie della Società Geologica Italiana* **36**, 165–174.

Pingitore, N.E., Meitzner, G. & Love, K.M. (1995): Identification of sulfate in natural carbonates by X-ray absorption spectroscopy. *Geochimica et Cosmochimica Acta* **59**(12), 2477–2483.

Piva, A., Asioli, A., Andersen, N., Grimalt, J.O., Schneider, R.R. & Trincardi, F. (2008a): Climatic cycles as expressed in sediments of the PROMESS1 borehole PRAD1-2, central Adriatic, for the last 370 ka: 2. Paleoenvironmental evolution. *Geochemistry Geophysics Geosystems* **9**(3), Q03R02, doi:10.1029/2007GC001785.

Piva, A., Asioli, A., Trincardi, F., Schneider, R.R. & Vigliotti, L. (2008b): Late-Holocene climate variability in the Adriatic Sea (Central Mediterranean). *The Holocene* **18**(1), 153–167.

Rahmstorf, S. (2002): Ocean circulation and climate during the past 120,000 years. *Nature* **419**, 207–214.

Reay, A., Johnstone, R.D. & Kawachi, Y. (1993): Anorthoclase, a second microbeam standard from Kakanui, New Zealand. *Geostandards Newsletter* **17**(1), 135–136.

Reveillaud, J., Freiwald, A., Van Rooij, D., Le Guilloux, E., Altuna, A., Foubert, A., Vanreusel, A., Olu-Le Roy, K. & Henriet, J.-P. (2008): The distribution of scleractinian corals in the Bay of Biscay, NE Atlantic. *Facies* **54**, 317–331.

Roberts, J.M., Long, D., Wilson, J.B., Mortensen, P.B. & Gage, J.D. (2003): The cold-water coral *Lophelia pertusa* (Scleractinia) and enigmatic seabed mounds along the north-east Atlantic margin: are they related? *Marine Pollution Bulletin* 46, 7–20.

Roberts, J.M., Wheeler, A.J. & Freiwald, A. (2006): Reefs of the Deep: The Biology and Geology of Cold-Water Coral Ecosystems. *Science* **312**, 543–547.

Rogers, A.D. (1999): The biology of *Lophelia pertusa* (Linnaeus 1758) and other deep-water reef-forming corals and impacts from human activities. *International Review of Hydrobiology* **84**, 315–406.

Romanek, C.S., Grossman, E.L. & Morse, J.W. (1992): Carbon isotopic fractionation in synthetic aragonite and calcite: Effects of temperature and precipitation rate. *Geochimica et Cosmochimica Acta* **56**, 419–430.

Rüggeberg, A. & Form, A. (Eds.) (2007): FS ALKOR Fahrtbericht / Cruise Report AL 275, Geobiological investigations and sampling of aphotic coral reef ecosystems in the NE- Skagerrak, Kiel – Kiel, 24.03. – 30.03.2006. – IFM-GEOMAR-REPORT Nr. 10.

Rüggeberg, A., Dullo, W.-Chr., Dorschel, B. & Hebbeln, D. (2007): Environmental changes and growth history of a cold-water carbonate mount (Propeller Mound, Porcupine Seabight). *International Journal of Earth Sciences* **96**(1), 57–72.

Rüggeberg, A., Fietzke, J., Liebetrau, V., Eisenhauer, A., Dullo, W.-Chr. & Freiwald, A. (2008): Stable strontium isotopes ($\delta^{88/86}$Sr) in cold-water corals - A new proxy for reconstruction of intermediate ocean water temperatures. *Earth and Planetary Science Letters* **269**, 570–575.

Schmidt, G.A., Bigg, G.R.. & Rohling, E.J. (1999): Global Seawater Oxygen-18 Database. *URL: http://data.giss.nasa.gov/o18data/*

Schröder-Ritzrau, A., Mangini, A. & Lomitschka, M. (2003): Deep-sea corals evidence periodic reduced ventilation in the North Atlantic during the LGM/Holocene transition. *Earth and Planetary Science Letters* **216**, 399–410.

Shirai, K., Kusakabe, M., Nakai, S., Ishii, T., Watanabe, T., Hiyagon, H. & Sano, Y. (2005): Deep-sea coral geochemistry: Implication for the vital effect. *Chemical Geology* **224**, 212–222.

Sinclair, D.J., Kinsley, L.P.J. & McCulloch, M.T. (1998): High resolution analysis of trace elements in corals by laser ablation ICP-MS. *Geochimica et Cosmochimica Acta* **62**(11), 1889–1901.

Sinclair, D.J., Sherwood, O.A., Risk, M.J., Hillaire-Marcel, C., Tubrett, M., Sylvester, P., McCulloch, M. & Kinsley, L. (2005): Testing the reproducibility of Mg/Ca profiles in the deep-water coral *Primnoa resedaeformis*: putting the proxy through its paces. *In* Freiwald, A. & Roberts, J. (Eds.): Cold-water Corals and Ecosystems, pp. 1039–1060, Springer-Verlag Berlin Heidelberg.

Sinclair, D.J., Williams, B. & Risk, M. (2006): A biological origin for climate signals in corals - Trace element "vital effects" are ubiquitous in Scleractinian coral skeletons. *Geophysical Research Letters* **33**, L17707, doi:10.1029/2006GL027183.

Skarđhamar, J. & Svendsen, H. (2005): Circulation and shelf-ocean interaction off North Norway. *Continental Shelf Research* **25**, 1541–1560.

Smith, J.E., Schwarcz, H.P., Risk, M.J., McConnaughey, T.A. & Keller, N. (2000): Paleotemperatures From Deep-Sea Corals: Overcoming 'Vital Effects'. *Palaios* **15**, 25–32.

Smith, J.E., Schwarcz, H.P. & Risk, M.J. (2002): Patterns of isotopic disequilibria in azooxanthellate coral skeletons. *Hydrobiologia* **471**, 111–115.

Squires, D.F. (1957): New species of caryophylliid corals from the Gulf Coast Tertiary. *Journal of Paleontology* **31**, 992–996.

Stenni, B., Nichetto, P., Bregant, D., Scarazzato, P. & Longinelli, A. (1995): The δ^{18}O signal of the northward flow of Mediterranean waters in the Adriatic Sea. *Oceanologica Acta* **18**(3), 319–328.

Stoll, H.M. & Schrag, D.P. (1998): Effects of Quaternary sea level cycles on strontium in seawater. *Geochimica et Cosmochimica Acta* **62**(7), 1107–1118.

Stuiver, M. & Grootes, P.M. (2000): GISP2 Oxygen Isotope Ratios. *Quaternary Research* **53**, 277-284.

Taviani, M., Freiwald, A. & Zibrowius, H. (2005a): Deep coral growth in the Mediterranean Sea: an overview. *In* Freiwald, A. & Roberts, J. (Eds.): Cold-water Corals and Ecosystems, pp. 137–156, Springer-Verlag Berlin Heidelberg.

Taviani, M., Remia, A., Corselli, C., Freiwald, A., Malinverno, E., Mastrototaro, F., Savini, A. & Tursi, A. (2005b): First geo-marine survey of

living cold-water *Lophelia* reefs in the Ionian Sea (Mediterranean basin). *Facies* **50**, 409–417.

Taviani, M., Correa, M.L., Zibrowius, H., Montagna, P., McCulloch, M. & Ligi, M. (2007): Last glacial deep-water corals from the Red Sea. *Bulletin of Marine Science* **81**(3), 361–370.

Turekian, K.K. & Bacon, M.P. (2003): Geochronometry of Marine Deposits. *In* Elderfield, H. (Ed.): The Oceans and Marine Geochemistry Vol. 6 Treatise on Geochemistry (Eds. H.D. Holland and K.K. Turekian), pp. 321–341, Elsevier-Pergamon, Oxford.

de Villiers, S. (1999): Seawater strontium and Sr/Ca variability in the Atlantic and Pacific oceans. *Earth and Planetary Science Letters* **171**, 623–634.

de Villiers, S., Shen, G.T. & Nelson, B.K. (1994): The Sr/Ca-temperature relationship in coralline aragonite: Influence of variability in $(Sr/Ca)_{seawater}$ and skeletal growth parameters. *Geochimica et Cosmochimica Acta* **58**, 197–208.

Waller, R.G. (2005): Deep-water Scleractinia (Cnidaria: Anthozoa): current knowledge of reproductive processes. *In* Freiwald, A. & Roberts, J. (Eds.): Cold-water Corals and Ecosystems, pp. 691–700, Springer-Verlag Berlin Heidelberg.

Wheeler, A.J., Beyer, A., Freiwald, A., de Haas, H., Huvenne, V.A.I., Kozachenko, M., Olu-Le Roy, K. & Opderbecke, J. (2007): Morphology and environment of cold-water coral carbonate mounds on the NW European margin. *International Journal of Earth Sciences* **96**(1), 37–56.

White, M., Mohn, C., de Stigter, H. & Mottram, G. (2005): Deep-water coral development as a function of hydrodynamics and surface productivity around the submarine banks of the Rockall Trough, NE Atlantic. *In* Freiwald, A. & Roberts, J. (Eds.): Cold-water Corals and Ecosystems, pp. 503–514, Springer-Verlag Berlin Heidelberg.

Willenz, P., Andre, L., Blust, R., Dehairs, F. & Dubois, P. (Eds.) (2006): Validation of alternative marine calcareous skeletons as recorders of global climate changes (CALMARS). Scientific Support Plan for a Sustainable Development Policy (SPSD II), Part 2: Global change, Ecosystems and Biodiversity, Belgian Science Policy, Brussels, 133 pp. – Report.

Zibrowius, H. (1980): Les scléractiniaires des la Méditerranée et de l'Atlantique nord-oriental. *Mémoires de l'Institut océanographique, Monaco* **11**, 1–284.

List of Figures

List of Tables

A Appendices

A.1 Lists of Stations and Samples

Station List

Table A.1: List of M70/1-, AL275-, and P325-stations.

Cruise & Station	Area	Coordinates at Bottom			Type of Sample
		Lat. [°N]	Long. [°E]	Depth	
M70/1-655	Malta Trough	35°50.802'	14°05.294'	1000 m	Water, CTD
M70/1-668-2	Linosa Trough	35°46.740'	12°59.120'	372 m	GKG
M70/1-669-1	Linosa Trough	35°46.510'	12°59.790'	362 m	GKG
M70/1-675	Malta Trough	36°28.776'	13°15.780'	1694 m	Water, CTD
M70/1-677	Urania Bank	36°50.340'	13°09.390'	644 m	Coral
M70/1-678	Urania Bank	36°50.344'	13°09.303'	615 m	Water, CTD
M70/1-679-2	Urania Bank	36°50.365'	13°09.344'	643 m	GKG
M70/1-705	SML	39°20.429'	18°30.808'	1013 m	Water, CTD
M70/1-708	SML	39°37.291'	18°04.815'	823 m	Water, CTD
M70/1-709	SML	39°37.260'	18°04.719'	871 m	Water, CTD
M70/1-710-2	SML	39°36.762'	18°04.726'	977 m	GKG
M70/1-712-1	SML	39°37.500'	18°04.998'	584 m	GKG
M70/1-721	SML	39°33.888'	18°27.123'	633 m	Coral, Water
M70/1-722	SML Transect	39°08.902'	18°05.441'	2482 m	Water, CTD
M70/1-723	SML Transect	39°23.757'	18°20.227'	1195 m	Water, CTD
M70/1-724	SML Transect	39°27.934'	18°24.190'	764 m	Water, CTD
M70/1-725	SML Transect	39°32.193'	18°26.181'	627 m	Water, CTD
M70/1-726	SML Transect	39°36.315'	18°27.343'	624 m	Water, CTD
M70/1-727	SML Transect	39°39.361'	18°28.457'	466 m	Water, CTD
M70/1-728	SML	39°33.298'	18°27.385'	623 m	Water
M70/1-735	Bari Canyon	41°17.477'	17°16.624'	663 m	Water
M70/1-736	Bari Seamount	41°30.036'	17°30.531'	1079 m	Water, CTD
M70/1-740	Bari Seamount	41°34.642'	17°28.018'	1167 m	Water, CTD
M70/1-745	Bari Seamount	41°17.810'	17°10.470'	557 m	Water
M70/1-746	Bari Canyon	41°19.499'	17°04.022'	195 m	Water, CTD
M70/1-747	Bari Canyon	41°18.976'	17°07.003'	417 m	Water, CTD
M70/1-748	Bari Canyon	41°18.498'	17°10.025'	524 m	Water, CTD
M70/1-749	Bari Canyon	41°18.000'	17°14.009'	629 m	Water, CTD
M70/1-750	Bari Canyon	41°16.983'	17°24.016'	874 m	Water, CTD
M70/1-752	Gondola Slide	41°43.510'	17°02.780'	710 m	Coral, Water

Cruise & Station	**Area**	**Coordinates at Bottom**			**Type of Sample**
		Lat. [°N]	**Long. [°E]**	**Depth**	
AL275-420-1#59	East Søster Isl.	59°05.770'	10°47.910'	x	Water
AL275-425-2#62	East Søster Isl.	59°05.900'	10°50.000'	x	Water
AL275-425-2#63	East Søster Isl.	59°05.700'	10°47.900'	x	Water
P325-383-2	Sveinsgrunnen	69°43.009'	16°07.477'	x	Water
P325-386-2	Sveinsgrunnen	69°42.457'	16°14.020'	x	Water
P325-373-2	Røst Reef	67°31.510'	09°29.402'	x	Water

Coral Samples

Table A.2: List of cold-water coral samples.

Sample ID	**Area**	**Lat.** [°N]	**Long.** [°E]	**Depth**	**Species**	**Age**[a] [YBP]
SE06-13L[b]	Bari Canyon	41°22.060'	17°06.720'	423 m	*Lophelia pertusa*	17550±56
CR-22L[c]	Santa Maria di Leuca	39°50.000'	17°37.750'	1102 m	*Lophelia pertusa*	12435±76
M70/1-721 Dive-106 (RED)	Santa Maria di Leuca	39°33.888'	18°27.123'	633 m	*Lophelia pertusa* (RED)	x
M70/1-721 Dive-106 (WHITE)	Santa Maria di Leuca	39°33.888'	18°27.123'	633 m	*Lophelia pertusa* (WHITE)	x
M70/1-752 Dive-111	Gondola Slide	41°43.510'	17°02.780'	710 m	*Lophelia pertusa*	x
M70/1-677 Dive-100	Urania Bank	36°50.340'	13°09.390'	644 m	*Lophelia pertusa*	x

a U/Th-Dating by Malcolm McCulloch (ANU-RSES, Canberra) in 2006/2007
b collected by Marco Taviani (CNR-ISMAR, Bologna) during R/V Urania cruise SETE-06.
c collected by Marco Taviani (CNR-ISMAR, Bologna) during R/V Urania cruise CORSARO.

Box Corer Samples

Table A.3: List of box corer (GKG) samples used in this study.

Sample ID	**Area**	**Lat.** [°N]	**Long.** [°E]	**Depth**	**Remarks**
M70/1-668-2	Linosa Trough	35°46.740'	12°59.120'	372 m	Recovery: 55 cm; hemipelagic sediment
M70/1-669-1	Linosa Trough	35°46.510'	12°59.790'	362 m	Recovery: 44 cm; hemipelagic sediment, one piece of *Madrepora*
M70/1-679-2	Urania Bank	36°50.365'	13°09.344'	643 m	Recovery: >55 cm; overpenetration, hemipelagic sediment
M70/1-710-2	Santa Maria di Leuca	39°36.762'	18°04.726'	977 m	Recovery: 32 cm; hemipelagic sediment with very few coral fragments
M70/1-712-1	Santa Maria di Leuca	39°37.500'	18°04.998'	584 m	Recovery: 32 cm; hemipelagic sediment

Water Samples

Table A.4: List of analyzed water samples. $\delta^{18}O_{sw}$ is in ‰ SMOW.

Cruise & Station	**Observations**				**Type of Analysis**
	Depth	**T [°C]**	**S [psu]**	$\delta^{18}\mathbf{O}_{sw}$	
M70/1-655	1007 m	13.85	38.68	1.29	ICP-MS, ICP-OES
M70/1-655	250 m	14.69	38.74	1.27	ICP-MS, ICP-OES
M70/1-655	100 m	16.25	38.11	1.21	ICP-OES
M70/1-675	1728 m	14.00	38.68	x	ICP-OES
M70/1-678	623 m	13.98	38.70	1.24	ICP-MS, ICP-OES
M70/1-678	620 m	13.98	38.71	1.26	ICP-OES
M70/1-705	1015 m	13.60	38.65	x	ICP-OES
M70/1-705	1000 m	13.61	38.65	x	ICP-OES
M70/1-705	920 m	13.67	38.65	x	ICP-OES
M70/1-705	880 m	13.73	38.64	x	ICP-OES
M70/1-705	500 m	13.90	38.68	x	ICP-OES
M70/1-705	200 m	14.27	38.71	x	ICP-MS, ICP-OES
M70/1-705	50 m	15.34	38.27	x	ICP-OES
M70/1-705	20 m	23.30	38.04	x	ICP-OES
M70/1-708 Dive-105	823 m	13.76_{ROV}	38.67_{ROV}	x	ICP-MS, ICP-OES
M70/1-709	882 m	13.75	38.66	x	ICP-OES
M70/1-709	600 m	13.71	38.66	x	ICP-OES
M70/1-709	460 m	13.80	38.67	x	ICP-OES
M70/1-709	280 m	14.06	38.71	x	ICP-OES
M70/1-709	50 m	15.34	38.48	x	ICP-OES
M70/1-709	20 m	22.15	37.82	x	ICP-OES
M70/1-721 Dive-106	633 m	13.58_{ROV}	38.66_{ROV}	1.39	ICP-OES
M70/1-722	2513 m	13.87	38.65	1.20	ICP-OES
M70/1-723	1198 m	13.61	38.64	1.18	ICP-MS, ICP-OES
M70/1-724	760 m	13.60	38.65	1.19	ICP-OES
M70/1-725	624 m	13.63	38.66	1.09	ICP-OES
M70/1-726	620 m	13.59	38.65	x	ICP-OES
M70/1-727	456 m	13.69	38.65	1.18	ICP-OES
M70/1-728 Dive-107	623 m	13.60_{ROV}	38.66_{ROV}	1.38	ICP-OES
M70/1-735 Dive-108	663 m	13.54_{ROV}	38.64_{ROV}	1.33	ICP-OES
M70/1-736	1078 m	13.12	38.61	x	ICP-OES
M70/1-740	1068 m	13.08	38.61	x	ICP-OES
M70/1-745 Dive-110	557 m	13.58_{ROV}	38.64_{ROV}	1.37	ICP-OES
M70/1-746	188 m	13.93	38.66	1.14	ICP-OES
M70/1-747	408 m	13.63	38.63	1.03	ICP-OES
M70/1-748	518 m	13.55	38.62	1.13	ICP-OES
M70/1-749	620 m	13.55	38.63	1.32	ICP-OES
M70/1-750	874 m	13.22	38.61	1.36	ICP-OES
M70/1-752 Dive-111	710 m	13.46_{ROV}	38.63_{ROV}	1.40	ICP-OES

Cruise & Station	**Observations**				**Type of Analysis**
	Depth	**T [°C]**	**S [psu]**	$\delta^{18}\mathbf{O}_{sw}$	
AL275-420-1#59	85 m	7.00	35.20	x	ICP-MS, ICP-OES
AL275-425-2#62	25 m	6.70	34.50	x	ICP-MS, ICP-OES
AL275-425-2#63	10 m	2.10	28.40	x	ICP-MS, ICP-OES
P325-383-2	593 m	4.10	35.08	x	ICP-MS, ICP-OES
P325-386-2	175 m	7.45	34.84	x	ICP-MS, ICP-OES
P325-373-2	298 m	7.06	35.25	x	ICP-MS, ICP-OES

A.2 Tables for Analytical Assessment

Accuracy of the EPMA

Table A.5: % deviation between analyzed and published standard values for EPMA-analyses.

Oxid	**Calcite USNM 136321**			**Reference**
	$\bar{\mu}\pm1\sigma$; N=30	publ.	dev. [%]	
CaO [wt.%]	55.28±1.46	56.10	-1.46	Jarosewich & MacIntyre (1983)
CO_2 [wt.%]	44.57±1.44	44.01	+1.27	Jarosewich & MacIntyre (1983)

Oxid	**VG-2 USNM 111240**			**Reference**
	$\bar{\mu}\pm1\sigma$; N=30	publ.	dev. [%]	
CaO [wt.%]	10.99±0.12	11.12	-1.18	Jarosewich et al. (1980)
MgO [wt.%]	6.79±0.10	6.71	+1.19	Jarosewich et al. (1980)
SrO [wt.%]	0.106±0.009	x	x	x
SO_3 [wt.%]	0.316±0.012	0.335	-5.48	Dixon et al. (1991)

Oxid	**KAN-1**			**Reference**
	$\bar{\mu}\pm1\sigma$; N=30	publ.	dev. [%]	
CaO [wt.%]	0.609±0.027	0.540	+12.7	Reay et al. (1993)
SrO [wt.%]	0.257±0.009	0.267	-3.92	Reay et al. (1993)

Oxid	**A-2 Modern Coral Standard**			**Reference**
	$\bar{\mu}\pm1\sigma$; N=19	publ.	dev. [%]	
CaO [wt.%]	52.79±0.53	x	x	x
MgO [wt.%]	0.126±0.025	x	x	x
SrO [wt.%]	0.432±0.012	0.946	-54.3	Ohde et al. (1978)
SO_3 [wt.%]	0.334±0.032	x	x	x

Accuracy of the ICP-MS

Table A.6: % deviation between analyzed (ICP-MS) and published IAPSO seawater standard values.

Element	**IAPSO**			**Reference**
	$\bar{\mu}\pm1\sigma$; N=2	publ.	dev. [%]	
^{7}Li [μg/l]	181±3.25	174	+4.02	Burton (1996)
^{85}Rb [μg/l]	132±1.48	120	+10.0	Burton (1996)
^{86}Sr [μg/l]	8696±466	7950	+9.38	Millero et al. (2008)
^{98}Mo [μg/l]	12.8±0.35	x	x	x
^{121}Sb [μg/l]	0.251±0.001	x	x	x
^{133}Cs [μg/l]	0.306±0.001	0.290	+5.66	Burton (1996)
^{138}Ba [μg/l]	154±0.85	14.0	+1000	Burton (1996)
^{238}U [μg/l]	3.05±0.07	3.30	-7.70	Burton (1996)

Precision of the ICP-MS

Table A.7: Relative standard deviation (RSD, 1σ) in % to assess the precision of the ICP-MS measurements.

Element	**M70/1-723, 1198 m**			
		Rep.1	Rep.2	RSD [%]
^{7}Li [μg/l]	201	183	182	4.76
^{85}Rb [μg/l]	134	139	136	1.71
^{86}Sr [μg/l]	9210	9497	9283	1.31
^{98}Mo [μg/l]	13.5	14.1	13.9	1.57
^{121}Sb [μg/l]	0.230	0.239	0.239	1.84
^{133}Cs [μg/l]	0.328	0.334	0.337	1.11
^{138}Ba [μg/l]	8.81	8.67	8.89	1.01
^{238}U [μg/l]	3.57	3.59	3.61	0.54

Accuracy of the ICP-OES (Concentrations)

Table A.8: % deviation between analyzed (ICP-OES) and published IAPSO seawater standard concentrations.

Element	**IAPSO**			**Reference**
	$\bar{\mu}\pm1\sigma$; N=16	publ.	dev. [%]	
Ca [mg/l]	412±10.3	412	-0.02	Millero et al. (2008)
Mg [mg/l]	1333±31.1	1284	+3.84	Millero et al. (2008)
Sr [μg/l]	7761±216	7950	-2.38	Millero et al. (2008)
B [μg/l]	5266±145	4489	+17.3	Millero et al. (2008)
Ba [μg/l]	151±10.6	14.0	+979	Burton (1996)

Precision of the ICP-OES (Concentrations)

Table A.9: Relative standard deviation (RSD, 1σ) in % to assess the precision of the ICP-OES measurements for element concentrations.

Element	**M70/1-655, 1007 m**				**M70/1-705, 920 m**			
1:50		Rep.1	Rep.2	RSD [%]		Rep.1	Rep.2	RSD [%]
Ca [μg/l]	9206	8938	8955	1.66	9210	8282	8852	5.33
Mg [μg/l]	29350	28657	28655	1.39	29460	26609	28267	5.09
Sr [μg/l]	173	168	168	1.90	173	154	165	5.80
B [μg/l]	104	101	101	2.01	101	94.5	98.4	3.14
Ba [μg/l]	0.0499	0.353	0.214	73.8	0.117	0.791	0.331	83.5

Element	**M70/1-709, 50 m**				**M70/1-735, 663 m**			
1:50		Rep.1	Rep.2	RSD [%]		Rep.1	Rep.2	RSD [%]
Ca [μg/l]	8259	8693	9137	5.05	8533	9290	9159	4.50
Mg [μg/l]	26629	28000	29191	4.59	27477	29769	29191	4.14
Sr [μg/l]	154	163	171	5.24	159	175	171	4.74
B [μg/l]	95.4	100	99.1	2.46	99.8	102	103	2.13
Ba [μg/l]	0.816	0.570	0.089	75.1	0.687	0.076	0.119	116

Element	**AL275-425-2#62, 25 m**			
1:50		Rep.1	Rep.2	RSD [%]
Ca [μg/l]	7470	7507	7616	1.00
Mg [μg/l]	23938	24072	24300	0.76
Sr [μg/l]	140	141	143	0.93
B [μg/l]	85.8	84.6	87.3	1.58
Ba [μg/l]	0.440	0.594	0.026	83.0

Accuracy of the ICP-OES (Ratios)

Table A.10: % deviation between analyzed (ICP-OES) and published IAPSO seawater standard ratios.

Ratio	**IAPSO**			**Reference**
	$\bar{\mu}\pm1\sigma$; N=16	publ.	dev. [%]	
Mg/Ca [mol/mol]	5.29±0.02	5.14	+2.94	Millero et al. (2008)
Sr/Ca [mmol/mol]	8.54±0.03	8.82	-3.19	Millero et al. (2008)
B/Ca [mmol/mol]	47.5±1.07	40.4	+17.7	Millero et al. (2008)
Ba/Ca [μmol/mol]	109±9.50	9.92	+1000	Burton (1996)

Precision of the ICP-OES (Ratios)

Table A.11: Relative standard deviation (RSD, 1σ) in % to assess the precision of the ICP-OES measurements for element ratios.

Ratio	**M70/1-655, 1007 m**				**M70/1-705, 920 m**			
		Rep.1	Rep.2	RSD [%]		Rep.1	Rep.2	RSD [%]
Mg/Ca [mol/mol]	5.21	5.24	5.23	0.28	5.23	5.25	5.22	0.31
Sr/Ca [mmol/mol]	8.54	8.53	8.49	0.32	8.54	8.46	8.47	0.53
B/Ca [mmol/mol]	42.0	41.9	41.6	0.50	40.3	42.2	41.1	2.33
Ba/Ca [μmol/mol]	6.55	16.2	11.8	42.0	8.61	32.2	15.6	64.3

Ratio	**M70/1-709, 50 m**				**M70/1-735, 663 m**			
		Rep.1	Rep.2	RSD [%]		Rep.1	Rep.2	RSD [%]
Mg/Ca [mol/mol]	5.27	5.27	5.23	0.49	5.27	5.24	5.21	0.50
Sr/Ca [mmol/mol]	8.46	8.50	8.49	0.23	8.48	8.53	8.48	0.33
B/Ca [mmol/mol]	42.7	42.5	40.0	3.60	42.9	40.7	41.5	2.67
Ba/Ca [μmol/mol]	33.1	23.6	7.80	59.4	27.9	7.33	8.70	78.5

Ratio	**AL275-425-2#62, 25 m**			
		Rep.1	Rep.2	RSD [%]
Mg/Ca [mol/mol]	5.24	5.24	5.22	0.26
Sr/Ca [mmol/mol]	8.52	8.51	8.51	0.09
B/Ca [mmol/mol]	42.5	41.7	42.4	1.08
Ba/Ca [μmol/mol]	21.9	27.5	5.99	60.4

A.3 Results

Mappings

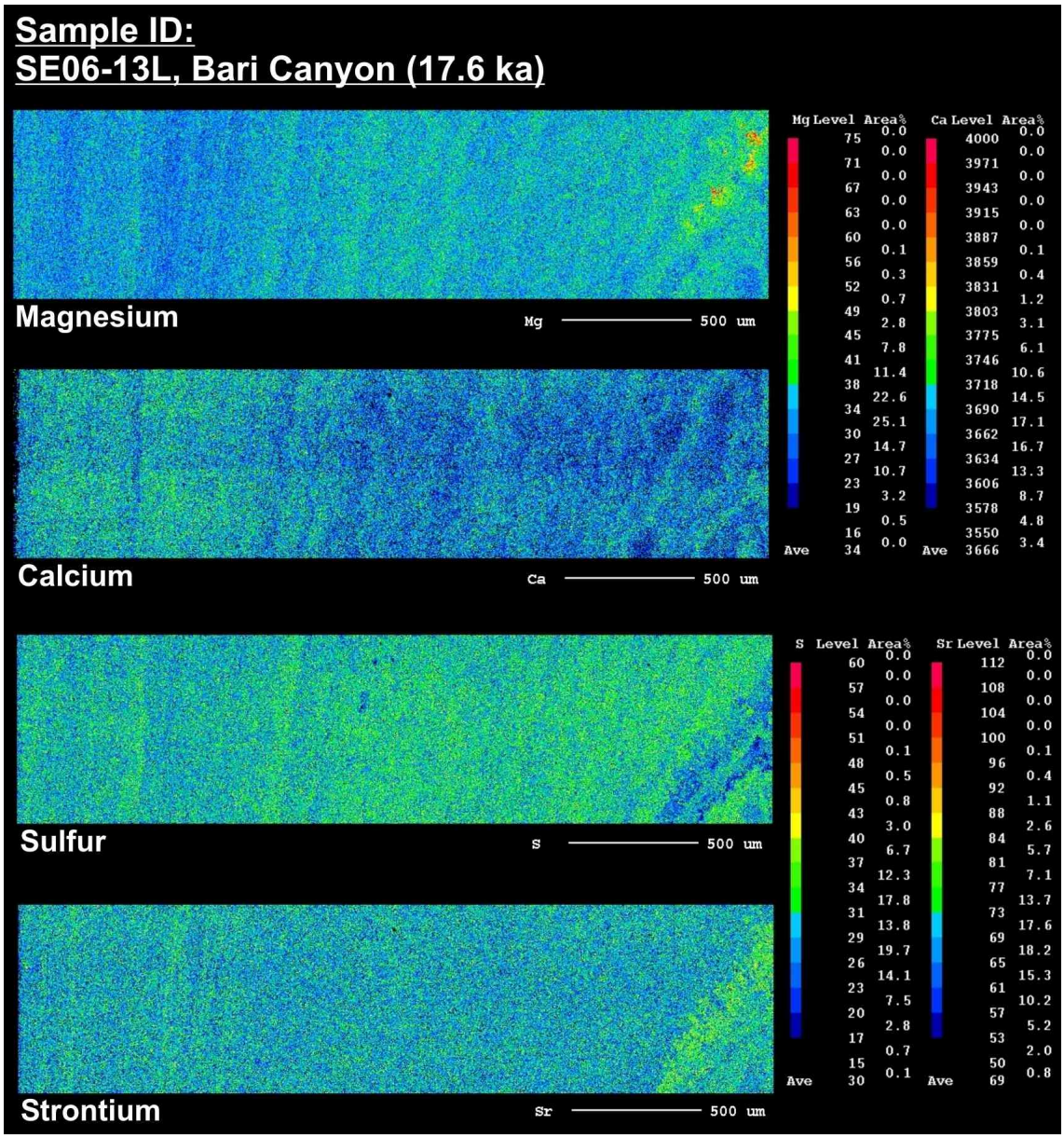

Figure A.1: Element mappings of sample SE06-13L (17.6 ka).

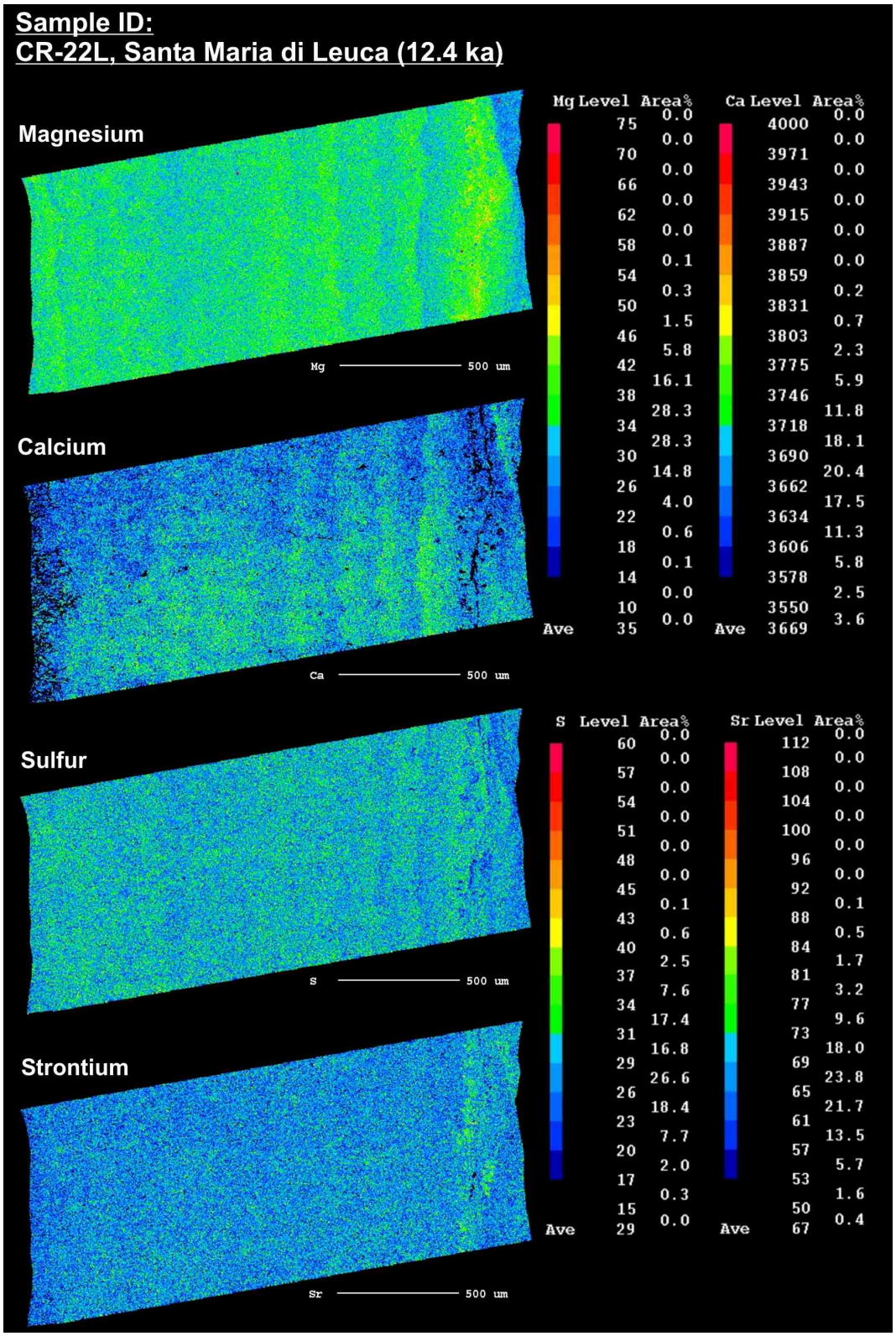

Figure A.2: Element mappings of sample CR-22L (12.4 ka).

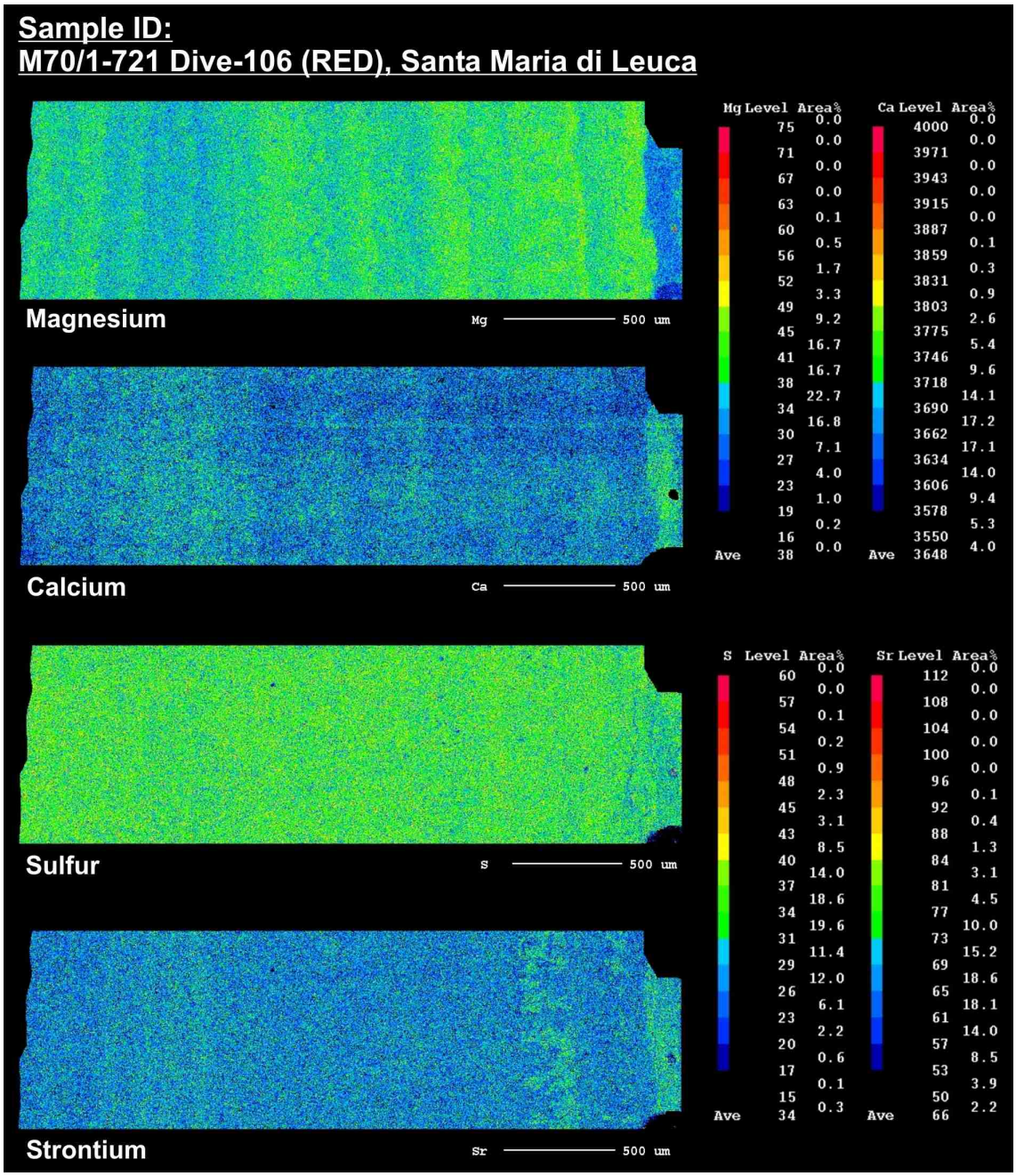

Figure A.3: Element mappings of sample M70/1-721 Dive-106 (RED).

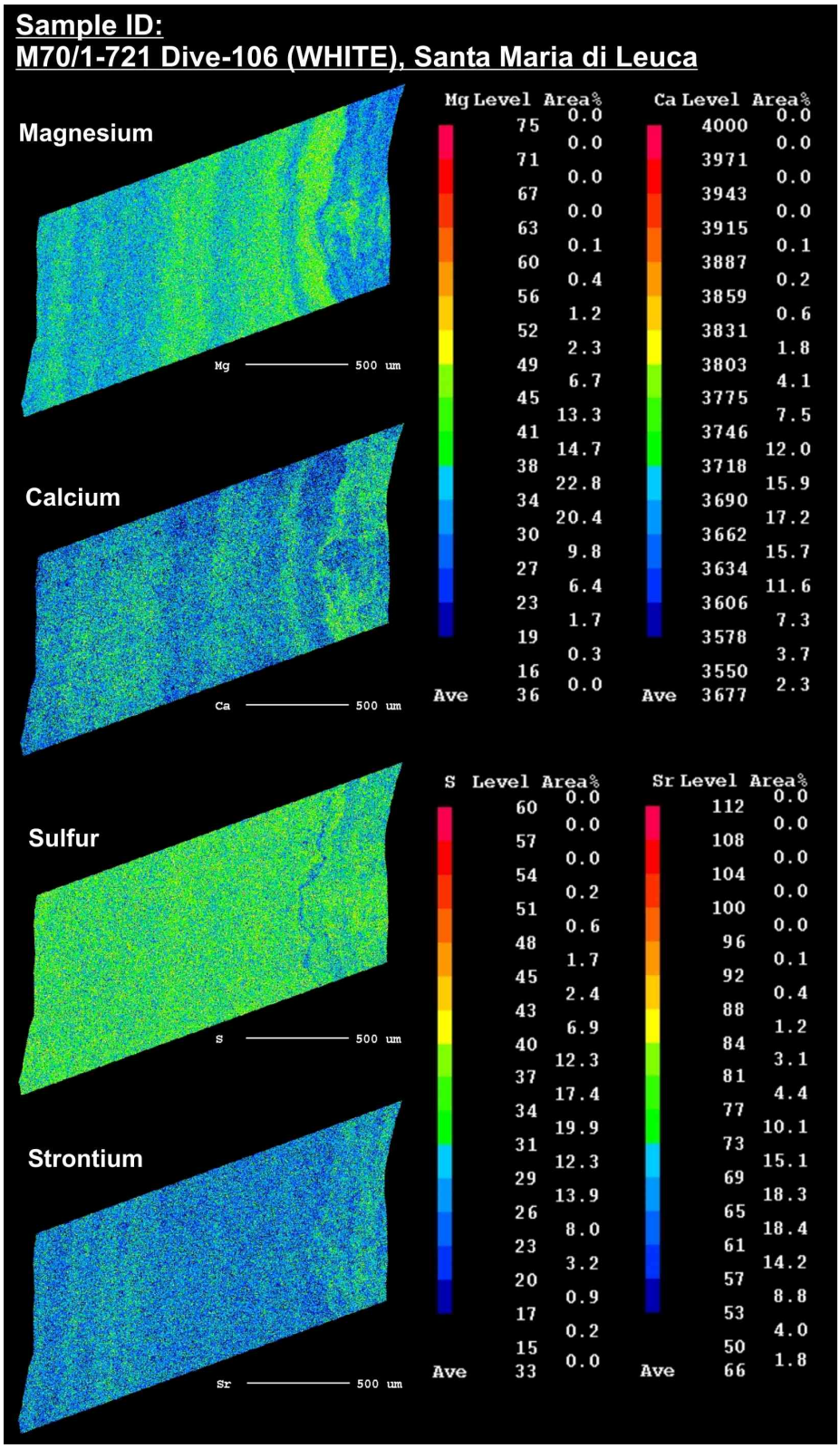

Figure A.4: Element mappings of sample M70/1-721 Dive-106 (WHITE).

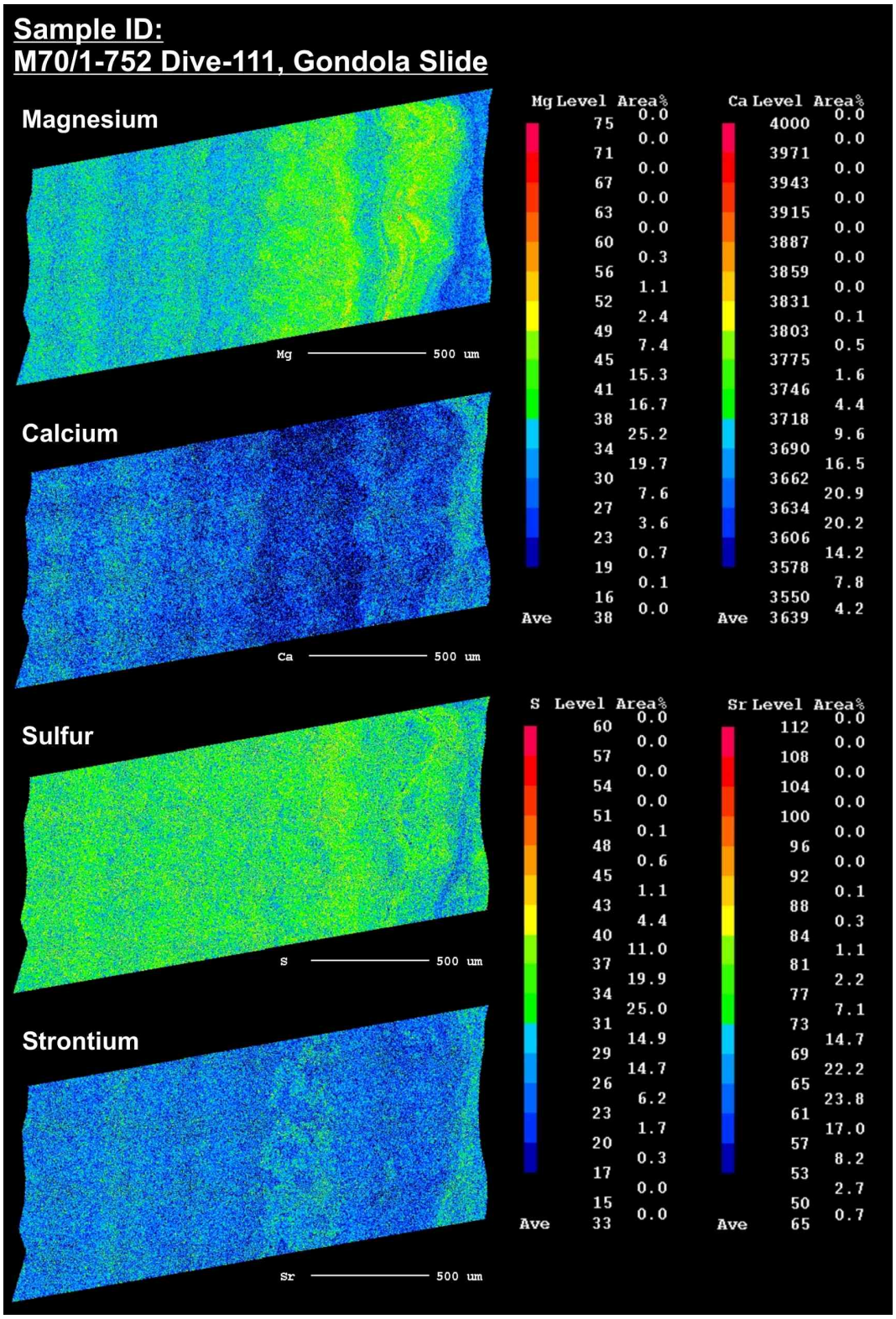

Figure A.5: Element mappings of sample M70/1-752 Dive-111.

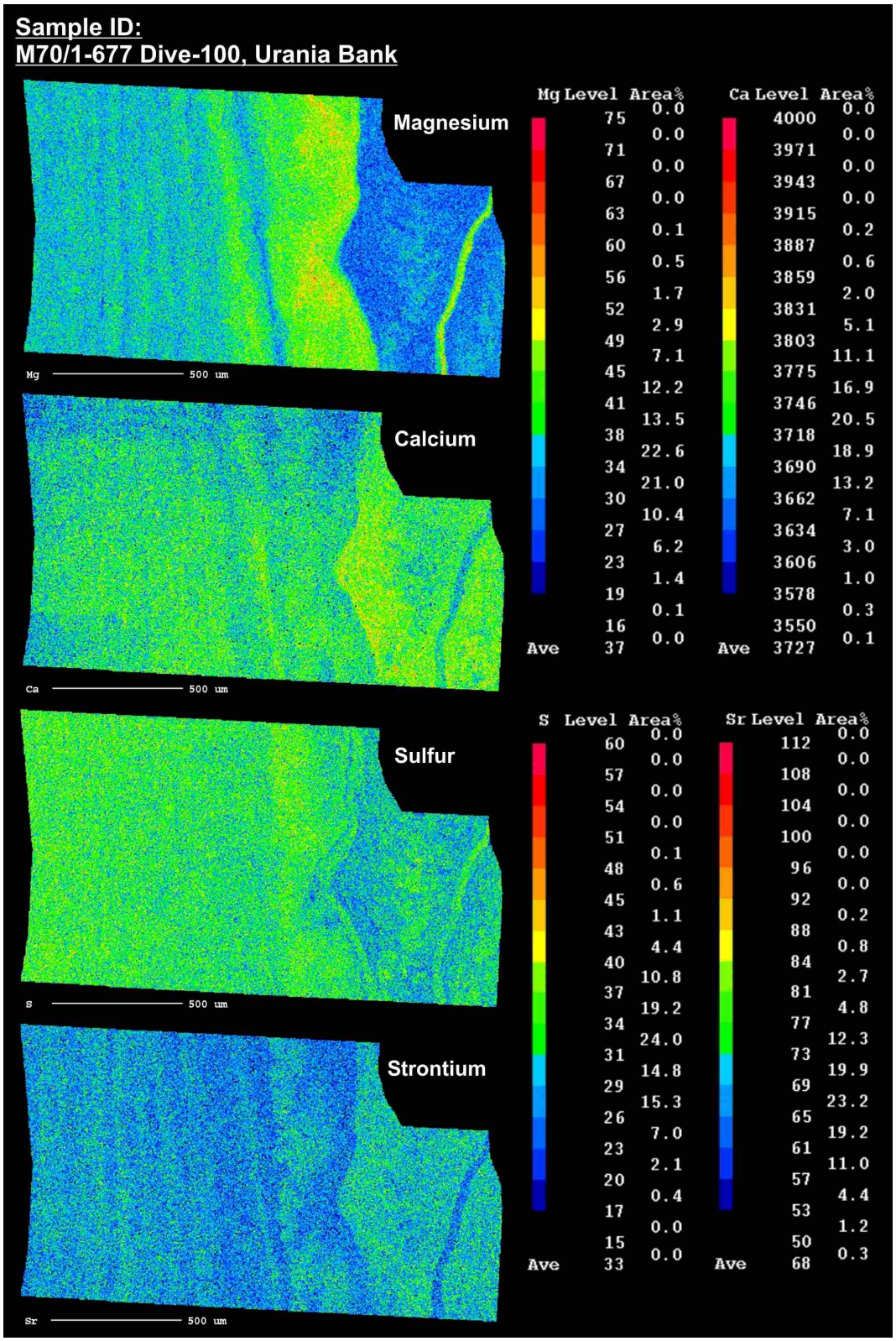

Figure A.6: Element mappings of sample M70/1-677 Dive-100.

Quantitative EPMA-Analyses

Sample ID: SE06-13L, Bari Canyon, (17.6 ka)

Table A.12: Results of quantitative EPMA-analyses of coral samples.

Dist. from Rim [μm]	**Mg/Ca**	**Sr/Ca** [mmol/mol]	**S/Ca**	**Dist. from Rim** [μm]	**Mg/Ca**	**Sr/Ca** [mmol/mol]	**S/Ca**
0	x	x	x	720	1.61	10.42	5.09
20	2.54	11.49	5.14	740	1.75	9.61	4.86
40	2.24	10.06	5.49	760	1.74	10.88	5.17
60	2.00	10.10	5.18	780	1.96	10.25	4.58
80	2.40	10.12	5.23	800	1.83	10.32	5.44
100	2.36	10.65	5.37	820	1.80	9.76	5.35
120	1.81	9.31	4.86	840	1.90	11.16	4.64
140	2.01	10.53	5.13	860	1.46	10.66	5.00
160	1.95	10.50	5.29	880	1.70	10.26	4.96
180	1.70	10.27	4.90	900	1.84	9.97	5.31
200	1.76	10.51	5.38	920	1.47	9.75	5.27
220	2.04	10.56	4.74	940	2.45	9.91	5.15
240	1.76	10.24	4.45	960	2.13	9.85	4.99
260	2.47	10.41	4.74	980	1.84	9.89	4.76
280	1.77	10.59	5.26	1000	2.06	10.04	5.10
300	1.99	9.98	5.08	1020	2.77	10.66	5.89
320	1.64	10.60	5.09	1040	2.57	10.15	5.84
340	2.44	10.34	4.79	1060	3.27	10.62	5.63
360	2.07	10.21	5.20	1080	3.58	10.81	5.66
380	2.25	9.95	4.91	1100	3.40	9.65	5.06
400	1.92	10.26	5.26	1120	1.46	10.11	5.02
420	1.64	9.93	5.21	1140	1.84	10.32	5.46
440	2.81	10.43	5.12	1160	1.59	9.76	4.72
460	3.12	10.07	5.40	1180	2.12	10.21	5.52
480	2.90	10.44	5.10	1200	1.55	10.71	5.01
500	2.18	10.23	5.18	1220	2.30	9.89	5.21
520	1.97	10.27	4.61	1240	3.27	10.42	5.75
540	1.61	9.91	5.05	1260	2.78	10.26	5.18
560	2.31	9.99	4.96	1280	2.35	9.86	5.52
580	2.45	10.62	5.33	1300	2.17	9.76	4.94
600	1.93	11.12	4.74	1320	2.94	10.38	5.89
620	1.55	11.10	4.64	1340	2.77	10.01	5.46
640	1.21	9.95	4.69	1360	2.92	10.18	5.45
660	1.19	10.49	5.07	1380	2.91	9.84	4.80
680	1.88	10.41	4.77	1400	2.82	10.44	5.32
700	2.53	10.34	4.98	1420	2.89	10.19	5.67

Dist. from Rim [μm]	**Mg/Ca**	**Sr/Ca** [mmol/mol]	**S/Ca**	**Dist. from Rim** [μm]	**Mg/Ca**	**Sr/Ca** [mmol/mol]	**S/Ca**
1440	2.22	10.24	5.58	2200	2.74	10.81	5.79
1460	2.40	10.02	5.06	2220	2.33	10.35	5.70
1480	2.14	10.76	5.42	2240	1.58	10.00	5.28
1500	2.68	10.66	5.25	2260	2.00	10.35	5.95
1520	3.17	10.68	5.18	2280	2.46	10.14	5.48
1540	2.45	10.30	5.79	2300	2.59	10.28	5.76
1560	3.08	10.48	5.62	2320	2.67	10.77	5.82
1580	2.70	10.28	5.69	2340	2.78	11.00	5.98
1600	3.33	10.64	5.54	2360	3.23	10.69	5.80
1620	2.41	10.24	5.80	2380	2.47	10.14	5.73
1640	2.98	10.14	5.54	2400	2.25	10.14	5.95
1660	1.62	9.60	5.21	2420	1.93	9.89	5.86
1680	2.06	11.02	5.48	2440	x	x	x
1700	2.72	10.12	6.27	2460	2.79	10.90	5.77
1720	3.11	10.29	5.55	2480	2.88	10.34	6.05
1740	2.80	10.33	5.64	2500	3.09	10.58	6.13
1760	3.06	10.41	5.84	2520	2.59	10.27	5.65
1780	2.21	10.01	5.60	2540	2.68	9.99	6.05
1800	2.24	10.03	5.44	2560	2.82	10.56	6.07
1820	2.46	10.75	5.92	2580	3.13	10.56	5.72
1840	2.22	10.59	5.74	2600	2.80	10.81	6.16
1860	2.52	10.09	5.79	2620	1.96	10.39	5.43
1880	1.89	10.41	5.19	2640	1.63	9.64	5.13
1900	2.55	10.26	5.36	2660	2.24	10.30	6.03
1920	2.51	10.26	5.70	2680	3.15	10.73	5.82
1940	2.22	10.49	5.46	2700	3.07	11.03	5.73
1960	1.83	10.33	5.36	2720	3.50	10.60	5.97
1980	2.52	10.13	5.51	2740	4.75	10.60	6.04
2000	3.13	10.37	5.76	2760	3.17	10.74	6.28
2020	2.27	10.04	5.84	2780	2.64	10.16	6.26
2040	3.13	10.70	6.03	2800	3.46	10.75	5.84
2060	2.56	10.45	5.38	2820	3.25	10.43	5.71
2080	2.32	10.20	5.05	2840	3.31	11.16	6.12
2100	2.42	10.10	5.94	2860	7.45	11.38	6.08
2120	2.47	10.21	5.56	2880	6.82	12.05	5.77
2140	2.21	10.39	5.77	2900	2.71	11.12	5.79
2160	2.58	11.03	5.33	2920	3.90	11.34	5.64
2180	2.68	10.70	5.56				

Sample ID: CR-22L, Santa Maria di Leuca, (12.4 ka)

Dist. from Rim [μm]	**Mg/Ca**	**Sr/Ca** [mmol/mol]	**S/Ca**	**Dist. from Rim** [μm]	**Mg/Ca**	**Sr/Ca** [mmol/mol]	**S/Ca**
0	2.00	9.53	5.70	800	2.66	9.95	5.70
20	3.02	9.86	5.27	820	2.09	9.78	5.47
40	2.93	10.00	5.45	840	2.17	9.85	5.16
60	2.75	9.71	5.34	860	2.39	10.18	5.64
80	3.12	10.80	5.55	880	1.95	10.22	5.03
100	2.28	10.34	5.49	900	2.15	10.10	5.19
120	3.46	9.76	5.27	920	3.06	10.18	5.17
140	2.44	9.77	5.31	940	2.83	9.96	5.72
160	2.94	9.56	4.86	960	2.66	9.92	5.67
180	3.08	9.84	5.31	980	2.84	10.20	5.57
200	2.93	10.05	5.52	1000	2.73	10.37	5.84
220	3.15	9.92	6.19	1020	3.01	9.69	5.77
240	3.29	10.51	5.90	1040	2.89	10.07	5.53
260	2.25	9.96	5.64	1060	x	x	x
280	2.08	9.77	5.24	1080	3.19	10.20	5.45
300	2.94	9.74	5.67	1100	2.19	9.41	5.27
320	2.70	9.77	5.09	1120	2.58	9.57	5.40
340	3.04	10.01	5.89	1140	2.18	9.36	5.68
360	2.83	10.10	5.06	1160	2.25	10.15	5.44
380	2.51	9.65	5.48	1180	3.22	9.45	5.73
400	2.04	9.83	5.16	1200	3.33	10.03	5.84
420	3.00	10.11	5.37	1220	3.73	9.62	5.46
440	3.04	9.44	5.29	1240	2.80	10.02	5.69
460	1.59	10.13	4.89	1260	2.11	10.48	5.38
480	3.17	10.01	5.72	1280	2.53	10.07	5.74
500	2.73	10.25	5.80	1300	2.00	9.50	5.29
520	3.19	9.99	5.54	1320	2.19	9.97	5.35
540	2.54	10.47	5.73	1340	3.04	9.27	5.64
560	2.57	9.64	5.33	1360	1.88	9.82	5.10
580	x	x	x	1380	2.68	10.44	5.71
600	2.53	10.01	5.61	1400	3.30	10.20	5.55
620	2.54	9.74	5.14	1420	2.47	9.58	5.27
640	2.21	9.99	5.43	1440	1.80	9.60	5.38
660	2.59	9.98	5.31	1460	2.26	10.08	5.08
680	2.71	9.88	5.20	1480	1.46	9.72	5.34
700	2.46	9.25	4.99	1500	3.40	9.14	5.47
720	2.56	9.60	5.23	1520	2.21	9.59	5.07
740	2.97	10.46	5.47	1540	3.20	9.19	5.22
760	2.28	9.58	5.24	1560	3.20	9.34	5.63
780	2.49	9.16	5.57	1580	3.43	10.43	5.69

Dist. from Rim [μm]	**Mg/Ca**	**Sr/Ca** [mmol/mol]	**S/Ca**	**Dist. from Rim** [μm]	**Mg/Ca**	**Sr/Ca** [mmol/mol]	**S/Ca**
1600	2.21	9.38	5.34	1840	4.47	10.00	5.58
1620	1.70	9.93	4.72	1860	3.80	9.89	5.68
1640	1.91	9.70	5.04	1880	3.88	9.27	5.15
1660	2.50	9.73	5.31	1900	2.97	10.24	5.25
1680	2.04	9.44	5.29	1920	3.29	9.95	5.66
1700	2.73	9.64	5.56	1940	3.17	10.05	5.50
1720	3.29	10.33	5.42	1960	3.05	9.92	5.00
1740	3.50	9.74	5.55	1980	2.84	9.95	5.05
1760	3.64	9.60	5.67	2000	1.60	9.70	5.31
1780	3.68	10.39	5.87	2020	1.19	10.34	5.19
1800	3.81	10.73	5.52	2040	1.54	9.88	4.87
1820	3.23	10.16	5.24	2060			

Sample ID: M70/1-721 Dive-106 (RED), Santa Maria di Leuca

Dist. from Rim [μm]	**Mg/Ca**	**Sr/Ca** [mmol/mol]	**S/Ca**	**Dist. from Rim** [μm]	**Mg/Ca**	**Sr/Ca** [mmol/mol]	**S/Ca**
0	3.23	9.73	6.29	800	3.08	10.17	6.34
20	3.41	9.27	6.13	820	3.55	9.59	6.36
40	4.09	10.04	6.51	840	2.87	10.02	6.25
60	3.07	10.12	6.51	860	3.16	10.03	6.27
80	2.33	9.79	6.39	880	3.16	10.08	6.90
100	2.96	9.92	6.80	900	1.47	10.42	6.02
120	3.03	9.55	6.20	920	3.25	10.18	6.48
140	3.56	10.34	6.11	940	3.47	9.82	6.49
160	3.11	10.12	6.37	960	3.16	9.63	6.24
180	3.02	9.87	6.59	980	2.63	9.92	6.87
200	2.03	9.00	6.06	1000	2.66	9.90	6.44
220	2.73	9.22	5.90	1020	3.34	9.80	6.35
240	2.56	8.84	6.86	1040	3.36	9.97	6.73
260	3.58	9.78	6.35	1060	3.89	9.80	6.50
280	3.57	9.87	6.65	1080	3.23	9.99	6.54
300	2.97	9.93	6.21	1100	3.08	10.11	6.53
320	2.80	9.73	6.62	1120	2.83	9.67	6.36
340	1.95	9.37	6.65	1140	3.45	9.66	6.52
360	3.08	10.05	6.42	1160	3.93	9.90	6.71
380	2.51	9.91	6.03	1180	3.49	9.82	6.69
400	2.50	9.77	6.72	1200	4.09	10.13	6.47
420	2.37	10.30	6.40	1220	3.11	9.99	6.20
440	3.30	9.81	6.39	1240	4.56	9.74	6.34
460	2.89	9.84	6.59	1260	3.60	9.20	6.36
480	3.66	9.78	6.34	1280	3.67	10.06	6.49
500	3.35	9.35	6.53	1300	3.50	10.54	6.45
520	2.00	9.48	6.11	1320	3.72	9.93	6.54
540	2.99	10.25	6.26	1340	3.32	9.63	6.88
560	3.23	9.67	6.10	1360	3.05	9.86	6.35
580	2.00	9.79	6.33	1380	3.07	10.05	6.43
600	2.98	10.07	6.93	1400	3.26	9.78	6.36
620	3.32	10.12	6.83	1420	2.99	9.50	6.35
640	2.89	10.46	6.76	1440	2.68	10.17	6.46
660	2.43	10.28	6.59	1460	3.47	9.89	6.29
680	x	x	x	1480	3.46	9.93	6.55
700	2.42	9.81	6.05	1500	4.09	9.58	6.56
720	3.30	9.31	5.82	1520	2.66	9.55	6.30
740	2.79	9.80	6.35	1540	3.09	9.40	6.27
760	3.10	9.41	6.55	1560	3.04	10.18	6.19
780	2.75	9.60	6.48	1580	2.68	9.82	6.33

Dist. from Rim [μm]	**Mg/Ca**	**Sr/Ca** [mmol/mol]	**S/Ca**	**Dist. from Rim** [μm]	**Mg/Ca**	**Sr/Ca** [mmol/mol]	**S/Ca**
1600	3.65	9.67	6.66	2260	3.60	11.16	6.26
1620	2.91	10.09	6.90	2280	3.43	10.93	6.31
1640	3.47	9.91	6.79	2300	3.21	10.08	6.21
1660	2.98	9.74	6.52	2320	3.73	10.64	5.88
1680	3.09	9.68	6.46	2340	3.89	11.51	6.52
1700	2.93	8.94	5.60	2360	3.30	10.78	6.06
1720	3.35	9.94	6.11	2380	3.65	10.86	6.16
1740	3.64	9.78	5.85	2400	3.38	11.05	6.28
1760	3.54	10.20	6.44	2420	4.21	9.95	6.11
1780	4.49	10.16	6.18	2440	4.04	9.81	6.41
1800	3.63	9.99	5.54	2460	3.78	9.89	6.31
1820	4.44	9.60	6.39	2480	4.04	10.20	6.87
1840	3.87	10.29	6.77	2500	2.83	9.72	6.42
1860	4.68	10.08	6.43	2520	3.33	9.81	6.11
1880	4.03	9.60	6.43	2540	3.19	10.06	6.39
1900	4.32	9.62	5.97	2560	3.49	9.59	6.34
1920	x	x	X	2580	3.16	9.34	6.47
1940	3.90	9.85	6.57	2600	3.42	9.30	6.47
1960	3.71	9.56	6.83	2620	3.65	9.32	6.52
1980	3.87	10.18	6.60	2640	4.60	9.84	6.70
2000	3.36	9.76	6.22	2660	4.57	10.48	5.94
2020	3.34	10.03	6.03	2680	4.03	10.36	6.64
2040	3.95	9.83	6.43	2700	4.68	9.58	6.15
2060	2.82	10.01	6.94	2720	4.04	9.77	6.31
2080	4.12	10.40	6.96	2740	3.98	9.39	6.18
2100	3.52	9.44	6.60	2760	2.45	9.86	5.80
2120	4.59	9.68	6.50	2780	1.21	10.34	4.92
2140	2.88	9.76	6.43	2800	x	x	x
2160	3.70	9.72	6.55	2820	1.20	10.48	5.57
2180	4.45	9.94	6.45	2840	1.18	9.93	5.19
2200	4.23	9.50	6.43	2860	0.95	10.86	5.73
2220	3.79	9.71	6.76	2880	1.50	10.44	5.69
2240	3.17	10.89	6.23	2900	2.46	10.97	5.56

Sample ID: M70/1-721 Dive-106 (WHITE), Santa Maria di Leuca

Dist. from Rim [μm]	**Mg/Ca**	**Sr/Ca** [mmol/mol]	**S/Ca**	**Dist. from Rim** [μm]	**Mg/Ca**	**Sr/Ca** [mmol/mol]	**S/Ca**
0	2.37	9.71	6.93	800	2.82	9.60	6.38
20	1.98	10.24	5.88	820	3.55	9.19	6.29
40	2.23	10.22	5.59	840	2.57	9.49	5.64
60	3.08	9.74	6.15	860	3.62	9.54	6.40
80	2.66	10.22	5.80	880	3.13	10.35	6.38
100	2.66	9.42	6.32	900	3.18	9.87	5.81
120	3.16	9.72	6.01	920	1.68	9.72	6.07
140	2.84	9.63	6.14	940	2.81	9.33	5.91
160	3.05	9.83	6.12	960	2.53	9.59	5.98
180	2.39	9.95	6.18	980	2.65	9.88	6.35
200	1.87	10.85	6.45	1000	1.84	9.96	6.04
220	2.28	10.53	5.91	1020	2.61	9.67	6.50
240	2.12	9.44	5.86	1040	2.98	9.21	6.16
260	1.98	9.61	6.10	1060	2.93	9.16	6.29
280	2.95	9.90	6.38	1080	3.63	9.57	6.22
300	3.22	9.80	6.51	1100	3.56	9.49	6.28
320	2.72	9.52	6.56	1120	3.30	9.48	6.06
340	2.76	9.49	6.01	1140	3.55	9.64	6.39
360	2.32	10.47	5.68	1160	3.29	9.66	6.48
380	1.84	10.58	6.04	1180	4.21	9.31	6.17
400	2.09	9.56	6.06	1200	4.46	9.71	5.86
420	2.06	10.23	5.78	1220	4.89	9.60	6.17
440	2.97	9.80	6.31	1240	3.19	9.63	6.62
460	3.68	9.88	5.73	1260	2.93	9.18	6.08
480	2.48	10.27	6.02	1280	4.58	9.34	6.46
500	2.63	10.25	6.05	1300	2.55	9.76	6.00
520	2.72	10.53	6.43	1320	2.56	9.57	5.69
540	2.19	9.52	5.56	1340	2.60	9.96	6.34
560	2.72	9.73	5.81	1360	4.31	9.56	5.88
580	3.52	10.34	6.47	1380	4.83	10.05	6.17
600	2.97	10.74	6.82	1400	3.36	9.84	4.45
620	2.78	10.58	6.37	1420	3.64	9.81	5.68
640	2.72	10.20	6.59	1440	4.32	10.23	6.16
660	3.63	9.77	5.91	1460	4.05	9.28	6.10
680	3.43	10.06	5.76	1480	4.56	9.02	5.04
700	3.44	9.30	6.27	1500	4.29	9.76	6.16
720	3.72	9.76	6.18	1520	4.74	10.05	6.46
740	3.81	9.41	6.06	1540	3.24	9.65	5.91
760	2.99	9.67	6.08	1560	2.60	10.37	5.14
780	3.04	9.65	6.13	1580	1.69	10.20	5.52

Dist. from Rim [μm]	**Mg/Ca**	**Sr/Ca** [mmol/mol]	**S/Ca**	**Dist. from Rim** [μm]	**Mg/Ca**	**Sr/Ca** [mmol/mol]	**S/Ca**
1600	1.00	9.08	5.36	1720	1.88	9.10	5.57
1620	1.66	10.65	5.43	1740	3.22	9.95	5.87
1640	2.01	9.58	6.16	1760	2.48	10.05	5.26
1660	2.46	9.44	5.92	1780	1.42	9.87	5.69
1680	2.26	9.39	5.74	1800	1.43	10.52	5.25
1700	2.36	9.78	5.48	1820	2.43	10.27	5.75

Sample ID: M70/1-752 Dive-111, Gondola Slide

Dist. from Rim [μm]	**Mg/Ca** [mmol/mol]	**Sr/Ca** [mmol/mol]	**S/Ca** [mmol/mol]	**Dist. from Rim** [μm]	**Mg/Ca** [mmol/mol]	**Sr/Ca** [mmol/mol]	**S/Ca** [mmol/mol]
0	2.96	9.96	5.65	800	2.04	9.82	5.84
20	3.06	10.30	6.21	820	3.08	9.59	6.00
40	2.91	10.30	5.95	840	2.34	9.40	5.91
60	3.71	10.00	6.00	860	2.70	9.80	6.22
80	2.15	9.85	6.37	880	x	x	x
100	x	x	x	900	1.50	9.51	5.65
120	3.23	9.77	6.26	920	2.75	9.69	6.62
140	3.36	10.06	5.94	940	3.28	9.68	6.09
160	2.68	9.83	5.83	960	3.08	9.66	6.14
180	3.46	9.59	5.99	980	2.64	10.23	6.13
200	3.09	10.01	6.07	1000	3.15	9.46	6.06
220	3.20	9.65	6.29	1020	3.12	9.36	6.13
240	2.96	9.55	6.76	1040	3.52	9.66	5.97
260	2.96	10.38	6.20	1060	2.83	10.87	6.02
280	3.20	9.76	5.98	1080	3.32	10.55	6.35
300	3.50	9.76	6.20	1100	4.34	10.11	6.19
320	3.37	9.97	6.32	1120	x	x	x
340	2.43	9.77	6.09	1140	3.68	10.16	6.20
360	2.55	9.89	6.22	1160	3.69	10.47	6.16
380	2.62	10.17	6.18	1180	3.88	10.02	6.66
400	1.84	10.25	6.05	1200	3.87	10.63	6.05
420	2.08	10.15	5.86	1220	3.60	9.79	6.31
440	2.28	10.03	6.41	1240	4.41	10.32	6.63
460	1.95	10.28	6.34	1260	3.86	10.40	6.29
480	3.41	10.08	6.57	1280	3.23	11.01	6.49
500	2.89	10.53	6.52	1300	3.86	10.34	6.86
520	2.92	9.88	6.13	1320	4.48	9.57	6.59
540	1.75	9.62	6.00	1340	5.39	9.90	6.36
560	2.43	9.83	5.79	1360	3.26	9.63	6.19
580	2.61	9.77	6.08	1380	3.40	10.12	6.13
600	2.30	9.67	6.11	1400	2.48	9.32	5.87
620	1.72	10.11	5.73	1420	2.91	9.51	6.08
640	2.11	9.54	5.54	1440	3.42	9.54	6.19
660	3.12	9.44	6.61	1460	2.16	9.54	6.01
680	2.72	9.59	5.77	1480	2.23	9.24	5.95
700	2.94	9.40	5.97	1500	3.96	9.22	6.01
720	2.41	9.09	6.07	1520	3.83	9.45	6.09
740	3.24	9.57	6.16	1540	4.17	9.69	6.07
760	2.99	10.30	6.40	1560	4.11	9.31	5.91
780	3.21	9.71	6.32	1580	4.34	9.57	6.08

Dist. from Rim [μm]	**Mg/Ca** [mmol/mol]	**Sr/Ca** [mmol/mol]	**S/Ca**	**Dist. from Rim** [μm]	**Mg/Ca** [mmol/mol]	**Sr/Ca** [mmol/mol]	**S/Ca**
1600	4.41	9.54	5.90	1780	3.60	9.79	6.14
1620	5.24	9.23	6.22	1800	4.96	9.11	6.15
1640	3.87	8.98	5.97	1820	4.88	9.44	6.35
1660	5.44	9.30	5.82	1840	4.86	9.19	6.26
1680	5.04	9.68	5.74	1860	2.84	8.83	6.06
1700	4.82	9.29	5.89	1880	2.96	9.13	5.61
1720	3.56	9.30	6.62	1900	2.00	9.98	5.65
1740	4.16	9.36	7.24	1920	1.45	10.40	5.27
1760	5.32	9.95	6.55	1940	1.99	10.32	5.43

Sample ID: M70/1-677 Dive-100, Urania Bank

Dist. from Rim [μm]	**Mg/Ca** [mmol/mol]	**Sr/Ca** [mmol/mol]	**S/Ca** [mmol/mol]	**Dist. from Rim** [μm]	**Mg/Ca** [mmol/mol]	**Sr/Ca** [mmol/mol]	**S/Ca** [mmol/mol]
0	3.30	9.79	6.54	800	4.14	9.65	6.69
20	2.26	10.40	6.49	820	3.72	10.06	6.18
40	3.40	10.13	6.92	840	4.29	10.34	6.35
60	2.91	10.43	6.62	860	3.77	9.72	6.39
80	2.92	10.87	6.60	880	3.83	9.75	6.14
100	2.64	10.39	6.71	900	1.90	10.08	5.40
120	2.84	9.60	6.58	920	3.97	9.62	6.25
140	2.50	9.73	6.50	940	5.11	9.46	6.05
160	3.22	9.39	6.15	960	4.31	9.28	6.32
180	3.30	10.51	6.65	980	4.36	9.51	6.44
200	2.46	10.28	6.52	1000	5.04	9.31	6.46
220	2.80	10.07	6.51	1020	5.45	9.60	6.18
240	3.06	9.90	6.84	1040	4.91	9.68	6.31
260	2.22	10.64	5.99	1060	4.28	10.18	6.59
280	3.27	9.57	6.63	1080	4.39	10.47	6.62
300	2.85	9.47	6.91	1100	4.87	10.11	6.32
320	3.04	10.43	5.93	1120	5.24	9.26	6.28
340	2.39	10.50	6.15	1140	5.65	9.41	6.05
360	2.56	10.24	6.11	1160	4.95	9.19	5.99
380	2.87	10.06	6.86	1180	4.96	9.34	6.17
400	2.83	10.20	6.56	1200	5.97	9.10	5.50
420	3.46	9.85	6.56	1220	5.54	9.63	6.20
440	2.44	10.15	6.51	1240	3.99	9.93	6.45
460	2.08	9.72	6.34	1260	1.04	9.52	5.08
480	2.09	10.78	6.63	1280	1.75	10.45	5.26
500	2.73	10.12	6.22	1300	1.72	9.64	5.42
520	2.56	9.40	6.43	1320	1.75	11.27	5.40
540	2.34	10.00	6.85	1340	1.82	9.66	5.39
560	2.54	9.75	5.99	1360	1.40	10.81	5.46
580	3.27	9.67	5.93	1380	1.02	10.64	5.71
600	3.33	9.63	6.25	1400	1.23	10.31	5.75
620	3.35	9.74	6.55	1420	2.54	10.08	6.44
640	2.60	10.38	5.82	1440	1.95	10.01	5.84
660	2.75	10.26	6.63	1460	1.85	10.63	5.92
680	2.13	9.50	6.44	1480	1.61	10.87	5.51
700	3.35	9.10	6.72	1500	0.96	10.97	6.13
720	2.76	9.89	6.23	1520	1.38	10.64	5.71
740	4.12	9.68	6.18	1540	1.46	10.05	5.54
760	3.57	9.36	6.49	1560	1.35	10.34	5.54
780	3.98	9.83	6.74	1580	5.66	8.91	6.43

Dist. from Rim [μm]	**Mg/Ca** [mmol/mol]	**Sr/Ca** [mmol/mol]	**S/Ca**	**Dist. from Rim** [μm]	**Mg/Ca** [mmol/mol]	**Sr/Ca** [mmol/mol]	**S/Ca**
1600	2.13	10.12	6.58	1700	1.73	11.29	5.50
1620	2.03	10.91	5.16	1720	1.91	10.48	5.67
1640	1.94	11.12	5.58	1740	2.57	10.09	5.67
1660	2.03	10.05	5.66	1760	1.83	10.55	5.77
1680	1.36	10.11	5.65	1780	2.29	9.46	5.85

Coral δ^{13}C- and δ^{18}O-Analyses

SAMPLE ID: SE06-13L, Bari Canyon (17.6 ka)

Table A.13: Results of stable isotope analyses of coral samples performed by Matthias López Correa (GZN-IPAL, Erlangen).

Dist. from Rim [μm]	δ^{13}**C**$\pm 1\sigma$ [‰ PDB]	δ^{18}**O**$\pm 1\sigma$ [‰ PDB]	**Dist. from Rim** [μm]	δ^{13}**C**$\pm 1\sigma$ [‰ PDB]	δ^{18}**O**$\pm 1\sigma$ [‰ PDB]
200	3.52±0.01	5.12±0.05	3600	1.80±0.01	4.50±0.02
300	3.15±0.01	4.99±0.05	3700	1.42±0.01	4.39±0.03
400	2.64±0.01	4.93±0.06	3800	0.54±0.01	4.17±0.03
500	2.88±0.01	4.99±0.05	3900	-0.64±0.01	3.50±0.02
600	3.56±0.01	5.45±0.02	4000	-0.74±0.00	3.70±0.04
700	3.56±0.02	4.98±0.06	4100	0.58±0.02	3.82±0.03
800	3.71±0.02	5.50±0.05	4200	1.75±0.01	4.69±0.03
900	3.41±0.01	4.80±0.07	4300	0.99±0.01	4.28±0.03
1000	3.49±0.01	5.47±0.04	4400	-0.06±0.01	3.92±0.01
1100	3.41±0.02	5.31±0.03	4500	-0.13±0.02	3.75±0.03
1200	3.40±0.01	5.35±0.02	4700	0.66±0.01	3.73±0.09
1300	3.22±0.01	5.21±0.03	4800	1.94±0.01	4.89±0.03
1400	3.29±0.02	5.38±0.02	4900	2.42±0.01	5.04±0.05
1500	3.42±0.01	5.38±0.05	5000	1.88±0.01	4.23±0.06
1600	3.50±0.01	5.36±0.04	5100	0.86±0.01	4.41±0.04
1700	3.61±0.01	5.21±0.03	5200	0.64±0.02	4.09±0.04
1800	3.72±0.01	5.33±0.02	5300	1.12±0.00	4.65±0.03
1900	3.69±0.01	5.27±0.02	5400	1.90±0.01	4.89±0.03
2000	3.57±0.01	5.07±0.03	5500	2.25±0.01	4.99±0.02
2100	3.57±0.01	5.34±0.04	5600	1.69±0.01	4.42±0.05
2200	3.43±0.01	4.69±0.07	5700	1.02±0.01	3.91±0.06
2300	3.43±0.02	4.78±0.08	5800	0.88±0.01	4.15±0.04
2400	3.41±0.01	4.93±0.04	5900	0.80±0.00	4.46±0.02
2500	3.48±0.01	4.95±0.04	6000	0.58±0.00	4.30±0.03
2600	3.49±0.01	5.04±0.05	6100	0.18±0.01	3.91±0.06
2700	3.45±0.01	5.19±0.04	6200	0.05±0.01	4.23±0.03
2800	3.32±0.01	5.08±0.04	6300	0.24±0.01	4.00±0.02
2900	3.15±0.01	5.13±0.03	6400	-0.16±0.01	3.97±0.02
3000	3.08±0.02	5.11±0.05	6500	-1.23±0.01	3.65±0.03
3100	2.11±0.01	4.51±0.03	6600	-2.49±0.01	2.74±0.06
3200	1.96±0.01	4.41±0.02	6700	-3.05±0.01	2.81±0.03
3300	2.05±0.02	4.61±0.03	6800	-3.77±0.01	2.65±0.03
3400	2.64±0.01	4.98±0.03	6900	-3.89±0.01	2.33±0.02
3500	2.56±0.01	4.88±0.03	7000	-4.14±0.01	2.37±0.03

SAMPLE ID: CR-22L, Santa Maria di Leuca (12.4 ka)

Dist. from Rim [μm]	δ^{13}**C**$\pm$**1**σ [‰ PDB]	δ^{18}**O**$\pm$**1**σ [‰ PDB]	**Dist. from Rim** [μm]	δ^{13}**C**$\pm$**1**σ [‰ PDB]	δ^{18}**O**$\pm$**1**σ [‰ PDB]
73	-0.45±0.01	2.99±0.05	1238	-2.51±0.01	2.58±0.02
146	-0.90±0.01	3.18±0.05	1311	-2.07±0.00	2.66±0.03
218	-1.72±0.01	2.71±0.05	1383	-1.55±0.02	2.70±0.02
291	-1.72±0.01	2.60±0.04	1456	-2.36±0.01	2.82±0.03
364	-1.74±0.01	2.56±0.04	1529	-2.82±0.01	2.51±0.03
437	-1.78±0.01	2.90±0.04	1602	-1.55±0.01	3.00±0.05
510	-1.42±0.01	2.53±0.02	1675	-2.06±0.01	2.85±0.03
583	-0.83±0.00	3.23±0.02	1748	-2.01±0.02	2.30±0.07
655	-0.74±0.01	3.24±0.02	1820	-0.94±0.02	2.93±0.05
728	0.51±0.03	3.10±0.08	1893	-1.31±0.01	2.88±0.04
801	1.32±0.01	4.06±0.03	2039	-2.77±0.01	2.63±0.03
874	0.70±0.01	3.66±0.05	2112	-5.09±0.01	0.96±0.04
947	0.53±0.01	3.29±0.03	2184	-3.76±0.01	1.62±0.05
1019	-0.35±0.01	3.40±0.04	2257	-1.59±0.01	2.74±0.04
1092	-1.00±0.01	3.22±0.01	2330	0.07±0.02	3.36±0.05
1165	-1.79±0.03	2.28±0.09			

SAMPLE ID: M70/1-752 Dive-111, Gondola Slide

Dist. from Rim [μm]	δ^{13}**C**$\pm$**1**σ [‰ PDB]	δ^{18}**O**$\pm$**1**σ [‰ PDB]	**Dist. from Rim** [μm]	δ^{13}**C**$\pm$**1**σ [‰ PDB]	δ^{18}**O**$\pm$**1**σ [‰ PDB]
100	1.09±0.01	2.56±0.04	900	-1.10±0.00	1.87±0.04
200	0.15±0.01	2.08±0.03	1000	-1.51±0.00	1.44±0.05
300	-2.46±0.01	1.04±0.06	1100	-3.16±0.01	0.93±0.04
400	-1.45±0.02	1.36±0.04	1200	-5.56±0.01	-0.24±0.04
500	1.25±0.01	2.59±0.03	1300	-6.89±0.01	-0.68±0.05
600	0.75±0.00	2.58±0.04	1400	-6.81±0.01	-0.75±0.04
700	-1.23±0.01	1.87±0.04	1600	-6.81±0.01	-0.92±0.05
800	-2.07±0.01	1.05±0.06	1600	-6.80±0.00	-0.86±0.04

SAMPLE ID: M70/1-721 Dive-106 (RED), Santa Maria di Leuca

Dist. from Rim [μm]	δ^{13}**C**$\pm 1\sigma$ [‰ PDB]	δ^{18}**O**$\pm 1\sigma$ [‰ PDB]	**Dist. from Rim** [μm]	δ^{13}**C**$\pm 1\sigma$ [‰ PDB]	δ^{18}**O**$\pm 1\sigma$ [‰ PDB]
100	-2.14±0.00	1.01±0.04	2600	-3.61±0.01	0.38±0.04
200	-2.76±0.02	0.38±0.04	2700	-3.03±0.01	0.80±0.02
300	-2.54±0.01	0.78±0.04	2800	-2.41±0.01	0.51±0.02
400	-2.80±0.01	1.15±0.00	2900	-2.68±0.01	0.52±0.03
500	-3.16±0.01	0.56±0.04	3000	-3.61±0.00	0.41±0.03
600	-2.19±0.01	1.00±0.02	3100	-4.36±0.01	0.13±0.04
700	-1.73±0.00	1.34±0.04	3200	-4.76±0.00	-0.22±0.03
800	-1.32±0.01	1.75±0.01	3300	-4.34±0.01	0.07±0.02
900	-0.84±0.00	2.02±0.02	3400	-4.26±0.00	0.16±0.03
1000	-0.30±0.01	1.76±0.03	3500	-4.38±0.02	0.05±0.03
1100	0.43±0.01	2.16±0.04	3600	-4.50±0.01	-0.02±0.02
1200	0.86±0.01	2.04±0.04	3700	-4.31±0.01	0.08±0.03
1300	0.75±0.03	1.60±0.07	3800	-4.20±0.01	0.16±0.04
1400	0.37±0.00	1.93±0.02	3900	-4.07±0.01	0.13±0.06
1500	-1.03±0.01	0.94±0.04	4000	-4.20±0.01	0.11±0.03
1600	-2.27±0.01	0.45±0.04	4100	-4.54±0.01	0.00±0.02
1700	-3.54±0.01	0.33±0.03	4200	-5.13±0.01	-0.31±0.02
1800	-4.61±0.01	-0.27±0.03	4300	-5.08±0.01	-0.12±0.01
1900	-5.17±0.00	-0.62±0.03	4400	-5.77±0.01	-0.65±0.03
2000	-5.05±0.01	-0.54±0.05	4500	-6.67±0.02	-0.98±0.02
2100	-4.40±0.01	0.05±0.03	4600	-7.17±0.02	-1.49±0.03
2200	-3.46±0.01	0.45±0.04	4700	-7.03±0.01	-1.71±0.04
2300	-3.13±0.01	0.58±0.04	4800	-7.39±0.01	-1.62±0.03
2400	-3.43±0.01	0.51±0.03	4900	-6.91±0.01	-1.16±0.02
2500	-3.79±0.01	0.51±0.01			

Box Corer δ^{13}C- and δ^{18}O-Analyses

Table A.14: Results of stable isotope analyses of epibenthic foraminifera in box corer (GKG) samples.

Sample ID	**Area**	**Species**	δ^{13}**C**$\pm 1\sigma$ [‰ PDB]	δ^{18}**O**$\pm 1\sigma$ [‰ PDB]
M70/1-668-2	Linosa Trough	*C. wuellerstorfi*	1.54±0.02	1.58±0.03
M70/1-668-2	Linosa Trough	*C. kullenbergi*	1.38±0.01	1.67±0.02
M70/1-669-1	Linosa Trough	*C. wuellerstorfi*	1.61±0.01	1.70±0.01
M70/1-679-2	Urania Bank	*C. kullenbergi*	0.56±0.01	1.76±0.02
M70/1-710-2	Santa Maria di Leuca	*C. wuellerstorfi*	1.63±0.01	1.90±0.02
M70/1-712-1	Santa Maria di Leuca	*C. wuellerstorfi*	1.56±0.01	3.58±0.02

ICP-MS Analyses

Table A.15: Results of ICP-MS-analyses.

Sample ID	^{7}**Li** [μg/l]	^{85}**Rb** [μg/l]	^{86}**Sr** [μg/l]	^{98}**Mo** [μg/l]	^{121}**Sb** [μg/l]	^{133}**Cs** [μg/l]	^{138}**Ba** [μg/l]	^{238}**U** [μg/l]
M70/1-655, 1007 m	197	140	9548	14.0	0.239	0.330	9.92	3.50
M70/1-655, 250 m	196	144	9768	14.4	0.237	0.336	8.47	3.59
M70/1-678, 623 m	193	143	9723	14.1	0.228	0.335	9.47	3.47
M70/1-705, 200 m	190	139	9566	14.1	0.213	0.336	8.66	3.54
M70/1-708, 823 m	188	140	9509	14.0	0.222	0.324	9.48	3.49
M70/1-723, 1198 m	201	134	9210	13.5	0.230	0.328	8.81	3.57
AL275-420-1#59, 85 m	166	123	8391	12.6	0.192	0.303	7.51	3.23
AL275-425-2#62, 25 m	150	112	7610	11.4	0.210	0.283	7.97	2.98
AL275-425-2#63, 10 m	133	96.3	6351	9.70	0.186	0.244	9.96	2.57
P325-383-2, 593 m	168	124	8511	12.7	0.236	0.297	5.70	3.22
P325-386-2, 175 m	164	124	8489	12.7	0.187	0.303	6.05	3.20
P325-373-2, 298 m	174	126	8528	12.8	0.192	0.298	5.76	3.26

ICP-OES Analyses

Table A.16: Results of ICP-OES-analyses.

Sample ID	**Ca** [mg/l]	**Mg** [mg/l]	**Sr** [μg/l]	**B** [μg/l]	**Ba** [μg/l]	**Mg/Ca** [mol/mol]	**Sr/Ca** [mmol/mol]	**B/Ca** [mmol/mol]	**Ba/Ca** [μmol/mol]
M70/1-655, 1007 m	460	1467	8670	5225	2.49	5.21	8.54	42.0	6.55
M70/1-655, 250 m	472	1510	8912	5204	x	5.24	8.57	40.8	x
M70/1-655, 100 m	459	1463	8636	5183	x	5.21	8.54	41.8	x
M70/1-675, 1728 m	442	1412	8275	4979	13.4	5.23	8.50	41.7	13.6
M70/1-678, 623 m	442	1417	8292	5051	22.0	5.25	8.51	42.3	19.1
M70/1-678, 620 m	440	1407	8244	4813	15.6	5.23	8.50	40.4	15.1
M70/1-705, 1015 m	449	1439	8446	4992	10.1	5.24	8.53	41.1	11.4
M70/1-705, 1000 m	448	1434	8428	5151	16.0	5.23	8.53	42.5	15.2
M70/1-705, 920 m	461	1473	8672	5027	5.83	5.23	8.54	40.3	8.61
M70/1-705, 880 m	445	1426	8366	4847	25.3	5.24	8.53	40.2	21.2
M70/1-705, 500 m	458	1465	8624	5076	x	5.23	8.54	40.9	x
M70/1-705, 200 m	456	1459	8590	5189	5.44	5.23	8.55	42.1	8.40
M70/1-705, 50 m	467	1494	8832	5303	x	5.23	8.58	42.0	x
M70/1-705, 20 m	452	1449	8500	5192	5.07	5.24	8.53	42.5	8.21
M70/1-708, 823 m	433	1393	8117	4920	35.2	5.26	8.50	42.0	28.1
M70/1-709, 882 m	445	1429	8371	4958	14.4	5.25	8.54	41.2	14.2
M70/1-709, 600 m	442	1423	8326	5091	19.7	5.26	8.54	42.6	17.7
M70/1-709, 460 m	437	1407	8206	4968	20.8	5.27	8.52	42.1	18.6
M70/1-709, 280 m	431	1381	8052	4827	29.1	5.24	8.47	41.4	24.1
M70/1-709, 50 m	413	1331	7702	4768	40.8	5.27	8.46	42.7	33.1
M70/1-709, 20 m	418	1346	7790	4884	36.4	5.26	8.45	43.3	29.8
M70/1-721, 633 m	437	1401	8170	5079	24.8	5.25	8.49	43.1	21.2

Sample ID	**Ca** [mg/l]	**Mg** [mg/l]	**Sr** [μg/l]	**B** [μg/l]	**Ba** [μg/l]	**Mg/Ca** [mol/mol]	**Sr/Ca** [mmol/mol]	**B/Ca** [mmol/mol]	**Ba/Ca** [μmol/mol]
M70/1-722, 2513 m	443	1413	8234	5029	26.6	5.22	8.44	42.0	22.1
M70/1-723, 1198 m	456	1463	8572	5115	26.4	5.25	8.53	41.5	21.5
M70/1-724, 760 m	453	1449	8487	5216	11.2	5.23	8.51	42.7	12.0
M70/1-725, 624 m	444	1428	8345	5179	24.1	5.26	8.52	43.2	20.4
M70/1-726, 620 m	431	1387	8080	4820	26.1	5.26	8.51	41.3	22.2
M70/1-727, 456 m	448	1440	8425	5181	9.66	5.25	8.53	42.8	11.2
M70/1-728, 623 m	439	1411	8232	5015	25.4	5.26	8.51	42.3	21.5
M70/1-735, 663 m	427	1374	7972	4938	34.3	5.27	8.48	42.9	27.9
M70/1-736, 1078 m	443	1421	8297	5025	19.6	5.25	8.50	42.0	17.6
M70/1-740, 1068 m	456	1466	8568	5192	16.3	5.26	8.53	42.2	15.1
M70/1-745, 557 m	457	1467	8616	5300	7.01	5.25	8.55	42.9	9.36
M70/1-746, 188 m	452	1452	8516	5163	17.0	5.26	8.55	42.3	15.7
M70/1-747, 408 m	453	1455	8537	5164	8.35	5.25	8.55	42.2	10.3
M70/1-748, 518 m	464	1489	8758	5288	3.66	5.24	8.56	42.1	7.25
M70/1-749, 620 m	447	1439	8410	5106	20.2	5.26	8.54	42.3	17.8
M70/1-750, 874 m	451	1447	8481	4977	14.5	5.24	8.53	40.8	14.1
M70/1-752, 710 m	469	1489	8786	5342	x	5.19	8.50	42.1	x
AL275-420-1#59, 85 m	415	1331	7866	4791	x	5.24	8.59	42.7	x
AL275-425-2#62, 25 m	374	1197	7016	4288	22.0	5.24	8.52	42.5	21.9
AL275-425-2#63, 10 m	320	1017	5973	3644	28.1	5.20	8.47	42.2	30.0
P325-383-2, 593 m	407	1312	7709	4588	9.4	5.28	8.60	41.7	11.6
P325-386-2, 175 m	423	1360	8031	4929	x	5.26	8.61	43.1	x
P325-373-2, 298 m	423	1364	8044	4805	x	5.27	8.62	42.0	x